UNIVERSITÀ
DEGLI STUDI
DI PADOVA

UNIVERSITA' DEGLI STUDI DI PADOVA

Sede Amministrativa: Università degli Studi di Padova

Dipartimento di Innovazione Meccanica E Gestionale

SCUOLA DI DOTTORATO DI RICERCA IN INGEGNERIA INDUSTRIALE
INDIRIZZO: INGEGNERIA DELLA PRODUZIONE INDUSTRIALE
CICLO XXIII

ACTIVE VIBRATION CONTROL SYSTEMS BASED ON MAGNETO-RHEOLOGICAL FLUIDS FOR SHEET METAL FORMING PROCESSES

Direttore della Scuola: Ch.mo Prof. Paolo F. Bariani
Coordinatore d'Indirizzo: Ch.mo Prof. Enrico Savio
Supervisore: Ch.mo Prof. Paolo F. Bariani

Dottorando: Paolo Regazzo

“Quousque tandem abutere, Catilina,
patientia nostra?”

M.T. Cicerone, *Catilinarie*

TABLE OF CONTENTS

ACKNOLEDGMENTS

The present work has been carried out under the supervision of Professor Paolo F. Bariani to whom I express my sincerest gratitude.

A special thanks is for Dr. Andrea Ghiotti, who has always help me to fight against the odds with his valuable advises and most of all his friendship.

I would also like to thank all my colleagues at DIMEG for their invaluable support, their friendly and bright atmosphere all during these years.
A thanks is also for the students who contributed with their efforts to the present work.

And the most important last thanks to my family, that endless supported me in these years.
This goal could not have been reached without them.

Paolo Regazzo

Padova, January 2011

ABSTRACT

Forming operations are among the most frequently used processes in sheet metal working. Dynamic phenomena occurring represent critical aspects for geometrical accuracy of products and service life of machines parts in high-tech forming machine sector. Stiff presses allow high repeatability and dimensional accuracies but, at the same time, determine rapid and excessive deterioration of tools by stresses and wear. On the other hand, softer ones improve the efficiency and the service life of tools, but with higher energy dissipation and bigger scatter in product dimensions that make processes unreliable with respect to precision.
The right trade-off is often the main prerequisite for the technical and economic success of the whole process and must therefore be found, especially with complex non-symmetric geometry and if vibrations take place during the process.
Since the interaction of different elements determines the dynamic efficiency of forming machines, controls systems for the compensation of elastic deformations result fundamental for the component accuracy and the required tolerances.
Conventional actuators devices present strong limitations in both performances and reliability, with restricted possibilities of closed-loop controls. The best solution is represented by new technologies, able to enhance the control of phenomena process.
Magneto-rheological (MR) fluids represent one of the most versatile and promising solutions for the development of high efficiency damping systems, capable to grant high versatility of configuration and effective closed-loop control capabilities.
The main objective of this work is to study magneto-rheological fluids technology, used up-to-now especially in anti-seismic and automotive fields, in order to extend to the industrial material forming processes.
Due to the complexity of the physics fields involved, the majority of models are based on analytical descriptions that, though easy and fast to implement, present strong limitations for the accurate design of the functional devices. A new approach is introduced, focused on a multi-physics coupled numerical model of the vibration dampers, based on calibrations by physical-simulation.
Different damper prototypes are realized for the laboratory tests, in order to experimentally analyse fluid and device behaviours.
On these bases, the application of these innovative damping systems and the evaluation of their performances are extended in the industrial context. The experimental tests, conducted on an hydraulic press using both commercially

available hydraulic dampers and MR dampers, are analysed with particular focus on the excited frequencies, the vibrations and the powers to quantify the impact of dynamic phenomena on the quality of final parts. The developed prototypes are able to elevated damping performances without complex adjustment calibration when setting up a new process, making flexible its design.

SOMMARIO

Le operazioni di formatura sono tra i processi più diffusi nell'ambito della lavorazione della lamiera metallica. La presenza di fenomeni dinamici è critica per l'accuratezza geometrica dei manufatti e per la vita di servizio delle attrezzature, in particolare per le aziende ad elevata tecnologia nel settore della produzione di macchine utensili. Ottime ripetibilità ed accuratezze dimensionali sono ottenute grazie a presse ad elevata rigidezza strutturale a discapito, tuttavia, della vita degli utensili, esposti a rapidi ed eccessivi fenomeni di usura. Dall'altro lato, l'uso di architetture poco rigide permette di aumentare la durata degli utensili, ma con limiti di efficienza energetica e degli standard di precisione dimensionale.

Pertanto il corretto bilanciamento dei differenti fattori rappresenta il prerequisito fondamentale per il successo tecnologico ed economico dell'intero processo. In particolare, nella produzione di geometrie complesse e non simmetriche, oppure quando fenomeni vibratori si manifestano durante il processo di lavorazione.

Poiché l'efficienza dinamica di una macchina per formatura è il risultato dell'interazione di diversi fattori, risulta fondamentale un sistema di controllo avanzato per la compensazione delle deformazioni elastiche, soprattutto in relazione alle specifiche richieste dei prodotti.

Gli attuatori tradizionali presentano grossi limiti sia nelle prestazioni sia in affidabilità, con poche possibilità di realizzare una catena chiusa nel controllo. La migliore soluzione è rappresentata dall'introduzione di nuove tecnologie, capaci di aumentare il controllo dei processi.

I fluidi Magneto–Reologici (MR) rappresentano una delle più versatili e promettenti soluzioni per lo sviluppo di sistemi di smorzamento ad elevata efficienza, capaci di ottima versatilità e controllo continuo dei fenomeni dinamici.

Il principale obbiettivo di questo lavoro consiste nello studio della innovativa tecnologia basata sui fluidi magneto–reologici, prevalentemente diffusa nell'ambito automotive e nei sistemi civili antisismici, in modo da estenderla anche ai processi di formatura dei materiali metallici.

In seguito alla complessità dei molteplici campi fisici interagenti, la maggior parte dei modelli si basano su descrizioni analitiche che, sebbene relativamente semplici e veloci da implementare, presentano grossi limiti per un'accurata progettazione di dispositivi. Pertanto viene introdotto un nuovo approccio, basato su una modellazione multi-fisica accoppiata dei sistemi di smorzamento e una calibrazione mediante simulazione agli elementi finiti.

Sono stati realizzati più prototipi di smorzatori magneto-reologici, in modo da analizzare le prestazioni sia dei fluidi che dei dispositivi stessi, attraverso test di laboratorio. Successivamente, l'applicazione di questi innovativi sistemi di smorzamento è estesa al contesto industriale e valutata mediante prove su una pressa idraulica per tranciatura. Attraverso test sperimentali che comprendono anche il confronto con dispositivi commerciali idraulici, le prestazioni degli smorzatori magneto-reologici vengono analizzate con particolare riferimento allo studio delle frequenze eccitate, alla tipologia di vibrazione e alle potenze in gioco, in modo da quantificare l'impatto dei fenomeni dinamici intervenenti sulla qualità dei prodotti finiti. I prototipi sviluppati sono in grado di elevare le performance di smorzamento senza complessi aggiustaggi durante il settaggio delle nuove sequenze di processo, rendendo flessibile la progettazione del processo

LIST OF FIGURES

CHAPTER 1

INTRODUCTION

1.1. CONTEXT

In a production system based on sheet metal working, forming operations are among the most frequently used. Therefore, a correct design of the forming sequence is one of the paramount issues of carrying out the process successfully.
The main motivations are the improvement of formability and product accuracy, that allows, for instance, the reduction of reject volume and of high cost of replacing tools and equipment after catastrophic failure.
Among various forming operation, blanking and, more generally, shearing operations are the most common operations in the process chains for sheet metal

parts. Studies on the optimization of the process design have been performed considering the control and the development of process control.
Depending on the geometry and the position of the cutting edges, various shearing processes are used, such as blanking, piercing and cutting off. According to the process parameters, complex stress and strain states influence the fracture formation, and may cause heavy vibrations, which propagate as strong detrimental noise in the working environment.
The sheet metal behaviour during blanking results in the characteristic load-stroke curve shown in Figure 1.1:

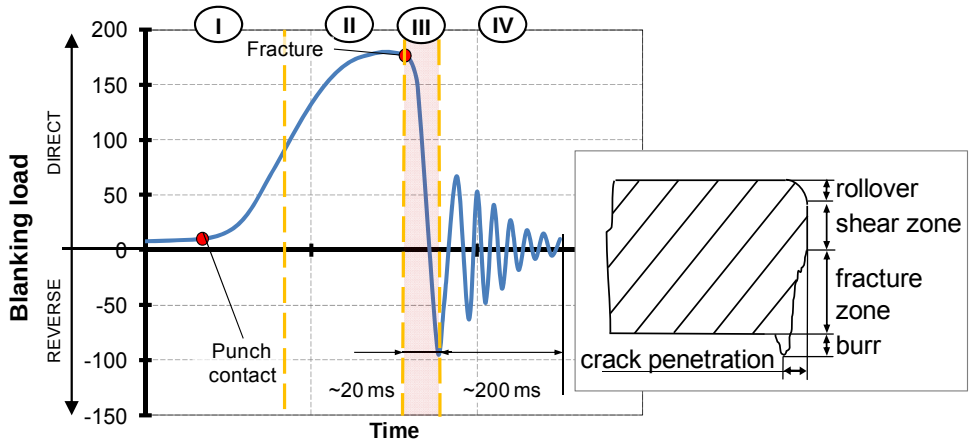

Figure 1.1 – The reverse load phenomenon in blanking (in the box, the corresponding rollover, smooth sheared zone and rough fracture surface are highlighted).

The first part of the curve that represents the material deformation during blanking can be divided into four stages. In the former stage, the punch comes in contact with the metal sheet and starts deforming elastically the blank (zone I). The sheet undergoes elastic compression, as well as tensile and bending deformation. With the penetrating of the punch, after the material yield strength is reached, the plastic deformation starts and determines the rounding of the edge of the blank. At first, the yielding point is reached by the surface fibres under the punch edge, and later by all the fibres interested by the material flow along the cutting edges. At this point, the shearing has not started yet, whilst the tensile stress and the bending moment in the material continue to increase. As the pressure increases, plastic shear deformation occurs, and the change of the force with the punch stroke reflects the strain-hardening characteristics of the material to be blanked. The material damage begins, followed by nucleation and growth of cracks. At this stage, the maximum value of the blanking force is reached and, although further strain-hardening may occur, the punch force decreases in proportion to the

decrease in the vertical area of shear (zone II). The arising dynamic phenomena determine high loads on the machine and the tooling and, as a consequence, considerable deflections of these components. The press and die set store up elastic energy.
Finally, after the shear strength of the material in the shearing zone is exceeded, ductile fracture starts and propagates towards the blank depth (zone III) and thus progressively cuts the material fibres one after the other (Figure 1.2) [1]. The punch still continues to penetrate into sheet, and the cracks near to cutting edges of the punch and the die become larger and expand into the material.

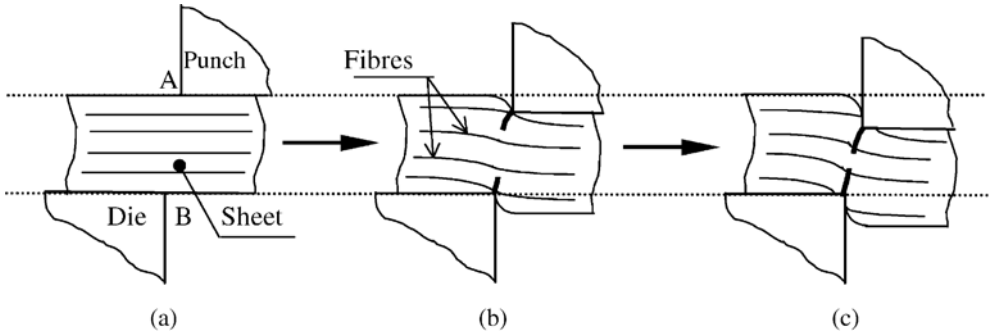

Figure 1.2 – Rupture of the sheet: (a) initial; (b) crack initiation; (c) crack propagation [1]

As the fracture propagates across the metal sheet, the energy accumulated in the machine frame is released abruptly, thus influencing the workpiece dimensions and accuracy. The energy subsequently dissipates through the high frequency oscillations shown in the tail end of the curve in Figure 1.1 (zone IV), depending upon the design of the press frame.
The sketch in Figure 1.1 shows the material flow, the plastic bending of the edge, the smooth sheared zone, the rough surface as a result of ductile fracture and the burr [2, 3].
The interactions between the workpiece, the machine and the tools make difficult the optimization of the processes and the respect of tolerances in the final product [4 – 6].
Stiff forming presses allow high repeatability and dimensional accuracies but, at the same time, can determine rapid and excessive deterioration of tools by stresses and wear. On the other hand, softer ones would be preferable for the efficiency and the service life of tools, but with higher energy dissipation and bigger scatter in product dimensions that make processes unreliable with respect to precision. The right trade-off is often the main prerequisite for the technical and economic

success of the whole process and must therefore be found. Especially when the formed part has a complex non-symmetric geometry and vibrations take place during the process, the stiffness and the damping performances of machine tools play a relevant role.

Shearing processes have been largely investigated in order to improve the monitoring and control of the quality of components, as well as to provide approaches for the parameter optimization and the reduction of the wear in tooling and in machines.

The most relevant contributions have been devoted to:

(i) *process optimization*, by investigating the influence of material behaviour (e.g.: rheology, microstructural constituent morphology, crystallographic texture, the intergranular structures), interface conditions (e.g.: coatings, lubricants, lubrication systems), process parameters (e.g.: clearance, punch speed, tools geometry), either experimentally or by using of FEM-based tools [7 – 9];

(ii) *dynamic phenomena reduction*, through the analysis of the elastic energy release during new surfaces generation, the unloading velocity of the machine frame and the system stiffness, taking into account the various nonlinear factors, such as the dies structure, the plastic deformation, the damping and the clearances [5];

(iii) *new devices and machines development*, for example new dampers for reducing the energy release rate stored within the press frame [10] and new servo-controlled presses that allow a closed control of the stroke curve during the fracture propagation [4].

Despite the importance of correlating the material shearing phenomenology and the process parameters, the first two approaches often clash with the limited flexibility that process designers have when setting up new processes, due to predetermined product features, such as shape geometry and product accuracy.

The best alternative, for improving both the quality of final products and the service life of machines and dies, is represented by the introduction of new technologies capable to enhance the control of those phenomena occurring during the shearing processes.

Conventional industrial devices techniques require additional machine power and higher loads, which make critical their use in many applications. Unlike, magneto-rheological (MR) fluids represent one of the most promising technologies for the development of high efficiency systems, capable to grant high versatility of configuration and effective closed-loop control capabilities, thanks to their rheological characteristics. Magneto-rheological actuators are very efficient on consumption, because they can require only a small fraction of the power of

traditional devices. Moreover on efficiency, allowing an active change of performances in a range of few milliseconds.
Besides their increasing importance, no investigations can be found for the control of forming machines.

1.1.1. Optimization of blanking operation: reverse load effect

Research in the control of forming operations in sheet metal working is currently being performed to improve the monitoring and control of the quality of components.
Considering blanking operations, since they represent among the most rapid operations in metal forming, it is imperative that the control of cutting process is correspondingly fast.
When the load has reached the maximum value (zone II of diagram in Figure 1.1), the machine has built up potential energy due to the deflections of the machine frame and the tools, as normal result of the pressure required to cut through the material. The punch breaks through the metal, generating a negative force, and the frame opens up, in the press gaps, when load is applied. As soon as the shearing strength of the material is exceeded and the fracture starts, the release of the stored up energy immediately occurs (zone III): the frame snaps back but closes beyond its "at rest" position. All the press components that are designed to function in compression are placed in tension while those that are normally in tension end up in compression, in a period whose duration is around 20 ms [11].
This sharp action is typically associated with the loud noise characteristic of the blanking processes and occurs while the punch is in the die cavity and engaged with the material.
This undesirable negative load effect is known as *Reverse Load*, often referred to as break through shock or snap through shock [11].
The punches not only oscillate vertically but also may experience significant lateral movement that will not only cause premature wear but often breakage to major press parts, such as the machine frame, the hydraulics, the dies or the suspension point components [12].
During the last part of the cycle (zone IV of load-stroke curve in the diagram of Figure 1.1), the rapid acceleration of the slide generates an impact compressive loading in the machine frame: depending upon the design of the press frame, this energy is dissipated through the high frequency vibrations shown at the end of the diagram. These oscillations increase in amplitude and duration as the reverse load goes up, and they represent the shock and vibration that are the greatest enemy of press and die life.

This damage does not usually appear after a single press stroke but manifests itself over many cycles. High shock, vibration and component deflection levels cause fatigue in the press and tooling components resulting in failure.

1.2. INDUSTRIAL-SCIENTIFIC PROBLEM

On the basis of previous observations, two fundamental aspects can be distinguished regarding sheet metal forming operation control:

- the industrial problem, such as the reverse load control and the reduction of its influence, in order to avoid uncontrolled mechanical vibrations and a loud noise that may cause problems such as fatigue cracks in the press components, premature wear in tooling and a great discomfort for press operators;

- the scientific problem, such as the analysis of innovative magneto-rheological fluids behaviour in forming operation, in order to gain a closed-loop control of dynamic effects and an evaluation, through full-scale experiments, of feasibility and practicability of implementation of magneto-rheological devices, understanding the potential benefits aspects in the active uses.

1.3. THE OBJECTIVES

The aim of the present work is to develop an innovative devices for the process control in sheet metal forming operation.
This can be express in a innovative solution for solve the reverse load problem in sheet metal forming, based on the smart capabilities of magneto-rheological fluids.
This aspect of the study is organized on numerical and experimental analysis, in order to investigate the damping device behaviour in the final working conditions and the accuracy of the final products.
The principal aim of the investigation is to evaluate, through full-scale experiments, the feasibility and practicability of implementing MR dampers and to understand the potential benefits when they are used in a semi-active manner in comparison with conventional dampers. Moreover the evaluation of the impact of

dynamic phenomena on the press frame and the tooling before and during the industrial implementation.
In order to achieve this main purpose, several goals can be distinguished:

- design and set up of an experimental damping devices to study magneto-rheological behaviour of MR fluids in order to reproduce, as close as possible, the process conditions that arise in typical sheet metal forming operations;
- development of a numerical procedure based on multi-physics coupled analysis for the evaluation of transmission of loads through the model domains and of physics field interactions;
- design and manufacturing of experimental damping devices to allow an experimental campaign conducted in the industrial context on an hydraulic press;
- design of an experimental procedure and of a laboratory equipment in order to testing MR fluids devices.

1.4. THE ORGANIZATION OF WORK

The work is organized in six chapters. The first one contains a short introduction of the work, the main problem approached and the objective.
The second chapter presents a general literature review effort, focused on the reverse load problematic connected to the sheet metal blanking and relative industrial solution, the magneto-rheological fluids proprieties and capabilities as well as the magneto-rheological device models and structures developed.
An novel multi-physics model approach is described in chapter three, in order to study the influence of different physical fields involved and to predict general performances of the magneto-rheological actuator.
In chapter four the experimental apparati for the study of MR fluid, as well as the laboratory testing campaign for the investigations about damping performances, working temperatures and pressure of materials are presented.
In chapter five the industrial implementation of the MR devices in a hydraulic press for blanking is presented, with the aim of evaluating, through full-scale experiments, feasibility and practicability of their implementation and understanding the potential benefits in comparison with conventional dampers.
The final chapter briefly presents the conclusions.

CHAPTER 2

LITERATURE REVIEW

2.1 INTRODUCTION

The present chapter presents a general literature review effort. The analysis of the problem is carried out starting from a presentation of the state of the arts considering the critical aspect of the industrial problem. In particular, the scientific author's works and several systems, that can be found in the industrial context, for the control of the blanking vibrations are analysed.
A description of the physical and rheological characteristics of the innovative Magneto-Rheological (MR) materials used are provided, focusing attention on the basic modes of operate of the materials, available in literature.

The typical damper architectures and the component configurations are presented, in order to understand the choices made in the following work.

2.2 REVERSE LOAD

Reverse load phenomenon, often referred to as break through shock or snap through shock, is an undesirable negative effect that affects the most common operations in the process chains for sheet metal parts.
As presented in Chapter 1, looking at a typical punch force vs. the penetration curve in blanking (Figure 2.1) [11], two main phases can be distinguished.

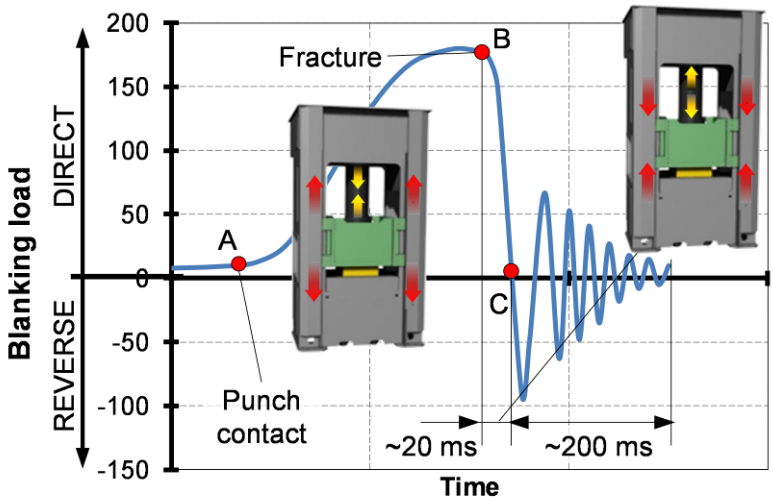

Figure 2.1 – The reverse load phenomenon in blanking.

In the first phase (from A to B in Figure 2.1), the punch penetrates the material causing the sheet metal to deform, first elastically and then plastically, until the pressure at the cutting edges starts the shearing.
Initially, the punch force increases steadily due to both the deformation and strain hardening of the material and, then, at the onset of shearing, it decreases due to the progressive reduction in the cross section despite the strain hardening. In this phase, the machine has built up potential energy due to the deflections of the machine frame and the tools, as normal result of the pressure required to cut through the material. As the ram descends downward and the die contacts the workpiece, a resistance force is built in the press frame [13]. The slide is counter pressured, eliminating all clearance in the mechanical or hydraulic linkage between the slide

and the crown. The latter, rigidly connected to the press bed through the side housing, resists this load and continues to store up elastic energy [11].
In the second phase (from B to C in Figure 2.1), the shear strength of the material in the shearing zone is exceeded and a fracture starts, causing the sudden release of stored up energy that dissipates through the high frequency oscillations (shown in the tail end of the curve in Figure 2.1). These oscillations increase in amplitude and duration as the reverse load goes up, and they represent the shock and vibration that are the greatest enemy of press and die life [14].
It has been measured [11] that all the energy is released in a period whose duration is around 20 ms: the press components that are designed to function in compression are placed in tension while those that are normally in tension end up in compression. The frame snaps back but closes beyond its "at rest" position [12].
The energy released has a direct relationship to amount of deflection. The magnitude of the actual energy released increases as the square of the actual tonnage developed at the moment of final breakthrough. (Eq. 2.1 [16] summarises the actual energy stored up:

$$E = \frac{F \cdot D}{2} \qquad \text{(Eq. 2.1)}$$

where F is the pressure at moment of breakthrough and D is the amount of total deflection to cut the metal blank.
Figure 2.2 represents the amount of energy stored in reverse load effect [17].

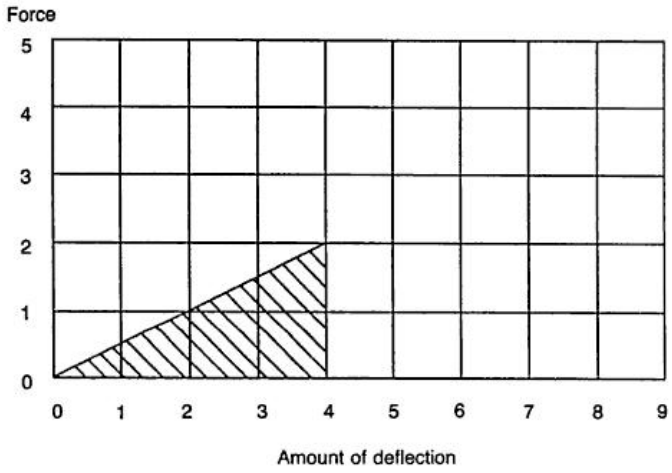

Figure 2.2 – Storage of energy in reverse load.

Reverse load is typically associated with the loud boom of the blanking processes and press vibration. It occurs while the punch is in the die cavity and engaged with

the material. Timing shear and punch entry sequences [17], to provide a gradual release of force prior to snap through, is a straightforward way to reduce the shock and noise associated with this problem (Figure 2.3).

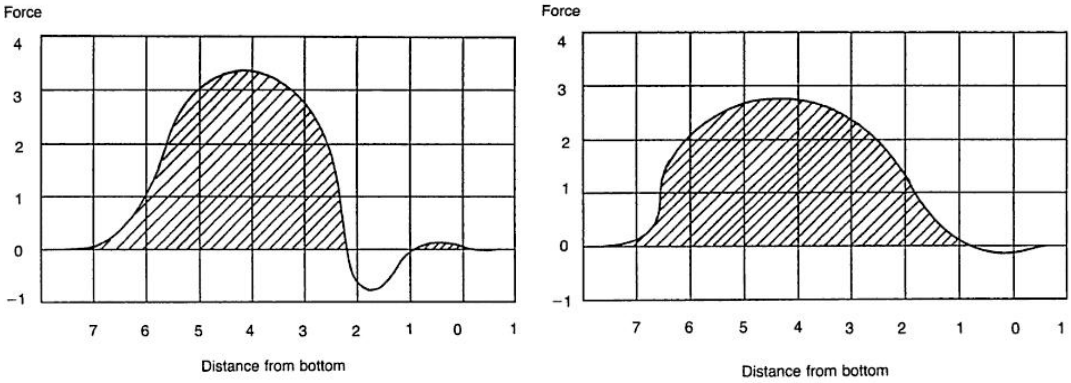

Figure 2.3 – Reverse load resulting from punch entry timing: on the left, no timing of entry condition; on the right proper timing of entry.

Reverse load damage does not usually appear after a single press stroke but manifests itself over many cycles. High shock, vibration and component deflection levels cause fatigue in the press and tooling components resulting in failure.

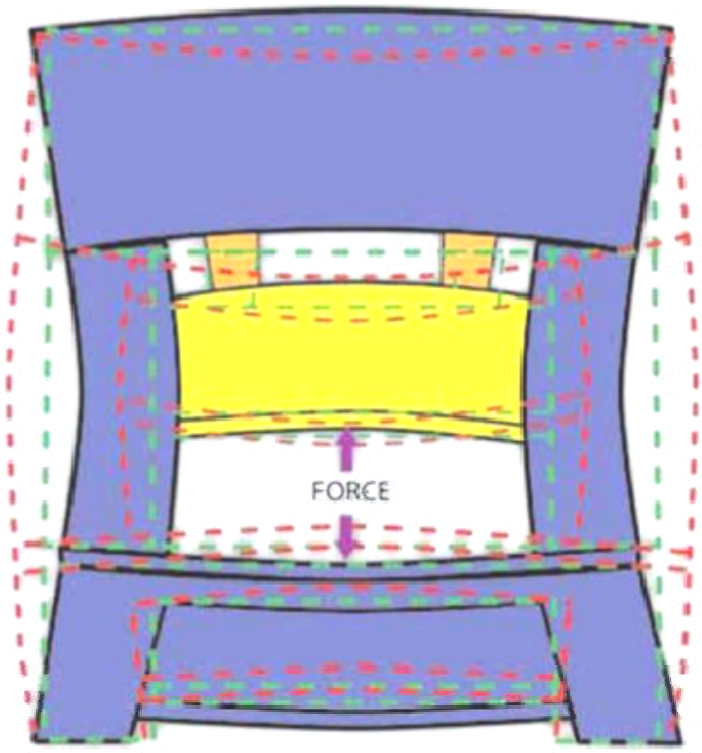

Figure 2.4 – Press deformation (amplified) during stamping operation.

The blue structure in Figure 2.4 illustrates a straightside press under load [12]. When the material fractures, the frame response is illustrated by the red outline and is well past the "at rest" position illustrated in green. As with the gap frame press, the frame oscillates many times before reaching a stable condition. This flexing of the frame and suspension point parts is what causes material fatigue because it occurs over and over with every press stroke

Several factors are influent to determine the level of reverse load: material types, hardness and thickness of metal sheet, clearances and sharpness in the press, punch stepping or shearing of the punches and die, punch velocity when it contacts the material, the characteristics of deflection in the press and die components [11, 12].

This break through shock generates uncontrolled high reverse loads, mechanical vibrations and a loud noise that may causes serious problems, such as fatigue cracks in the ram, drive linkage, crown, housings and, in the bed of the press, premature wear in punches and dies and a great discomfort for press operators.

To withstand the harmful effects caused by reverse load shocks, mechanical and hydraulic presses are normally oversized. The conventional general industry standard is to have presses designed to accept a reverse load that does not exceed 10% of the maximum forward capacity of the press, even if an over tonnage of 50% is not unusual for continuous blanking and punching of high strength materials [12].

The basis for this rating is dependent on the overall clearances, suspension point design and deflection characteristics of the press.

Relations that link the reverse load to the mechanical proprieties of materials can be found in literature. An example is shown in Figure 2.5 [11], where the reverse load factor (RLF) relates direct to reverse load.

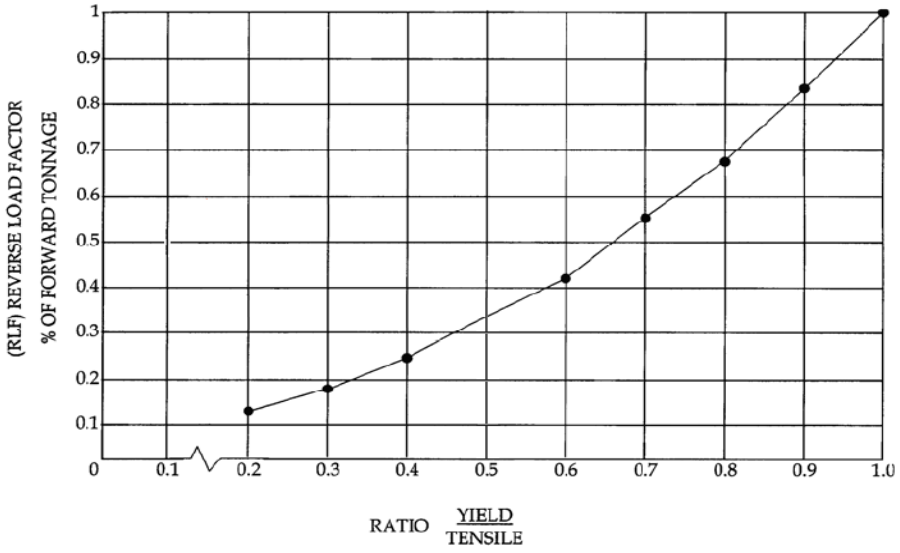

Figure 2.5 – Influence of mechanical proprieties of material in reverse load

Guo [5] analyzes blanking vibrations connected with the press stiffness by using the unloading slope of the blanking force – stroke curve.
The unloading characteristics at break-through step can be expressed by the unloading-slope (Figure 2.6), stated as the slope of the second part of force-stroke curve (from B to C in Figure 2.1), where the load decrease with the continued expansion of the crack (Eq. 2.2):

$$\psi = \left|\frac{\boldsymbol{dF}}{\boldsymbol{dS}}\right| = \tan\alpha \qquad \text{(Eq. 2.2)}$$

Its value is determined by the blanking material, the blanking conditions (blanking clearance and velocity), the blanking method and any retarding system in operation.

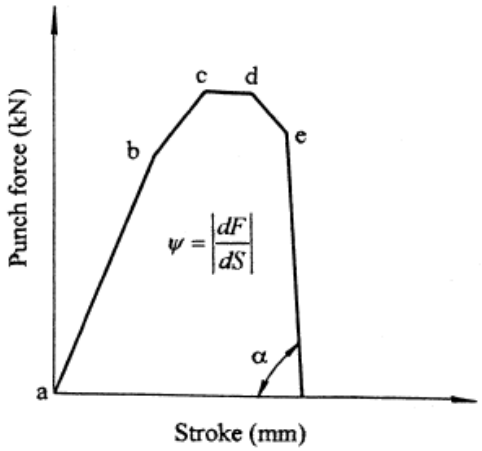

Figure 2.6 – Unloading-slope definition according to Force vs. stroke press curve.

When break through occurs, the differential displacement value deviates from the ideal nominal stroke curve, due to vibrations.
Neglecting any gaps between the parts, as well as any friction between the punch and the materials, the simplified proposed theoretical model that describes press behaviour treats the upper die and the moving mechanism of the press (stiffness K_u, quality m_u), and the lower die and the bed and bolster (stiffness K_d, quality m_d) as simple two-degrees-of freedom elastic model of an overall elastic model, that moves downwards with a nominal velocity of sliding V.
Figure 2.7 shows the main parts of the model.

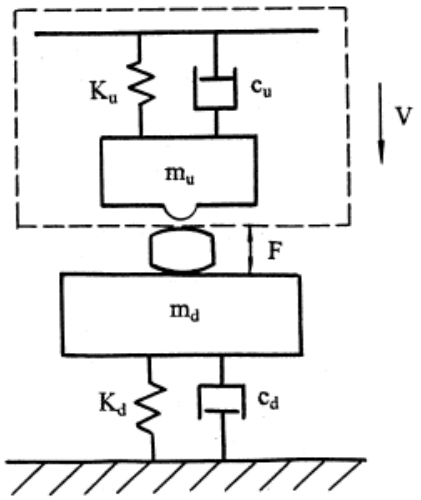

Figure 2.7 – Guo theoretical press model

The following relationship (Eq. 2.3) relates frame stiffness to reverse load vibration:

$$\psi \leq \boldsymbol{K} \qquad \text{(Eq. 2.3)}$$

where K is the stiffness of elastic model, such as relatively K_u or K_d.
When satisfied, the heave vibration caused by the abrupt unloading during break through decreases, showing that an excessive increase of the stiffness of the equipment (over sizing the press), besides could not be practical, will not have much significance and it will be wasteful economically.

Therefore, other industrial measures can be found to reduce the effects of reverse load in the press machine [11, 12].

- Limitation of the applied tonnage, considering stepping punches, using punches and dies sharp and preventing punch to die clearance that provides the lowest force requirement to accomplish the shearing process;
- Staggering of the punches, in order to minimize the forward load, as well as the reverse one;
- Shearing of the punches if the slug is to be scrap (if the punch is for blanking and the part must remain flat, shear should be ground on the die section, taking to account that grinding all the shear in one direction would create lateral forces on the punch that could cause excessive wear or chipping);
- Reduction of the punch velocity, by slowing the press down (usually not acceptable), reducing the press stoke length or using a special link motion drive;

- Reduction of the press deflection, since it has a direct relationship to reverse tonnage. A decrease of the overall deflection can be accomplished by housing the die in a significantly higher tonnage capacity press or by using a press that is designed specifically for blanking and perforating work, or by placing sufficient structure in the proper areas of the machine Conventional presses have deflection ratings that are based on the load being equally distributed over two thirds of the bolster area. Placing a concentrated load in the large bed press causes the reverse tonnage to increase due to the increased deflection.
- as with deflection, overall bearing clearance is a significant contributor to the negative effects of reverse tonnage, because they produce the over-travel of a punch into the die cavity once the material fractures, that is extremely detrimental to die life and part quality, as well as increasing shock and vibrations in the press;
- building a cushion that absorbs the shock energy generated during material shearing;
- use of shock dampers, that is the most versatile solution to reverse load problem and the resulting damage, although the forward tonnage increases.

The break through shock in blanking operations has been considered by a number of researchers. The most notably based the work on the modelling of the ductile fracture that causes the sheet metal separation and the associated energy release.
Breitling et al. work [7] investigated press performances by a die sensors analysis for controlling all the different phases and the numerous parameters in a stamping process. Piezo based, as well as strain gage based in-die sensors signals were compared with load curves of press frame mounted sensors and the acoustic emission acquired from a triaxial acceleration sensor. Figure 2.8 presents the experimental setup used and the different sensor locations within the progressive die.

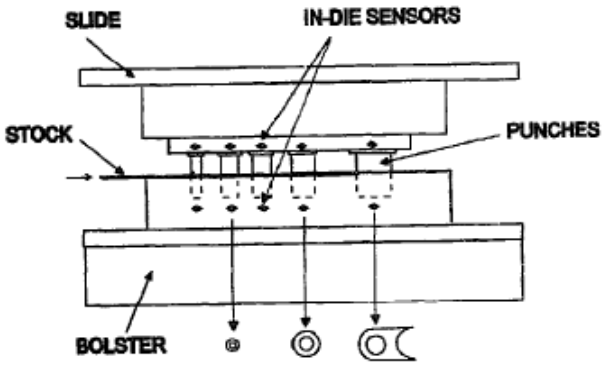

Figure 2.8 – Experimental setup and in – die sensor location.

Several blanking parameters (such as punch-die clearance, stock material, cutting tools, tool wear, punch velocity, lubrication) were changed, while continuously monitoring and saving the load-stroke curves and the acceleration sensor signals.
The results showed that it was possible to detect the different phases of blanking by means of in-die sensors, especially located in the machine line of force, as close as possible to the point where the load was generated. Every combination had its own load-stroke curve and most of these curves were slightly different.

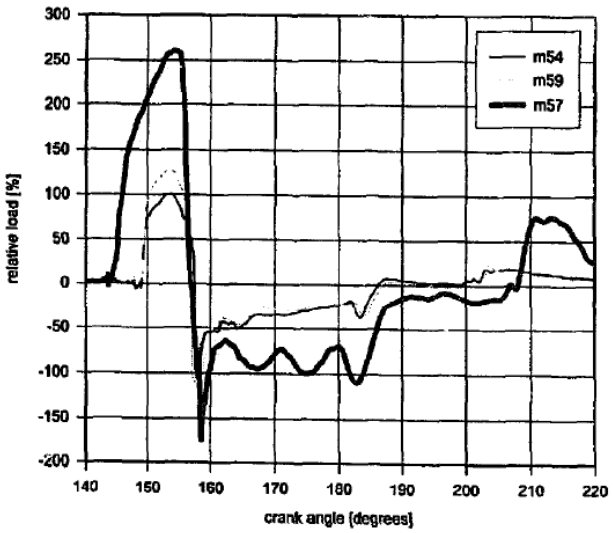

Figure 2.9 – Load – stroke curves by piezo sensor signal for different material at 200 spm.

Detecting problems, as poor punch-die alignment and change in material proprieties, energy release after material fracture, especially severe with progressive blanking dies, was registered for all materials tested in a distinct negative peak close to the crank angle (160°) at witch fracture occurred (Figure 2.9). The amplitude of the snap through peak depended on the initial blanking force: the higher the blanking force, the more snap through was seen.
Moreover, thanks to the monitoring and the control of the stamping process directly inside the die, an improvement of part quality and a reduction of the production of scrap parts was proved. However, no indication on realize the process control was provided.

Farzin et al.[8] discussed modelling issues of blanking processes, studying the effects of various damage criteria on the blanking parameters. *Gurson, Shear* and *Goijaerts* damage models were compared by their implementation in a plane strain numerical analysis for the description of the damage growth and fracture processes.

Gurson model crack prediction was not in agreement with experimental observations; therefore Goijaerts criterion was used to investigate the crack initiation position by changing the die–punch corner radii and material properties.
Novel 'Die to Punch corner ratio' was introduced for the definition of crack initiation and its effect on the stress distribution in the die wall.

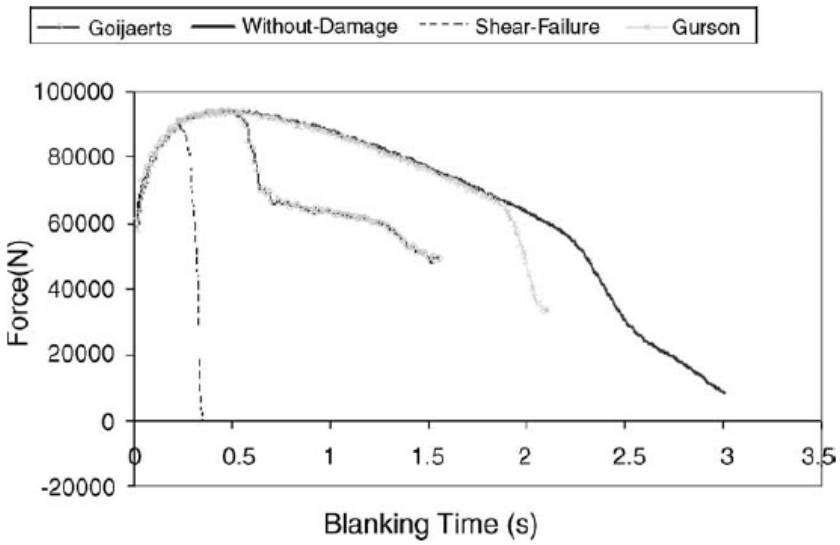

Figure 2.10 – Force–time diagrams for various damage models

Force–time diagrams for various damage models tested (Figure 2.10) showed that the maximum force calculated was the same with or without a damage criterion, concluding that when stress distribution in the die and punch had to be studied, no damage criterion was required. Therefore, particularly, any effect of reverse load in the stress distribution of both the punch and the die was valued.
Always relates to the numerical modelling of the ductile fracture, a study of the displacement and strain fields was carried out using a digital image correlation technique by Stegeman et al. [9].

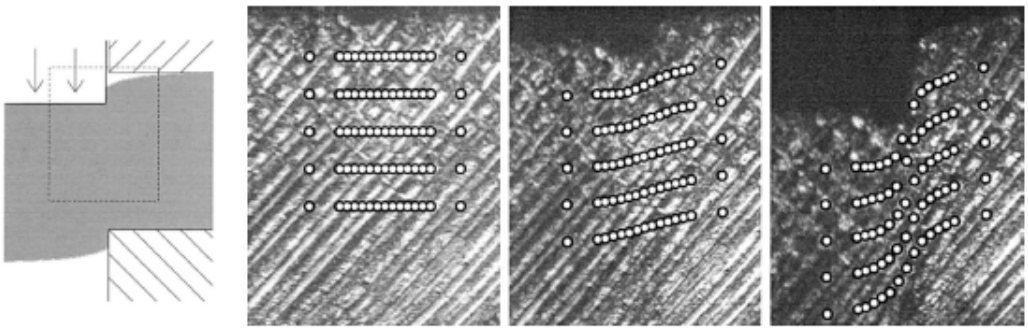

Figure 2.11 – Example of images recorded during the blanking process

Despite other research, not only the load–penetration curve at distinct stages of the punching process, but also the deformation was recorded in situ, through a planar blanking configuration.
Local deformations were monitored, and subsequently compared with numerical predictions, focusing on the deformation behaviour in a planar blanking process in order to obtain a methods useful for characterization of fracture and load–penetration machine curves. The numerical approach proved to a first approximation of the actual deformation at the surface, but not an adequate quantitative description, lacking in several parameter definition.

Many people have concentrated their studies on the effect of impact unloading behaviour on system vibration during break-through correlating the stiffness of the system components (press, stripper and die set) and their noise and vibrations during shearing [6, 18-19].
Doege [18] studied noise emission on punch presses in order to avoid the impulsive noise at breakthrough generated by the rapid unloading of the press frame.
An amount of the energy stored in the machine frame was reduced, using an electronically controlled hydraulic element in the force – flow of the power press
Figure 2.12), respectively to made use of it for the blanking process. By controlling the oil pressure within this element, it was possible to influence the effective shearing load during the blanking operation, reducing the oil pressure immediately after reaching the maximum cutting force. The true tool velocity has been controlled, allowing a reduction on the rapidly unloading of the force at a large scale.

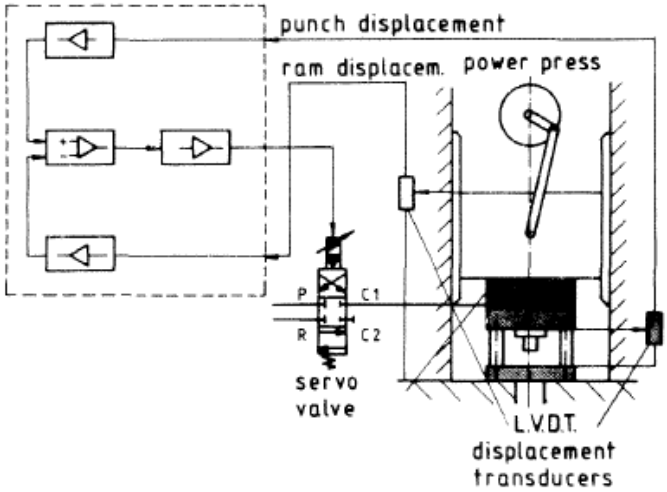

Figure 2.12 – Scheme of the hydraulic system.

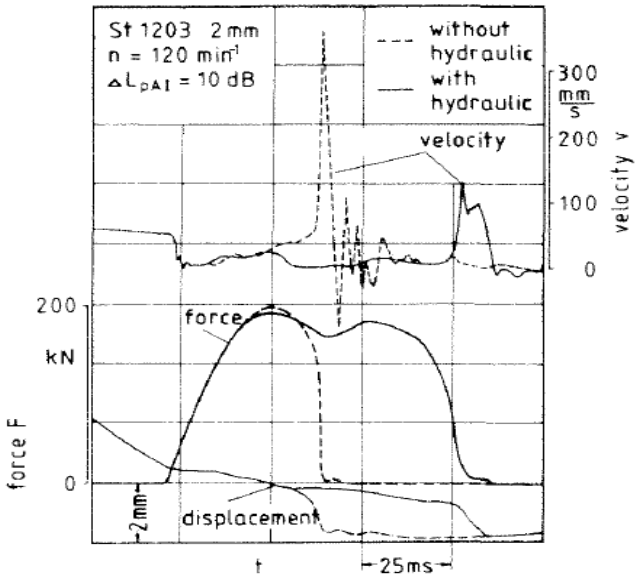

Figure 2.13 – Force-displacement-velocity curves

The hydraulic system allowed a reduction of both the true tool velocity after reaching the maximal force and the total force peak even if, however, the last one was not so remarkable. Instead of a sharp decrease of the process force, a gradual slope has been provided, for the same machine power.

Lai [20] and Shinaishin [21] examined various noise control options in continuous metal-cutting and in impact–shearing processes in factories for an analysis of numerical methods for prediction of noise and machine vibrations as required by government standards. Thanks to a noise source diagnosis, the total energy in a cutting process was distinguished in the work done on the product, the work transferred to the ground, the energy dissipated as heat through structural damping and the energy dissipated by structural vibrations and radiated as noise.

The main solutions proposed to solve the problem are not as a general rule and focused on a changing of the force and the speed generated by the machine and on a reduction of the force transmission to the connecting parts, even if it sometimes affected the product's quality.

Otsu et al. [4] proposed an accurate control of the punch motion combined with a "continuous two-steps blanking" to limit the noise level accompanying the break through shock. Through a servo controlled press, cutting operation has been divided in two steps: the former, when the punch movement was stopped at an intermediate position before breakthrough and soon moved, in the latter, again to finish the process (Figure 2.14).

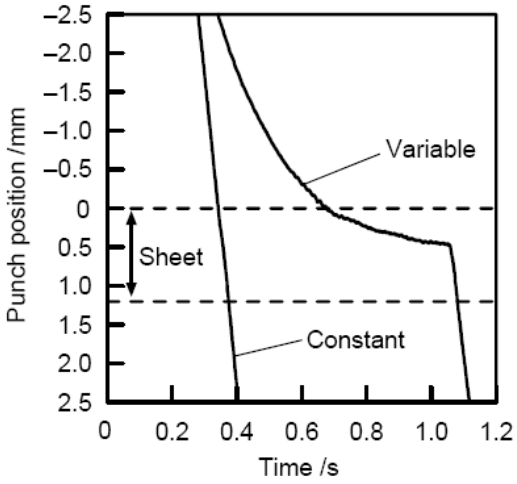

Figure 2.14 – Punch motions of constant and variable punch speeds.

Otsu demonstrated that the noise level of the variable punch speed process was lower than that for the constant punch speed process. As the stopping position of the punch increases, the noise level was again lower, especially in the high strength carbon steel. Moreover, linked to noise reduction, continuous two steps blanking allowed that the vertical vibration of the machine became smaller, as a direct result of load reduction before breakthrough.

However, few contributions in the scientific literature have dealt with new possible solutions to effectively control shearing process and reduce the reverse load, vibrations and noise.

2.2.1 Shock Damping Systems

In the industrial context, several systems for the control of the blanking vibrations can be found housed in the presses in order to prevent and limit reverse load. These devices are used to reduce the release rate of elastic energy stored up in the machine, and, consequently, the impulsive reverse load produced by the crack propagation.
On the basis of their working principle, they can be divided into the following categories.

a) *conventional long springs*

These spring systems [22], that use a compression of an internal spring characterized by a well-known spring constant go in contact with the machine ram just after the material rupture;

b) *inertial dampers*

Mechanical dampers [23] presents an architecture where a weight element (e.g. flywheel) is forced to move along an axial worm connected with the sliding parts when the reverse load appears, thus directly carrying out a damping action on the system vibrations. The conversion in rotational motion mitigates punches speed peaks. An example of mechanical dampers is presented in Figure 2.15.

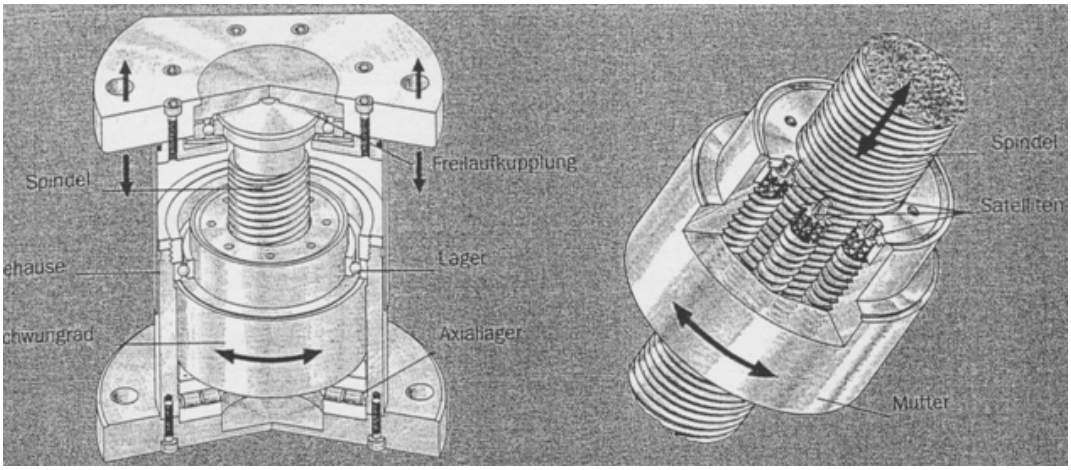

Figure 2.15 – Mechanical dampers.

Murakawa [10] developed a "hydraulic inertia damper", where an inertia counter force caused by an inertia mass was transmitted through a hydraulic conduit against the blanking punch force. This means of either a pin provided beneath the punch bottom or the piston above the blank holder. This system, represented in Figure 2.16, was installed within the die plate connected to the blank holder.
This passive system proved to be quite effective in lowering the punch force reduction rate thereby causing a reduction in vibration and noise, even if not easy to implement in the industrial enclosures and requiring several high inertial mass for the several blanking operations performed.

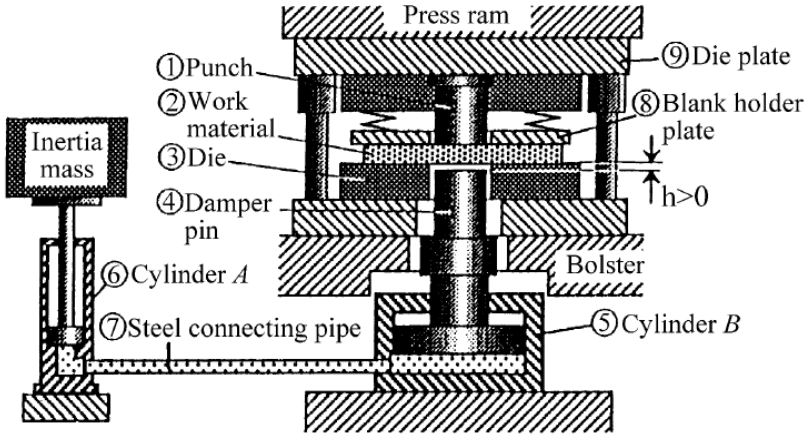

Figure 2.16 – Hydraulic inertia damper.

c) *hydraulic dampers*

In the industrial contest [12, 24–25], two types of hydraulic devices can be found. The first typology is designed to provide an upward counter-force through the compression of the oil inside a cylindrical chamber, as well as an oil cushion (Type I). In the second ones, an upward counter pressure is generated through control valves that restrict the flow of oil in an external hydraulic power unit out of the cylinder when it is subjected to an instantaneous velocity increase (Type II).
The main architectural characteristics are schematized in Figure 2.17, where the external reservoir and the close-coupled hydraulic circuit can be distinguished.

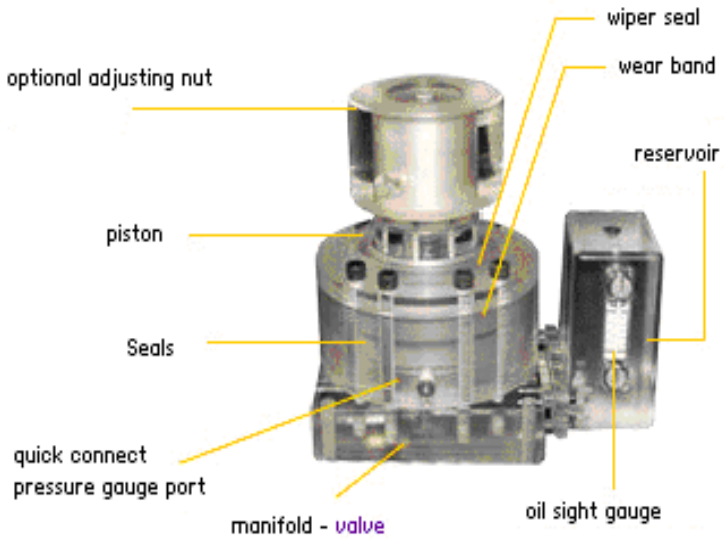

Figure 2.17 – Hydraulic shock damper.

On break through of the blanking punch, its speed increases to a multiple of the value just before break through, and the resulting increase in the hydraulic cylinder of the damper produces the damping effect. After the downward force has been taken off, the piston of the damper is moved back to the starting position by the oil flow into the cylinder through a non return valve.

The orifice area conditions the final damping capacity of the device (Figure 2.18). It is sized to minimize the upward counter pressure during normal cycling at the speed characteristic of the machine, passing the required volume in the accumulator.

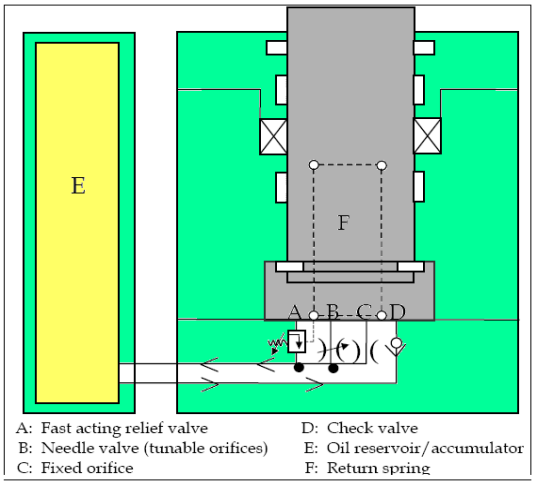

Figure 2.18 – Sketch of reservoir system for an hydraulic shock damper.

d) *magnetic dampers*

Behrens [3] develops a damper based on the physical principle of the Lorentz force. It consists of two parts. The upper part (actor) is attached to the ram and contains a short-circuited coil. The lower part (stator) is situated on the bolster plate and consists of a pile of permanent magnets. The voltage induction into a copper ring allows the operating, where the intensity of the magnetic field depends on the material of the permanent magnets and on the size of the air gap between the upper and the lower part of the damper.

Hence, the force involves the deceleration of a moving closed loop electrical conductor circuit in a magnetic field. The deceleration force increases with the intensity of the magnetic field and with the velocity of the conductor. Figure 2.19 presents the positioning of the damper and, in the sketch, the main parts of it.

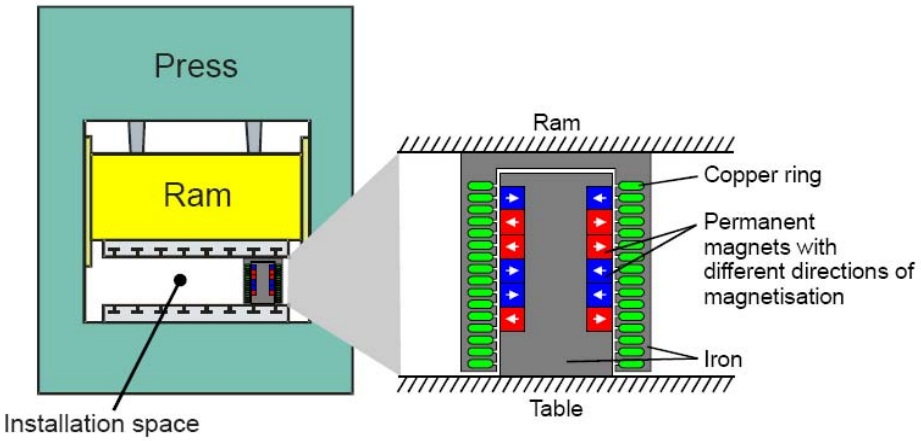

Figure 2.19 – Installation space in the press and a sketch of main components of a magnetic damper.

2.2.2 Available damping system limits

Available damping systems, discussed in previous section 2.2.1, present several limits in their damping performances and control.
Most of devices allow a passive control of the vibrations, that is they provide results only after an application of an external load and without any possibilities of changing the response during the process.
Passive control is the least expensive in the sense that a good design and the use of inherent system damping can achieve a sufficient response characteristic. But it is invariably a compromise that doesn't allow an optimal suppression capability of reverse load effects.
Traditional spring systems are limited by the spring constant and they are not suitable when the loads are greater or the punch speeds are higher.
Hydraulic cushions allow a good possibility of integration in the blanking machine, both considering the spatial positioning (usually placed inside the press bed) and the possibility of an integrated control with the control press unity. Therefore, the efficiency of this damping system is quite low: they provide a slow response, mainly due to the improper use of the press equipment.
Hydraulic damper are the most widely used in industrial contest, thanks to their relative limited costs and their rapid reconfiguration when the production process change. Due to the flow of oil through the orifice, damping performances are limited at the end of the piston device displacement and in a limited range of stroke (less than 20 mm). The needed external oil reservoir affects the versatility in the

positioning in the press bed plate. Also the effective minimum number of units needed for the same blanking process is not defined.
Magnetic damper developed, although they allow a control of the ram oscillation of the press at high frequency (when the rate are high), are affected by a strong influence of the material of the permanent magnets. Great magnetic fields are required in order to provide a relative low damping response, at the expense of energy machine consumption.
Magneto-rheological devices, on the contrary, allow to high versatility of configuration and effective closed-loop control capabilities, by modifying the way energy stored to the system is dissipated. Damping performances can be varied during the process along the whole machine stroke, without any addiction of load to the machine in their off-state. The usually range of current intensity required are less than 4 A, while the needed voltage is less than 20V, also for large scale dampers (i.e. 35 tons), with clear positive implications on the safety and on the economy of the process.
Architectural configurations allow to do without any external reservoir unit, facilitating the positioning in the press bed plate and increasing the versatility and flexibility in setting up new processes.

2.3 MAGNETO-RHEOLOGICAL FLUID

Magneto-rheological (MR) fluids belong to the Smart Materials category. The initial discovery and development can be credited to Jacob Rabinow at the US National Bureau of Standards in the 1940 even if their applications in the industrial fields are recent [26].
The most important advantage of these fluids, over conventional mechanical interfaces, is their ability to achieve a wide range of viscosity (several orders of magnitude) in a fraction of millisecond.
MR fluids are suspensions of micron sized iron particles in a liquid carrier. The average diameters of not colloidal particle go from 10^{-5} to 10^{-7} m, while the density are 7–8 g/cm^3.
They present controllable and reversible changes in its rheological properties [27], [28], from free flowing linear viscous liquids to semi-solids, having a controllable yield strength. Typical material carriers are mineral oil, silicon oil or water.
When exposed to a magnetic field [29], the ferrous particles, that are dispersed throughout the fluid, form magnetic dipoles. These magnetic dipoles align themselves along the lines of magnetic flux.

The interaction between the resulting induced dipoles causes the particles to form columnar structures, parallel to the applied field, as shown in Figure 2.20. These chain-like structures restrict the motion of the fluid, thereby increasing the viscous characteristics of the suspension. The mechanical energy needed to yield these chain-like structures increases as the applied field increases resulting in a field dependent yield stress.

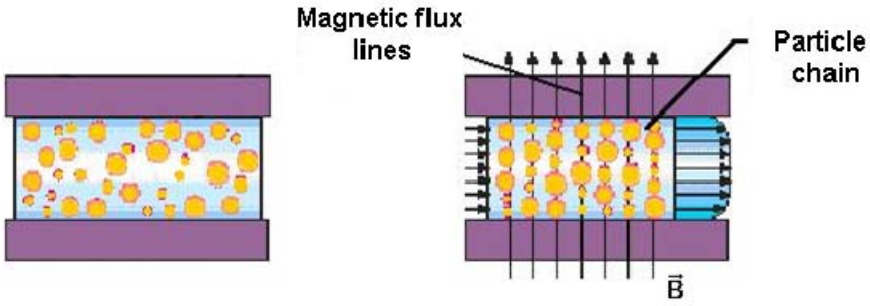

Figure 2.20 – Effects of external magnetic fields on the MR fluid rheology

This change is manifested by a very large change in viscosity and, consequently, in the resisting force when activated by an external magnetic field [30]. In the semi-solid state, the fluid exhibits viscous-plastic behaviour that is characterized by the field-dependent yield stress.

An advantage of MR fluids is their relative insensitivity to temperature extremes and contaminants [31]. This arises from the fact that the magnetic polarization of the particles, and therefore the yield stress of the MR fluid, are not strongly influenced by temperature variations. Similarly, contaminants (e.g. moisture) have little effect on the fluids magnetic properties.

Several additives, similar to those in commercial lubricants, can be added in the MR suspension in order to discourage gravitational settling and to promote particle suspension, enhance lubrication, modify viscosity and inhibit wear at material interfaces.

A typical MR fluid consists of 20-40% by total fluid volume of relatively pure, soft iron particles (e.g. carbonyl iron) [32, 33]. Commonly pure soft iron particles are used, obtained by chemical resolution (CVD) of $Fe(CO)_5$. Low carbon steel are also suitable materials. Even if the best available particles are alloys of iron and cobalt, because they have higher magnetic saturation (2.4 T), such alloys are prohibitively expensive for most practical applications. So the best practical particles are simply pure iron, as they have a lower magnetic saturation (2.15 T). Virtually all other metals, alloys and oxides have magnetic saturation significantly lower than that of iron, result in substantially weaker MR fluids.

The thermal range of working of these materials without a decay of their properties are -40 °C ÷ 150 °C, depending mostly on carrier properties [31, 32].
The rheological properties of controllable fluids depend on concentration and density of particles, particle size and shape distribution, properties of the carrier fluid, additional additives, applied field, temperature, and other factors. The interdependency of all these factors is very complex [28, 32].
The magneto-rheological response of fluids is the result of polarization in the particles by applying an external magnetic field. At particle level, a dipole structure is assumed.

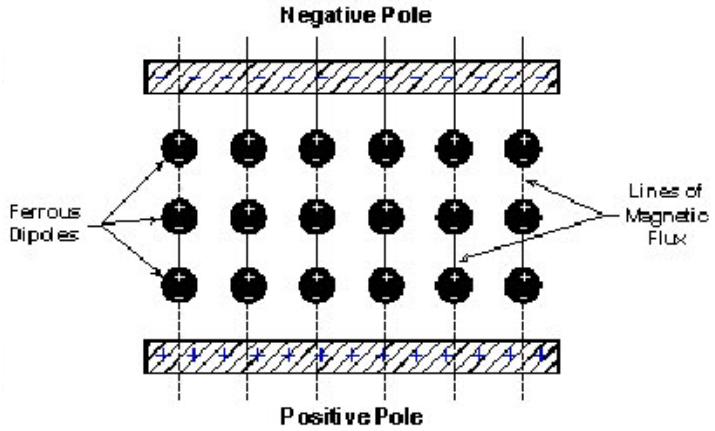

Figure 2.21 – Magnetic dipole generation in micro sized particles of MF fluid

As shown in Figure 2.21, without an applied magnetic field the particles are evenly distributed [34]. The fluid has a consistency similar to a common mineral oil. Its behaviour is similar to a Newtonian fluid, with a linear dependency of the shear stress versus the tangential velocity gradient.
With the application of an external field, a dipole momentum is introduced on the ferromagnetic micro-particles, in the same direction of the field [34]. The results are radical changes in the metal powder distribution. The magnetic interaction between dipoles brings the system into a state of balance and forces to move towards a new state of minimum energy, causing the formation of chains and columns linear structure parallel to the flow lines of the applied field [35]. These structures restrict the section for the movement of the fluid. An increase of the local viscosity of the suspension is generated. This behaviour, known as magneto-rheological effect, can lead to the apparent solidification of the fluid. A significant reduction in the mobility of the fluid and a strong variation of viscous resistance of the material result. Consequently, they induce a high increase in yield strength, directly dependent on the applied field, since it grows with the mechanical energy required to break the columnar structures [36].

In the selection of the right magneto-rheological fluid for the different applications, is fundamental a careful assessment of the magnetic properties [31-32].
Magnetic proprieties exhibit approximately linear behaviour, as shown in Figure 2.22, where there's a typical induction curve (*B-H* curve) of commercial MR fluids.

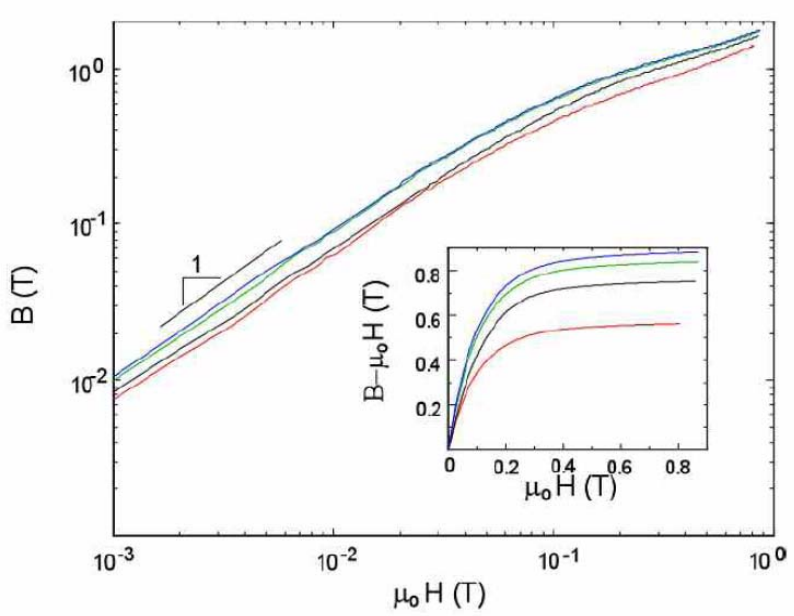

Figure 2.22 – Magnetic proprieties of MR fluids.

As can be seen, the MR fluids magnetic properties up to an applied field of about $0.02/\mu_o$ A/m, where μ_o is the permeability of a vacuum. In this region, the differential permeability of the MR fluids, that is the slope of B(H), varying between 5 and 9 times that of a vacuum, can be considered relatively constant. Magnetic saturation can be observed out of linear regime, which becomes complete for fields more than $0.4/\mu_0$ A/m [36].

The magnetic properties of MR fluids vary significantly considering the properties of most ferromagnetic materials properties. Ferromagnetic induction can typically be linearized over a much broader range of applied field and the corresponding permeability is several orders of magnitude greater [37].
Little or no hysteresis can be observed in the induction curves. This super-paramagnetic behaviour is a consequence of the magnetically soft properties of the iron used as particulate material in these fluids and the mobility of this particulate phase [36].

2.3.1 Analitical and Mechanical models

Several theoretical models are proposed in literature in order to describe magneto-rheological behaviour. These models are classified as the quasi – static and dynamic models. Quasi – static models are capable of describing force – displacement behavior of the MR damper reasonably well. Dynamics models allow also a description of the non linear force – velocity behaviour of the damper at high speed. The most widely used for the description of MR fluid behaviour is the visco– plastic Bingham model [27, 36], effective in describing the essential field dependent fluid characteristic [28] (Eq. 2.4):

$$\tau = \tau_0(H)\,\mathrm{sgn}(\dot{\gamma}) + \eta\dot{\gamma} \qquad \tau \geq \tau_0(H) \qquad \text{(Eq. 2.4)}$$

$$\tau = G\dot{\gamma} \qquad \tau < \tau_0(H) \qquad \text{(Eq. 2.5)}$$

$$\dot{\gamma} = 0 \qquad \tau < \tau_0(H) \qquad \text{(Eq. 2.6)}$$

where τ_0 is the yield stress caused by the applied field, G the shear modulus of fluid, H the amplitude of the applied magnetic field, η the field-independent post-yield plastic viscosity, $\dot{\gamma}$ the shear strain rate.
Without magnetic field (i.e. B=0) MR fluid is as a conventional Newtonian fluid, while, for B>0, a shearing stress τ emerges.
The Bingham model consists of a Coulomb friction element placed in parallel with a viscous damper. For nonzero piston velocities, $\dot{x}$, the force generated by the device is defined in (Eq. 2.7 [35]:

$$F = f_C \ \mathrm{sgn}(\dot{x}) + c_0\dot{x} + f_0 \qquad \text{(Eq. 2.7)}$$

where c_0 is the damping coefficient and f_C is the frictional force, which is related to the fluid yield stress. An offset in the force f_0 is included to account the presence of the accumulator. If at any point the velocity of the piston is zero, the force generated in the frictional element is equal to the applied force. Figure 2.23 represents that previously stated.

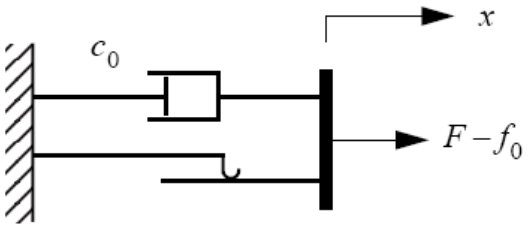

Figure 2.23 – Bingham model

The Bingham model has been employed in a number of models used to describe the behaviour of specific MR fluid devices. Many such models are derived from the work of Phillips [39], who developed Bingham flow in channels with parallel walls. He introduced non – dimensional forms of the Bingham flow equations (Eq. 2.8), and corresponding polynomial solutions, to determine the pressure gradient of flow through a parallel duct and to give the volume flux due to piston motion:

$$P^3 - (1+3T)P^2 + 4T^3 = 0 \qquad \text{(Eq. 2.8)}$$

Where the non-dimensional pressure gradient P and yield stress t are respectively defined as (Eq. 2.9 – 2.10):

$$P^3 = -\frac{dp}{dx}\frac{h^2}{12u_m\eta} \qquad \text{(Eq. 2.9)}$$

$$T = \frac{\tau_0 h}{12u_m\eta} \qquad \text{(Eq. 2.10)}$$

$\frac{dp}{dx}$ is the pressure gradient, h is the channel height, u_m is the fluid velocity, η is the fluid viscosity and τ is the yield stress.

A parametric viscoelastic – plastic model based on the Bingham model was proposed by Gamota [41]. The model consists of the Bingham model (a frictional element in parallel with a dashpot) in series with a standard model of a linear solid. The governing equations for this model are given by (Eq. 2.11-2.12):

$$\left.\begin{aligned} F &= k_1\left(x_2 - x_1\right) + c_1\left(\dot{x}_2 - \dot{x}_1\right) + f_0 \\ &= c_0\dot{x}_1 + f_0\,\mathrm{sgn}\left(\dot{x}_1\right) + f_0 \\ &= k_2\left(x_3 - x_2\right) + f_0 \end{aligned}\right\} \quad |F| \geq f_C \qquad \text{(Eq. 2.11)}$$

$$\left.\begin{aligned} F &= k_1\left(x_2 - x_1\right) + c_1\left(\dot{x}_2\right) + f_0 \\ &= k_2\left(x_3 - x_2\right) + f_0 \end{aligned}\right\} \quad |F| \leq f_C \qquad \text{(Eq. 2.12)}$$

where:
C_0 is the damping coefficient associated with the Bingham model; k_1, k_2 and C_1 are respectively the two stiffness and the damping coefficient associated with the linear solid material. Figure 2.24 resumed Gamota theoretical model.

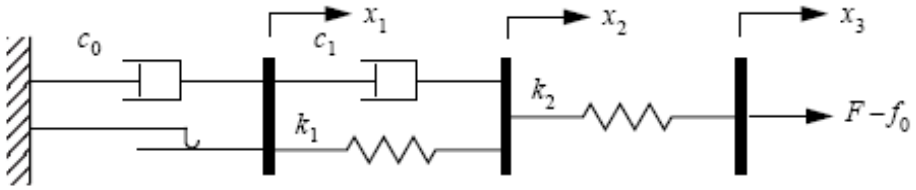

Figure 2.24 – Theoretical Bingham model in series with a standard model of a linear solid proposed by Gamota

Namaduri et al. [42] used a *Quasi-Steady-State* force model to predict MR performances, assuming laminar flow of the MR fluid with Newtonian behaviour in the off-state and Bingham plastic behaviour in the on-state.
Gavin et al. [43] presented a parallel plate approximation to the exact solution of Bingham flow in channels with parallel walls by a high order non dimensional polynomial to determine the pressure gradient in flow and mixed – mode valves. He also described the conditions under which simplified solutions to this polynomial could be developed. His approximation was useful in analysis of flow using the damper displacement and velocity information.
Because the gap size of the damper is normally very small in comparison to the annulus diameter, the fluid flow through the annular gap can be approximated by flow through parallel plates, witch pressure, stress and velocity profile through an annular duct are presented in Figure 2.25:

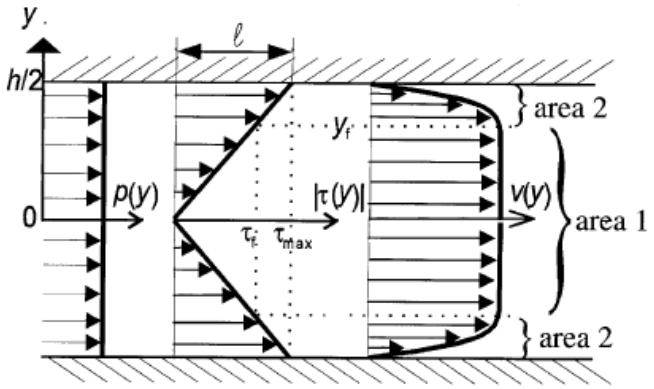

Figure 2.25 – Distribution of pressure and velocity across a channel in parallel plate approximation

In a similar work, Wereley and Pang [45] performed a no dimensional analysis of MR fluid dampers using the parallel plate approximation. The authors introduced another set of non-dimensional groups, that Hong et al. [46], basing on the Bingham plastic constitutive equation of the MR fluid, developed in:

$$\phi_C = \frac{\tau_y h}{\eta v_p} \qquad \text{(Eq. 2.13)}$$

$$\phi_R = \frac{r}{h} \qquad \text{(Eq. 2.14)}$$

where the non-dimensional parameter Φ_c is the Bingham number, that represents the ratio of the dynamic yield shear stress to the viscous shear stress and the influence of the magnetic field on the damping force of the MR damper. The non-dimensional parameter Φ_R represents the geometric ratio characterized by the piston radius r and gap h. This parameter allowed to better correlate the geometrical damper dimensions and its final damping force.
Hu and Wereley [47] used Bingham number, no dimensional geometric parameter and also non-dimensional damping force and dynamic range D (section 4.3), while Choi and Lee [48] used a polynomial model that included the excitation current as variable, in order to control the fluid performances. The final force was defined as:

$$F = \sum_{i=0}^{n} \left(b_i + c_i I \right) v^i \qquad \text{(Eq. 2.15)}$$

where *b* and *c* are experimental coefficients, determined from the curve fitting, while *v* is the fluid velocity.
Wereley et al. [48] developed a non-linear hysteretic biviscous model that could allow an improved representation of the pre – yield hysteresis. Using a set of no dimensional groups, consisting of no dimensional plug thickness and Bingham number *Bi*, an equivalent viscous damping coefficient at field-on status and at field-off status has been stated as (Eq. 2.16):

$$C_{eq} \begin{cases} \dfrac{\mu_{po} bL}{d}\left[1+\left(1-\bar{\mu}\right)Bi\right] & \bar{\tau} > 1 \\ \dfrac{\mu_{pr} bL}{d} & \bar{\tau} \le 1 \end{cases} \qquad \text{(Eq. 2.16)}$$

where μ_{PO} is the post yield viscosity and μ_{PR} the pre yield viscosity of fluid in a gap *d* between two plates of length *L* and width *b.*
Moreover*:*

$$\bar{\tau} = \frac{\tau}{\tau_{ys}} = \frac{\tau\left(1-\bar{\mu}\right)}{\tau_{yd}} \qquad \text{(Eq. 2.17)}$$

$$\bar{\mu} = \frac{\mu_{po}}{\mu_{pr}} \qquad \text{(Eq. 2.18)}$$

Where τ_{ys} and τ_{yd} are static and dynamic yield stresses.

Stanway et al. [49] made a no dimensional analysis for a flow mode damper by considering dimensionless numbers, such as *friction factor* $\pi 1$, *Reynolds number* π_2 and *Hedstrom number* π_3. In this case, a flow mode damper was experimentally analyzed to show the effectiveness of the model, showing a improvement in the prediction of device behaviour.

An alternative to the Bingham model is the Herschel – Bulkley model [28, 32, 50], which accounts for the post-yield shear thinning or thickening behaviour of MR fluids, as presented in Figure 2.26. In this model, shear thinning and thickening effects influence the post-yield plastic viscosity, now dependent on shear strain rate:

$$\tau = \left(\tau_0(H) + K|\dot{\gamma}|^{\frac{1}{m}} \right) \mathrm{sgn}(\dot{\gamma}) \qquad \text{(Eq. 2.19)}$$

where K is called the *consistency* and m as *flow (behaviour) index*; they are both fluid parameters that are influenced by the intensity of applied magnetic field, the particle content, the magnetic proprieties of fluid and the dosages of surfactants [44] For $m > 1$, (Eq. 2.19 represents a shear thinning fluid, while shear thickening fluids are described by $m < 1$. The pre-yield behaviour is assumed to be rigid, similar to the Bingham–plastic model. If $m = 1$ the Herschel–Bulkley model reduces to the Bingham plastic model [51]. Figure 2.27 shows the relationship between viscosity and shear rate in a MR fluid [31].

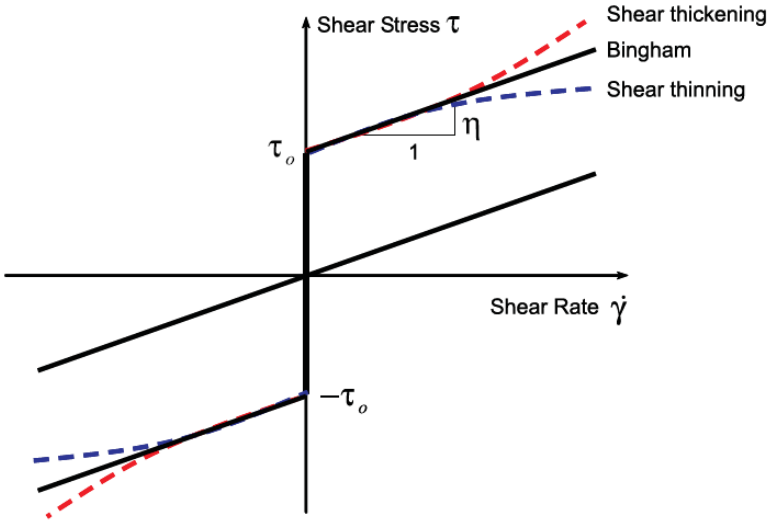

Figure 2.26 – Visco-plastic models used to describe MR fluids.

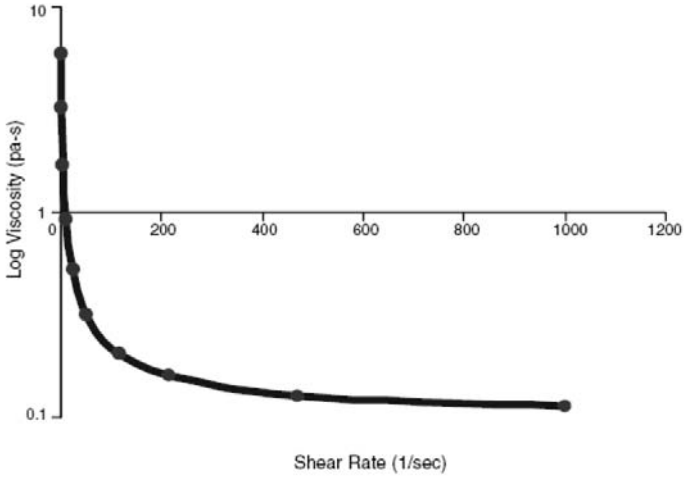

Figure 2.27 – Viscosity vs. shear rate in MR fluid.

Wang and Gordaninejad [52], assuming one-dimensional steady laminar flow, used the Herschel-Bulkley model to describe MR fluid flow through tubes and parallel plates. Lee and Wereley [53] developed the previous model for an magneto-rheological flow mode damper. Yang [54] developed axisymmetric models of a large-scale MR fluid damper using both the Herschel - Bulkley model and the Bingham model in a axisymmetric models. Every author's work was focused on to better describe the relationship between dampers dimensions, fluid motion conditions and final damping force.

One model that is numerically tractable and has been used extensively for modelling hysteretic systems is the Bouc-Wen model. It is versatile and it can exhibit a wide variety of hysteretic behaviour, since it possesses the force–displacement and force–velocity behaviour, which resembles that of the real life MR dampers [54, 55].
The Bouc–Wen model is a set of differential equations describing the hysteretic characteristic of the damper force/velocity response (Eq. 2.20-2.21).

$$F = c\dot{x} + kx + \alpha z - f_0 \qquad \text{(Eq. 2.20)}$$

$$\dot{z} = \delta\dot{x} - \beta\dot{x}|z|^n - \gamma z|\dot{x}||z|^{n-1} \qquad \text{(Eq. 2.21)}$$

where F is the damping force, c is the viscous coefficient, k is the stiffness, x are the damper displacement, α is a scaling factor, z is the hysteretic shape evolutionary variable and f_0 is the initial damper displacement contributing to the force offset.
By adjusting the characteristic parameters of the model γ, β, and δ, the linearity in the unloading and the smoothness of the transition from the pre-yield to the post-yield region can be controlled. One of the major problems in the Bouc–Wen model is the accurate determination of its characteristic parameter. In addition, the force f_0 due to the accumulator can be directly incorporated into this model as an initial deflection x_0 of the linear spring k_0 (Figure 2.28).

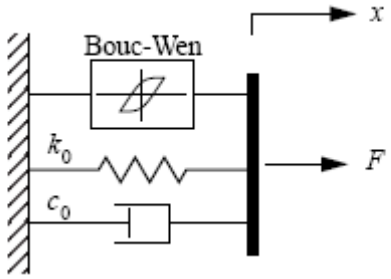

Figure 2.28 – Bouc-Wen model

Kwok et al. [55] proposed a non-symmetrical Bouc–Wen model considering the effect of non-symmetrical hysteresis, which has not been taken into account in the original Bouc–Wen model and adjusting the effect of the velocity as (Eq. 2.22):

$$\dot{z} = \left(\delta - \left(\beta + \gamma \operatorname{sgn}\left(z\dot{x}\right)\right)|z|^{n}\right)\dot{x} \qquad \text{(Eq. 2.22)}$$

The Bouc-Wen model predicts the force-displacement behaviour of the damper well. However, similar to the Bingham model, the nonlinear force-velocity response of the model does not roll-off in the region, where the acceleration and velocity have opposite signs and the magnitude of the velocities are small.
To better predict the damper response in this region, Spencer et al. [37] proposed a mechanical model (Figure 2.29) in which the total force and the velocity can be written as:

$$F = c_1\dot{y} + k_1\left(x - x_0\right) \qquad \text{(Eq. 2.23)}$$

$$\dot{z} = -\gamma|\dot{x} - \dot{y}|\,z|z|^{n-1} - \beta\left(\dot{x} - \dot{y}\right)|z|^{n} + A\left(\dot{x} - \dot{y}\right) \qquad \text{(Eq. 2.24)}$$

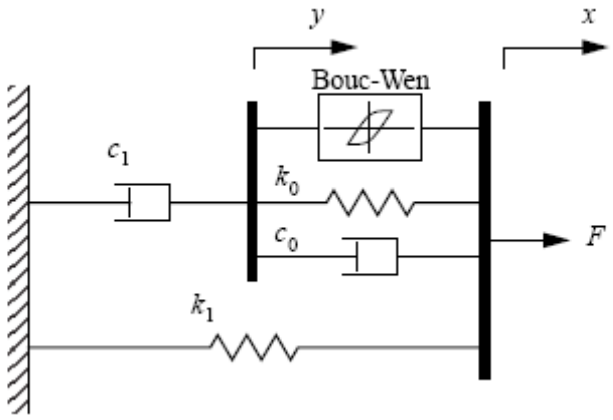

Figure 2.29 – Mechanical model proposed by Spencer

The accumulator stiffness is represented by k_1 and the viscous damping at larger velocities is represented by c_0. A dashpot c_1 is included in the model in order to produce the roll-off that was observed at low velocities, k_0 is present to control the

stiffness at large velocities, and x_0 is the initial displacement of spring k_1 associated with the nominal damper force due to the accumulator.
In order to accurately describe the quasi-steady behavior of MR dampers, Kamath et al. [56] developed an axisymmetric model of fluid dampers.
Yang et al. [28] proposed a phenomenological model which considers inertial and shear thinning effects in the MR fluid behaviour, modifying the damping constant in the Bouc–Wen model by a mono-decreasing function with respect to absolute velocity.
A non-linear new model, based on the Bouc–Wen model proposed by Dominguez et al. [57], allowed to simulate the hysteresis behaviour of dampers, considering the frequency, amplitude and current excitation as input dependent variables. This methodology suggested the relations such that the characteristic parameters can be directly determined using key information of the experimental data, eliminating errors and high computational costs inherent in optimization procedure.
Sapinski [58] linearized the MR Bouc–Wen behaviour, focusing on equivalent viscous damping and complex modulus models: the damper was approximate as an ideal dashpot at every operating conditions, allowing to predict damping and stiffness with accuracy also neglecting hysteresis effects.
Chang and Roshke [59], starting from Bouc–Wen theories, developed a neural network model to emulate the dynamic behavior of MR dampers. On these basis, the trained direct identification neural network model proposed by Wang et Liao [60] predicted the damping force of the MR fluid damper on line, employing the dynamic responses across the MR fluid damper and the command voltage.
Zhou et al. [61] suggested a different definition of MR hysteresis based on a modified Dahl model, where hysteresis model instead of the Bouc-Wen model was adopted to simulate Coulomb force to avoid too many parameters.

2.3.2 MR fluid working mode

The properties of magneto–rheological fluids allow their use in devices active-controlled by an electric input current [62]. In Figure 2.30 the characteristics of damping force change, as a function of velocity and current in electromagnetic coil, are shown. The operational envelope shows the area in which the damping force can be generated as a function of velocity, acceleration, pressure by changing the coil current. Therefore, the damping force acts only in a direction opposite to the direction of the velocity and only absorbs mechanical energy.

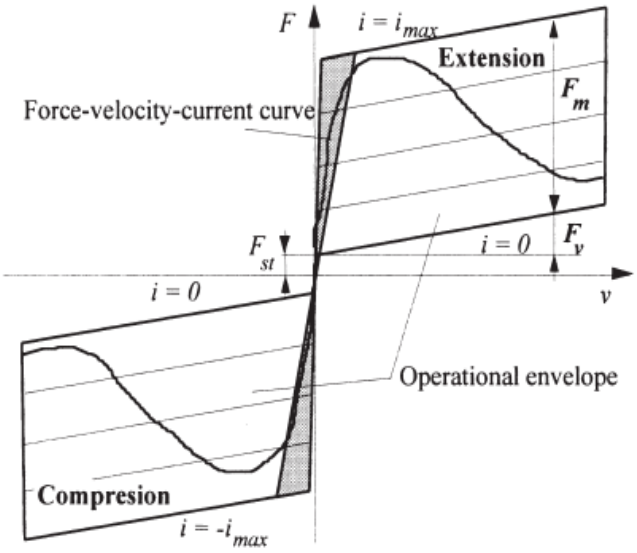

Figure 2.30 – Force-velocity-current curves for MR fluids.

Considering the different ways of use of magneto – rheological fluid, MR fluids can be operated in three working modes, depending on the type of deformation employed: *valve mode, shear mode* and *squeeze mode* [27 – 30]. Figure 2.31 schematizes the different fluid working modes.

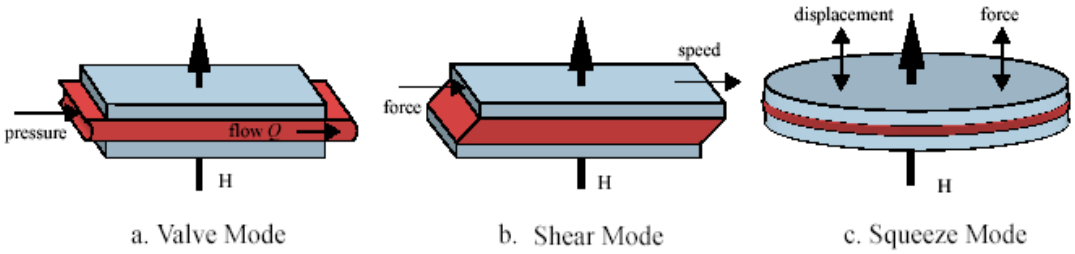

Figure 2.31 – MR fluid working modes: a) valve mode; b) shear mode; c) squeeze mode.

In the case of the *valve mode* (case a), known also as *Flow mode*, the MR fluid is located between metallic surfaces that move to each other. The magnetic flux lines are perpendicularly to the direction of motion of these surfaces.
Examples of flow mode devices include servo – valves, shock absorbers, dampers and actuators.
On the basis of the parallel – plate model [28, 63], the total damper force F can be decomposed into a controllable force F_τ, due to the controllable yield stress $\tau_{0,}$ and an uncontrollable force F_{uc}. The uncontrollable force includes two other parts, a

viscous force F_η and a constant friction force F_f . Therefore, the total damper force may be expressed as:

$$F = F_\tau + F_\eta + F_f \qquad \text{(Eq. 2.25)}$$

where controllable and viscous forces can be write respectively as:

$$F_\eta = \left(1 + \frac{wh}{2A_p}\right)\frac{12\eta L A_p}{wh^3} A_p v_0 \qquad \text{(Eq. 2.26)}$$

$$F_\tau = \frac{\tau_0 L A_p}{h}\operatorname{sgn}\left(v_0\right) \qquad \text{(Eq. 2.27)}$$

Where L is the effective axial pole length, A_p is the cross sectional area of the piston, w is the width of the rectangular plate, h is the width of the gap between two parallel plates, η is the Newtonian viscosity and τ_0 is the fluid yield stress and C parameter is bounded to the interval (2.07 ÷ 3.07).
In the *shear mode* (case b), the MR fluid is forced to flow directly between static plates. The fluid flow is still normal to the magnetic field direction.
Applications can be found in biomedical prosthesis, compact clutches and brakes, chucking and clamping systems.
In a like manner as flow mode parallel – plate theory [36, 64], the force developed by a direct-shear mode device is:

$$F = F_\tau + F_\eta = \frac{\eta S A}{g} + \tau_y A \qquad \text{(Eq. 2.28)}$$

where S is the relative pole velocity and A = Lw is the shear (pole) area.

Eq. 2.26 and Eq. 2.27 are useful in the design of controllable fluid devices, but they often do not provide the best insight into the significance of the various parameters.

In the *squeeze mode* (case c), the MR fluid is squeezed by a normal pressure in the direction of the magnetic field under dynamic or static (compression or tension) loadings. MR fluid is sandwiched between the two paramagnetic moving surfaces.

The displacements engaged in squeeze mode are relatively very small (few millimetres) but require large forces.
The geometrical arrangement designated squeeze mode can produce compressive and tensile stresses, which can be greater.

Examples of valve mode systems are pressure driver flow devices, servo valves, automotive dampers, actuators and shock dampers.
The total force acting on the MR mount can be expressed as follows [65 – 66]:

$$F_t(t) = F_S(t) + F_V(t) + F_{er}(t) \quad \text{(Eq. 2.29)}$$

Where:

$$F_V(t) = c_f(t)\dot{h}(t) = \frac{3}{2}\frac{\pi\eta R^4}{\left(h_0 + h(t)\right)^3}\dot{h}(t) \quad \text{(Eq. 2.30)}$$

$$F_{er}(t) = \frac{4}{3}\frac{\pi R^3}{h_0 + h(t)}\tau_y(E)\,\mathrm{sgn}\left(\dot{h}(t)\right) \quad \text{(Eq. 2.31)}$$

In the above [67], $F_v(t)$ and $F_{er}(t)$ are respectively viscous damping force and controllable damping force. η is the viscosity of the fluid, $\tau_y(E)$ is the field-dependent yield stress of the fluid, $C_f(t)$ is the damping coefficient in the absence of an electric field, $h(t)$ is the exciting displacement, h_0 is the initial gap between lower and upper poles, and R is the radius of the circular plates.

2.3.3 Architectural Configurations Of Dampers

In technical and laboratory context, the most common configuration used with magneto-rheological fluids is based on a modification of the typical hydraulic actuator structure (Figure 2.32) [68]. An outer cylinder is filled up with MR fluid and an inner piston moves inside. Between the two main components, a constant annular gap is ensured, in which MR fluid is free to flow during the piston displacements in the device chamber.

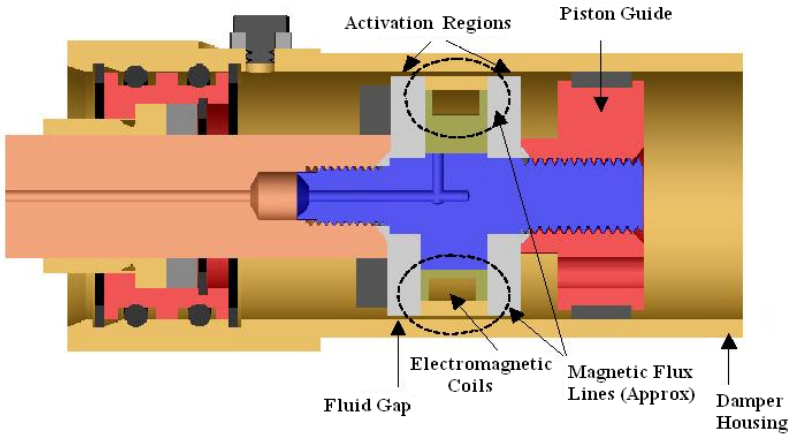

Figure 2.32 – MR damper: main components.

The piston, which is one of the two paramagnetic elements, has a central groove along its lateral surface, where one or more electric coil of copper are housed. The cylinder corresponds to the second pole of the field. When current is supplied to the coil, some areas of the fluid in the gap piston-cylinder are "activated" (i.e. material is polarized) and the formation of particle chains starts.
Increasing the intensity of the magnetic field, the number and strength of the chains of particles between the two poles of the circuit increase. The flow resistance can be adjusted, starting from the total absence of magnetic field to the state of magnetic saturation of the fluid, where a complete alignment of ferromagnetic particles takes place and a further increase in current does not produce, at constant speed, greater damping force.
In this solution, an external oil reservoir must to be used in order to collect the fluid volume moved by the entrance of the piston rod in the cylinder chamber.
In technical applications, essentially three architectural configurations can be distinguished, in order to optimize the performances of the fluid and to solve the constructive problem of flow of material by inner piston rod movement: *monotube*, *twin tube* and *double ended* configuration [68 - 69].

Monotube configuration is the most common and widely used in damper design. It exhibits simplicity and compactness of design with the ability to be mounted in any orientation. It has an oil reservoir in order to accommodate the change of MR volume that occurs when the piston rod enters the housing. In the solution with inner accumulator piston (Figure 2.33), the last provides a barrier between the MR fluid and a compressed non-oxidizing gas (usually nitrogen), that is used to accommodate the volume changes. Often external oil reservoir is considered.

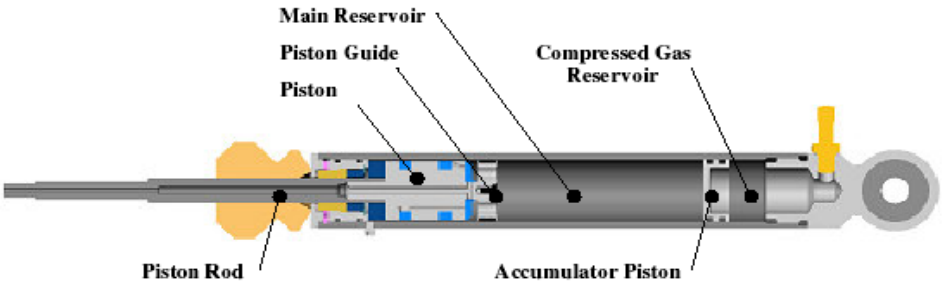

Figure 2.33 – Monotube configuration damper

Twin tube, shown in Figure 2.34, configuration uses inner and outer cartridges to negotiate the changing volume of MR fluid, separated by a foot valve. The inner housing guides the piston/piston rod assembly just as the housing of a monotube damper does, filled with MR fluid. To accommodate changes in volumes, due to piston rod movement, an outer housing, partially filled with MR fluid, is present. As the piston rod enters the inner housing, the extra volume of MR fluid displaced by the piston rod is forced from the inner housing to the outer housing via the foot valve. When the piston rod retracts, MR fluid flows back into the inner housing, therefore preventing the creation of vacuum in the inner housing and cavitation of the damper. Drawbacks of this design includes size and orientation. In effect, this damper must be mounted with the foot valve at the bottom to ensure no cavitation.

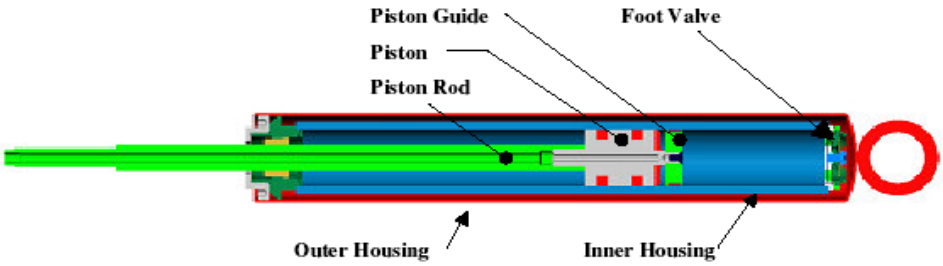

Figure 2.34 – *Twin tube* configuration damper.

With this type of MR damper, keeping the iron particles (which are an integral part of MR fluid) in suspension is a major concern, since these iron particles can settle into the valve area and prevent the damper from operating properly. All MR dampers are affected by MR fluid settling, but this problem is particularly prevalent in the twin tube variety.

Finally, in the *double ended* dampers (Figure 2.35), the problem of fluid storage is radically solved by making a piston rod that protrudes through both ends of the damper. It ensures a constant volume of the rod inside the cylinder, maintaining a continuous centering of the piston without requiring extra devices. Since there is no change in volume as the piston rod moves, the double-ended damper does not require an external accumulator.

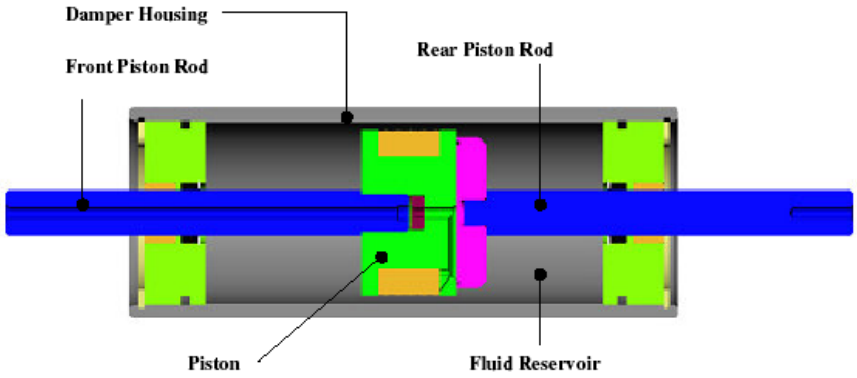

Figure 2.35 – Double ended configuration damper.

The twintube and double-ended damper provide a significant advantage over the monotube design. The pressurized charge in the accumulator of the monotube design adds a spring force to the damping rod, so not only does the damper have force vs. velocity characteristics, it also has a spring rate, that the second ones do not demonstrate. On the contrary, they don't have a great facility in positioning.

The development of MR damper has received a respectable improvement recently, thanks to new attention in civil, biomedical and mechanical applications. Hong et al. [46] used a non-dimensional representation for the development of a design methodology for an MR damper in mixed-mode operation. Four dimensionless parameters were defined: the Bingham number (the ratio of dynamic yield stress to viscous stress), the damping force, the dynamic range, and the geometric ratio (hydraulic amplification). These parameters allowed the physical design of the device. In his work (a sky-hook controller adopted to study vibration isolation using an MR-based mount), two different Bingham numbers are proposed, in terms of piston velocity or average valve-gap duct velocity, showing that the Bingham number and hydraulic amplification parameter determine MR damper characteristics.
In order to testing the applicability of MR technology in civil engineering applications [70], a device whose nominal maximum damping force was 20 tons and the dynamic range was equal to 10, has been created. It was based on double-ended architecture (Figure 2.36). The electromagnetic coil, divided in three parts,

determined 4 activates areas and consisted of 1.5 km of copper wire. The device was about 1 m long, had a mass of 250 kg and used about 5 litres of MR fluid.

Figure 2.36 – MR damper 20 ton for civil applications.

Using similar device, Sunakoda et al., [71] connected the solenoid directly to the bypass valve, in their experimental study of the frequency response of magneto-rheological materials. It was connected at end of the cylinder and regulator of fluid flow, in order to recreate, in the orifice, the uniform magnetic field directed perpendicular to the flow. This bypass configuration simplified the dynamics of the test, providing the advantage of a more flexible design in the electromagnet dimensions.

Within the several possible piston-valve configurations [42], the simplest one is the open-piston MR valve in Figure 2.37a. It uses the tube of the actuator as part of the magnetic circuit, with the coil wound directly on the piston, which is centred within the tube by a guide ring. Since the tube is part of the magnetic circuit, multi coil piston (two coils shown in Figure 2.37a) may be necessary to reduce the tube thickness and the overall mass of the actuator.
The open-piston geometry maximizes the working diameter and hence the damping forces of the MR actuator of given overall diameter.
A mono-tube MR damper with an enclosed piston can be found (Figure 2.37b). There is no annular gap and the MR material is forced to flow through a series of circular openings in the head of the rod. Although the design and construction of the piston is much more complex than the previous one, because an inner wire coil needs, the complexity may be offset by the advantages of precise control of the valve gap, minimum tube thickness and ease of qualifying the piston valve prior to assembly. Since the working diameter of the active area of the piston is reduced, performances, in terms of damping force, are smaller, when compared with the open piston design of equal length.

There is a third configuration, such as stationary coil with standard piston (Figure 2.37c), which incorporates the twin - tube solution: the coil is fixed and realized in a central position in the annular space created by the two concentric cylinders. Between them, the gap is also guaranteed for the flow and the control of the MR fluid. In the inner cylinder, therefore, a standard piston moves with no special features, however characterized by a minor stroke.

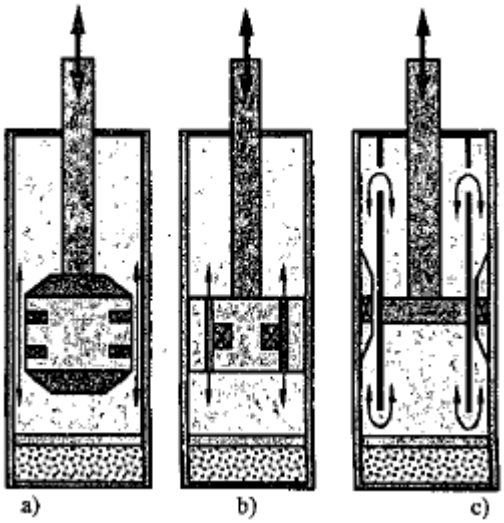

Figure 2.37 – Possible piston-valve configurations: a) open-piston MR valve; b) enclosed; c) stationary coil with standard piston.

Some prototypes [72] were designed to have the electrical coil fully isolated and outside around the device (Figure 2.38). This approach had the advantage of requiring significantly simplified design, especially regarding to the piston, but it generates smaller performances and it is difficult to commercial use.

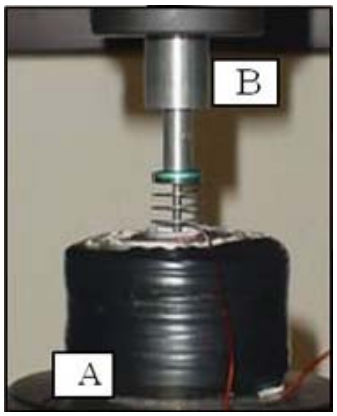

Figure 2.38 – External electric coil configuration.

The type of construction of the electric coil can be significantly varied [73]: single or multi coil can be chosen (Figure 2.39a), according to forces or special performances required (Figure 2.39b and c).

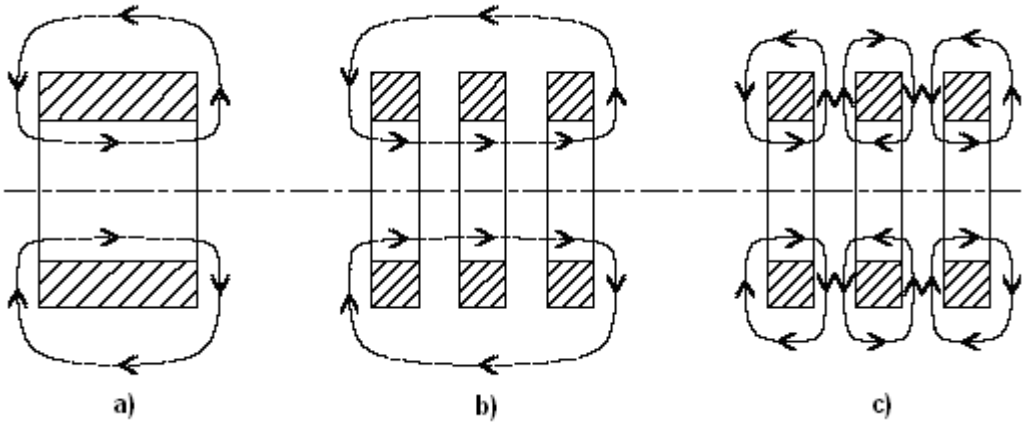

Figure 2.39 – Coil configurations: a) single; b) multi coil mono flux; c) multi coil, multi flux.

The latter two configurations have similar characteristics, except for the polarity of the magnetic field. In configuration b), the magnetic flux lines have all one only direction from the centre of the solenoid. In configuration c), there is a trade-off between the different coils, which also affects the circuit length. The main advantage of this solution is a decrease of the overall inductance of the circuit that allows, compared to other, less response time of the same device.

2.4 CONCLUSIONS

The present Chapter presents first a description of reverse load phenomenon and its effect on blanking presses. A summary of main scientific and commercial solutions to reduce its influence is reported, in order to underline advantages and disdvantages for the introduction of the originality of present work.
A description of magneto-rheological fluids and their proprieties is presented, focusing on analytical and mechanical models mainly used to describe their behaviour in application.
MR Fluid working modes are discussed and the principal damper architectural configuration are analyzed, in order to prepare to future constructive design choices.

CHAPTER 3

FINITE ELEMENT MODELLING OF MR DAMPER

3.1 INTRODUCTION

Finite element analysis are the most widely instruments used to predict how a part or a system works and responds to the effect of a set of load and boundary conditions.
Critical working conditions have to be also valued in order to study and design new mechanical devices.
In the present chapter, a magneto-static simulation was performed for the analysis and the representation of the levels of magnetic saturation in the MR fluid.
Once stated, a multi-physics model was developed in order to study the influence of different physical fields involved and to predict general performances of the final damper device.

3.2 THE APPROACH

The effects of multiple physical phenomena influencing a process were usually investigated by separately analyzing each phenomenon individually. Thermal, electric, or mechanical fields were studied without regard to any physics interaction, usually using several simplifications. Advances in computer hardware and software, nowadays make it practical for analyses to account for the effects of more interacting physical phenomena that work at the same time [74].
The essence of multi-physics analysis is coupled-field analysis, which allows to determine the combined effects of multiple physical phenomena (fields) on a design.
Two numerical techniques are available for combining physics fields: *direct-coupled* and *sequential-coupled fields*.[75]
Direct-coupled analysis assembles all the physics fields as finite-element equations in one matrix and solves the matrix as a whole.
In sequential coupling (often referred to as load-vector or staggered coupling), the equation for one field is partially solved and the results passed as loads (the results of one physics field interacting with another) to the next physics field to drive its partial solution. The analysis software then passes this iteration to the next physics field, and so on, down to the last field. Then the sequential iteration process begins all over and continues until a final solution is achieved.
In order to develop an innovative solution for the industrial problem described in previous chapter, a predictive model that studies magneto-rheological behaviour has to meet the two main requirements:

(i) to predict the changes in MR fluid viscosity determined by the applied magnetic field, and
(ii) to couple the phenomena occurring in the fluid and metallic regions, both mechanical and thermal, in order to account for their mutual interactions.

With these goals the task of the numerical techniques is to provide coupled simulations of the interactions between the MR fluid, the magnetic field that acts as fluid activator and the thermo-mechanical behaviour of the damper structure.
The numerical simulations were performed using the commercial finite element code ANSYS Mechanical and ANSYS CFX to solve bidirectional fluid-solid interaction.

3.3 DEVELOPMENT OF MULTI-PHYSICS NUMERICAL MODEL

3.3.1 Geometrical model settings

The models of device useful for the numerical analysis were introduced starting from a typical configuration of industrial dampers, as seen in section 2.3.3, where an inner

metallic piston is housed inside a metallic cylinder (Figure 5.1). Both diameters were organized in order to ensure an annular gap between the outer piston surface and the internal cylinder surface.
At piston centre, is localized one or more volume, corresponding to electrical coils, where an electrical current flows. In the internal chamber and in the gap is positioned a fluid volume, where viscosity and magnetic performances of magneto-rheological fluid are defined.
Coil volumes were modeled as rigid body, while other metallic components were modeled by elastic properties. Fluid volume was defined according to Bingham model laws.
Because of the device is completely axisymmetric, the studies were reduced to the analysis of 15° slides, as presented in the following sections, implementing in the software relative boundary conditions [76].

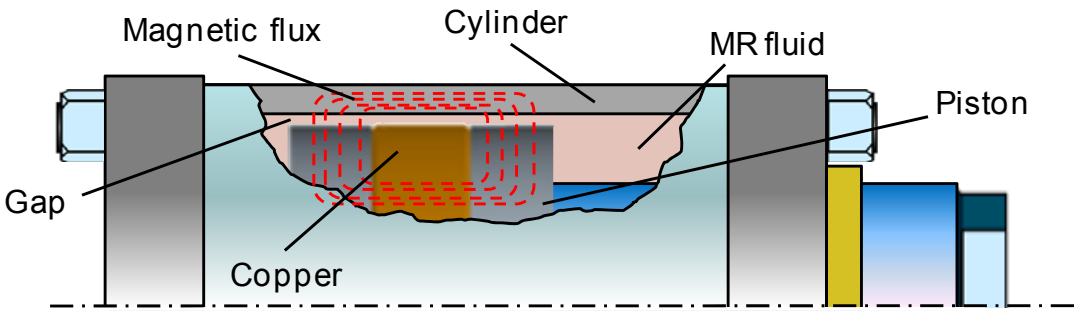

Figure 3.1 – MR fluid dampers model configuration.

3.3.2 Magneto-static numerical model

The magnetic induction of the magnetic field in the several component and, first of all in the fluid volume, is a critical parameter in controlling the performances of a magneto-rheological devices and, of course, its final performances.
A magnetic simulation was performed in order to determine the viscosity of the magneto-rheological fluid for different magnetic fields. It was solved by Finite Element Method (FEM).
The magnetic induction vs. magnetic field strength curves (B-H curves) of the fluid have been implemented in the model to define the properties of MR fluids interested by the magnetic flux. Figure 3.2 presents B-H curve of MRF 132 DG fluid implemented [77], while Figure 3.3 presents typical magnetic curves of low carbon steel [78]. Maximum magnetic induction value in the fluid has been set equal to 750 kA/m, while in the metallic components it has been set equal to 780 A/m. The magnetic analysis assumed that all surfaces of the model are flux-parallel (i.e. no

dispersion of the flux in the air) and avoided ill-conditioned problems related to the convergence at the boundary by single node constrains.
An optimization of architecture's design device was also possible. Details of the model can be found in [80].
Starting from the configuration introduced in previous section, the model parts used for the analysis are resumed in Figure 3.4. Diameters of models have been designed in order to ensure an annular gap of 1 mm wide. Coil sections were design in order to house the desired number of coils useful to the generation of the magnetic field, that allowed the viscosity change in the MR fluid.

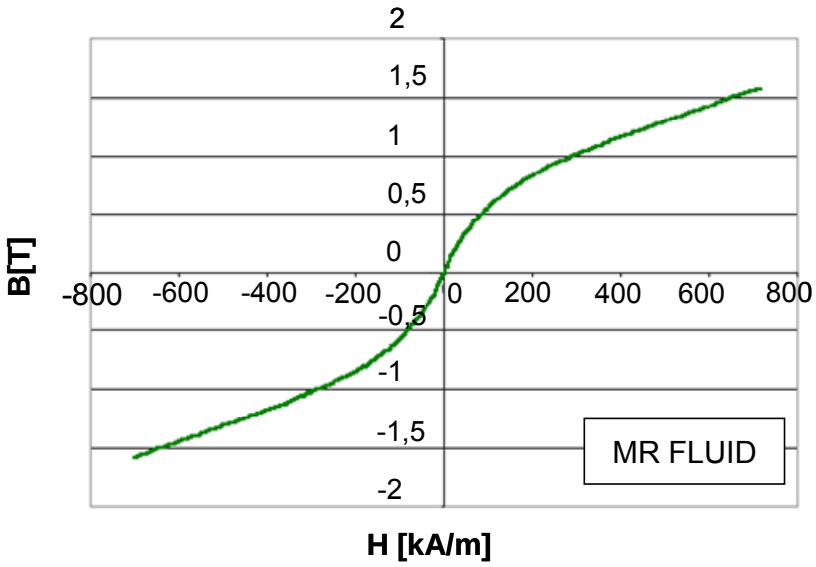

Figure 3.2 – Induction vs. magnetic field curves of MRF132DG magneto-rheological fluid.

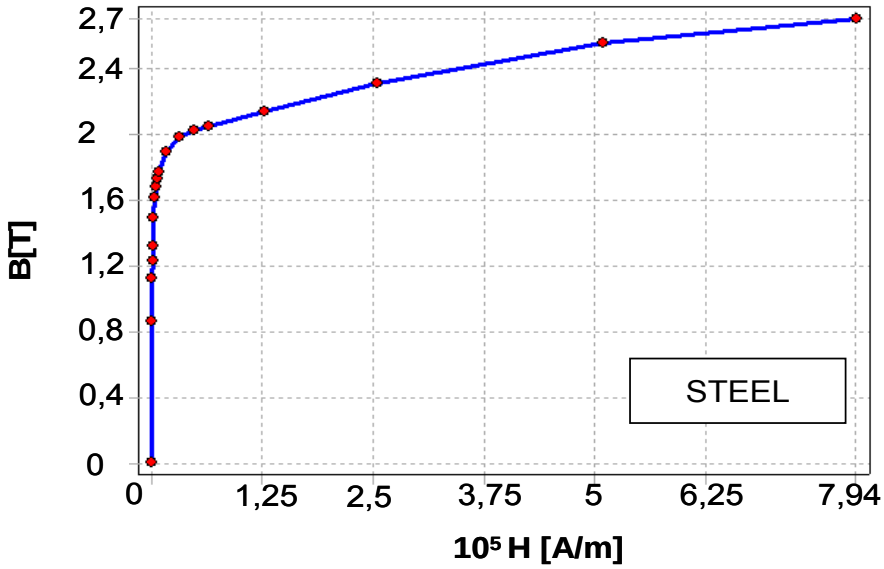

Figure 3.3 – Induction vs. magnetic field curves of AISI 1040 steel.

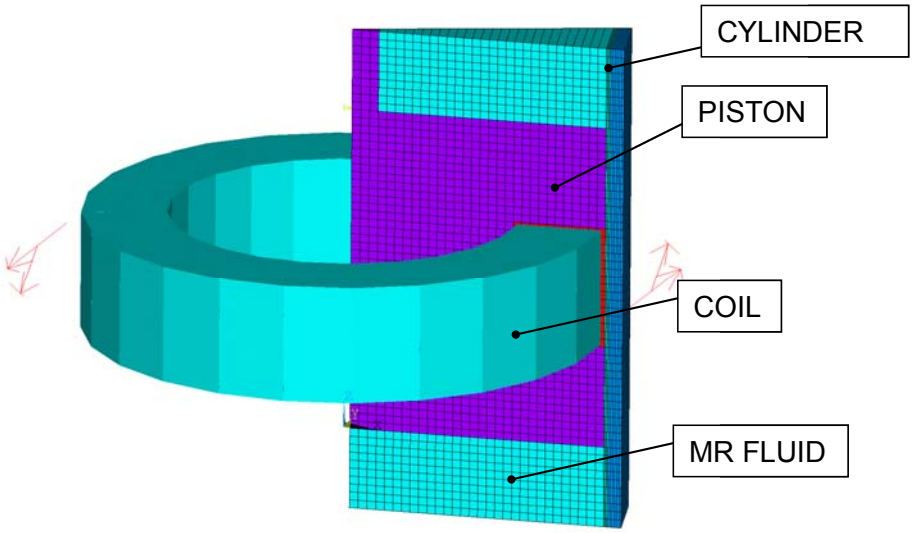

Figure 3.4 – Part models used in magneto-static analysis.

Magnetic analysis was fundamental for:

- Detection of magnetic induction in the models, in order to evaluate possible conditions of magnetic saturation (i.e. inability to further increase the magnetic flow and the possibility of permanent magnetization of elements);
- Geometrical end positional evaluations in the design of the models and of the device;
- Revelation of the mutual value of magnetic induction in each node of the model, in order to generate the input magnetic distribution for the coupled multi-physics analysis.

3.3.3 Multi-physics numerical model

Always in the models defined in section 3.2.2, two different regions were identified (Figure 3.5):

- *structural domain*, consisting on inner piston, coils and cylinder parts;
- *fluid domain*, consisting on MR fluid volume in the chamber and in the gap.

The mutual thermo-mechanical interactions between the MR fluid and the metallic structure were solved separately as different physics: the first region, representing the MR fluid domain, was solved using Finite Volume Method (FVM) while the second region, representing the structural domain of the damper, was solved by Finite Elements Method (FEM) calculations [75].

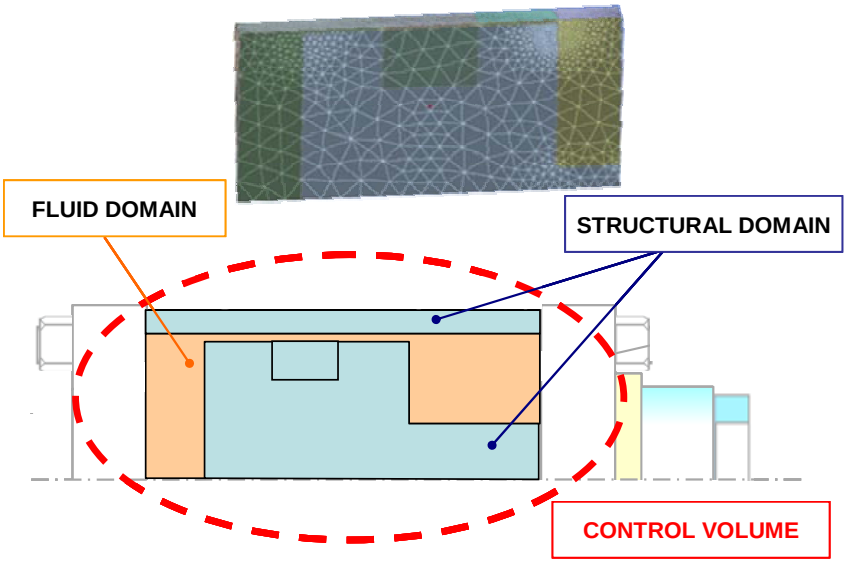

Figure 3.5 – Fluid domain and structural domain in the control volume for the multi-physics analysis.

The magnetic induction values, previously defined by the magneto-static analysis, were introduced in the coupled analysis, in order to define the viscosity configuration in the fluid volume.
The interface between the domains transmitted the loads generated by the MR fluid, in terms of temperature, deformations and stresses, to the metal and passes the deformed shape and temperature of the metal structure back to the MR fluid. In fluid–structure interaction, fluid flow exerted pressure on a solid structure, which caused it to deform such that it perturbed the initial flow. Thermal–mechanical coupling was omnipresent, and structures changed their shapes and material properties as a result of a temperature increase or decrease.
A sequential coupling analysis was set: the software passed results between the different domains that represented each of the physics fields involved. This procedure was repeated in the stagger loop within each time step (Figure 3.6) until convergence of the load transfer between fields. After that, the simulations then continued to the next time step, until the convergence of the entire analysis.
In this way, the effects of different fields starring were studied and, above all, the mutual effects of interactions when more than one fields were involved.
The proposed model allowed a reliable prediction of the fluid-thermal-structure interactions, taking into account the different viscosity conditions due to the application of the magnetic fields and evaluating the contribution of the complex thermal and mechanical events at the interface.

The main structural parameters that were implemented were:

- Fluid rheology;
- Magnetic and thermal parameters;

At the interface, following definitions had been implemented:

- Thermo-physical properties;
- Elastic-plastic properties;
- Magnetic-fluid properties;
- Thermal-magnetic properties.

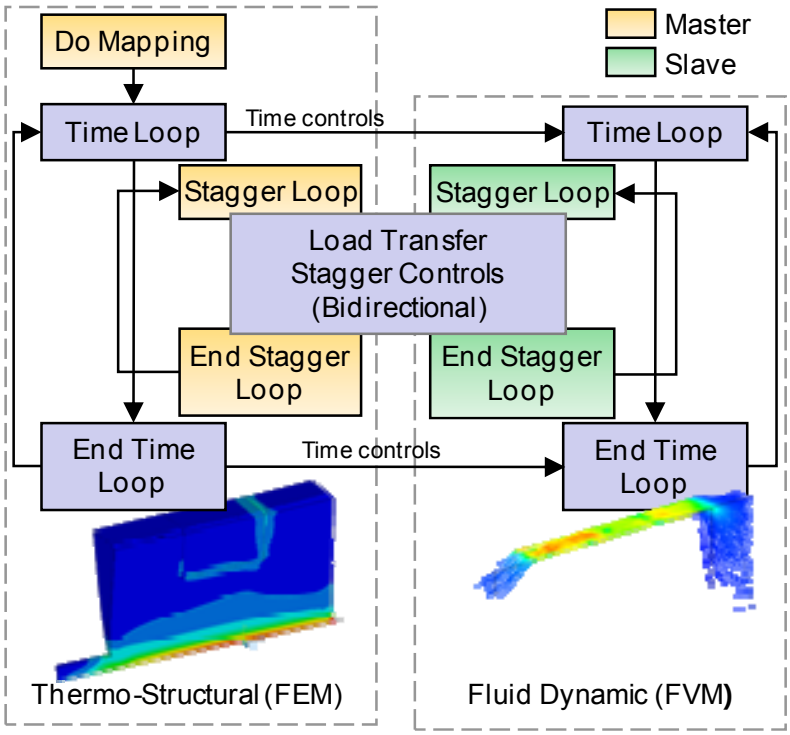

Figure 3.6 – The multi-physics model philosophy, adapted from [79].

The models used were the same of magneto-static simulation, because it was necessary the correspondence of the mesh in the initial step. Mesh definitions were set as conservative interface flux mesh motion option [75], in order to allow that motion of nodes in all domains adjacent to the interface influenced, and were influenced by, the motion of the nodes on the interface.

The material of the structural domain was set as AISI 1040 steel, while coil region was defined by generic copper material and current density. Simulation time was set equal to 20 ms, according to the industrial conditions (see Section 2.2).

The simulation type was set as transient.

In the fluid domain, a law (Eq. 3.1) that defined the viscosity variation with the magnetic induction distribution, function of damper length (L, r) and shear strain

rate, has been written, according to Newton law and Bingham rheological model [81].

$$\mu = \mu\left(\eta, \tau_0, \dot{\gamma}, \tau(\boldsymbol{H}), \boldsymbol{L}, \boldsymbol{x}\right) \qquad \text{(Eq. 3.1)}$$

where η is the Dynamic viscosity, τ_0 the carrier fluid shear stress, $\dot{\gamma}$ the shear rate, $\tau(H)$ the magnetic induction dependent shear stress.
Initial model temperature was set equal to room temperature, according to the industrial or laboratory conditions. In hypothesis of relative motion of MR fluids an piston and open flux, a different distribution of pressure have been fixed, assigning a boundary inlet condition in the entry (air pressure) and an opening type condition in the exit (air pressure equal until 10 MPa).

3.4 NUMERICAL RESULTS

3.4.1 Magneto-static analysis

FEM simulation was used to verify the risks of magnetic saturation in the device, which could limit the damping performances of the device. Numerical simulations were performed spacing the range of current available (i.e. range 1÷3 A). The results are presented in Figure 3.7, considering an input current of 3 A.

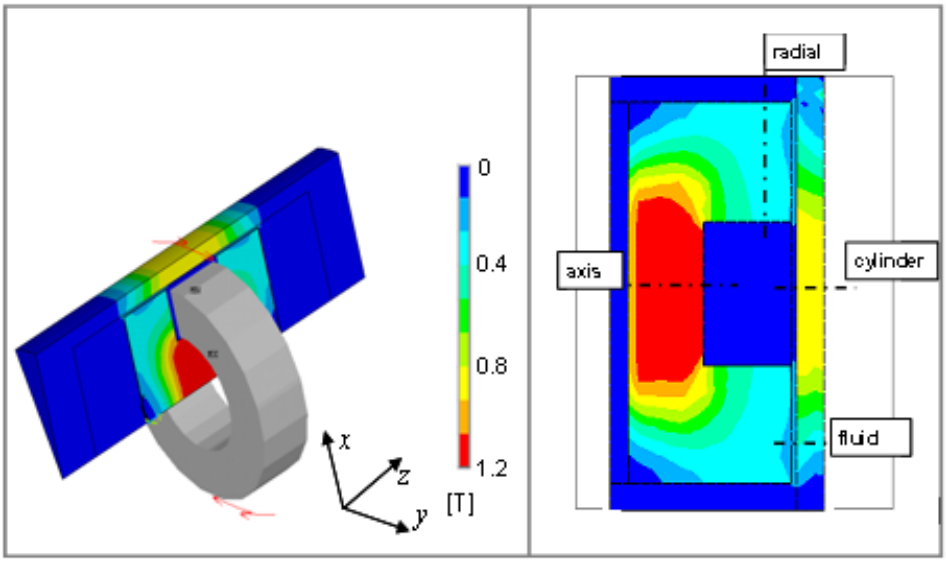

Figure 3.7 – Magnetic flux density distribution of simulated device.

Results in terms of local magnetic flux density and magnetic field intensity, highlighted that the maximum values of magnetic flux density are located in the

sections near the piston axis. This fact reduces the magnetic performances (i.e. damping performances) of the MR fluid.
Similar values for the peak of magnetic flux density were calculated by analytical formulations (see Table 3.1) [82].

Table 3.1 – Magnetic flux density values in MR device

	FLUX DENSITY B (T)			
RESULTS	Axis	Radial	Fluid	Cylinder
Theoretical	1.13	0.19	0.20	0.44
Simulation	1.10	0.25	0.31	0.41

The magneto-static analysis, showing the flux density or the magnetic field strength into the device, were used also for the optimization of the number and the distribution of coils in the device, in order to assure the homogeneousness and the right value of project of magnetic flux.
Even better numerical results were obtained using two coils in terms of uniformity of magnetic induction, as shown in the left part of Figure 3.8, the configuration with a single coil, shown in the right part of the same figure, was implemented. This solution was preferred for the lower risk of saturation of the magnetic fluid and the lower temperatures due to friction at interfaces.

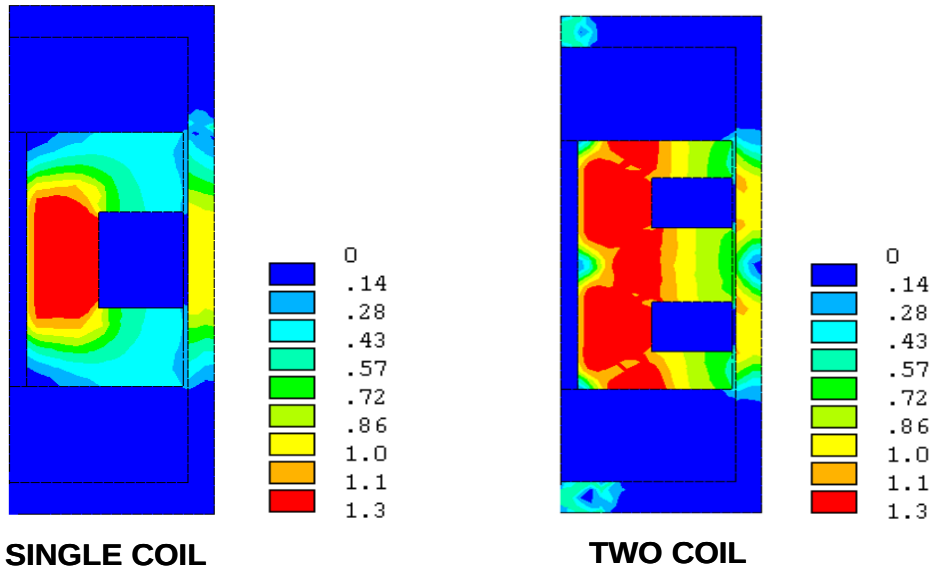

Figure 3.8 – Comparison between the magnetic flux density distribution of one coil solution and two coil solution device with input current of 3 A.

Magneto-static simulation allowed, in addiction, preparatory design considerations in the magnetic field distribution. The presence of an internal hole in the inner piston was considered, as shown in Figure 3.9.

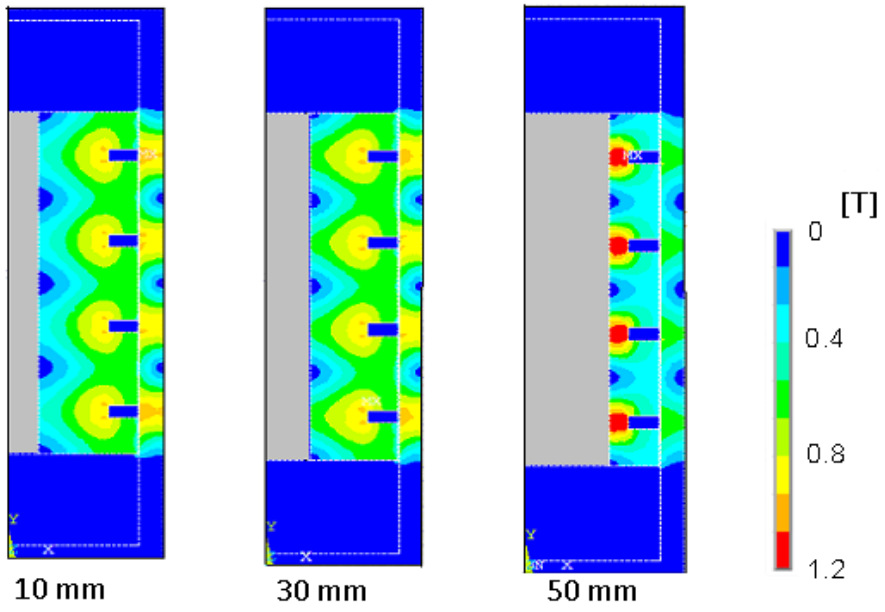

Figure 3.9 – Evaluation of an internal hole in the piston part: effects on the magnetic field distribution.

It was verified that induction distribution changed passing from an internal hole of 10 mm of diameter to greater values. Magnetic induction increased because magnetic flux section decreased, so flux was forced to pass in a constricted zone. Diameter of 50 mm was consider as design limit.
Influence of coils geometry housed was also valued: as shown in Figure 3.10, the effects of different height – width couple of the electric coil (at the same number of coils) were studied in order to optimize the design device.

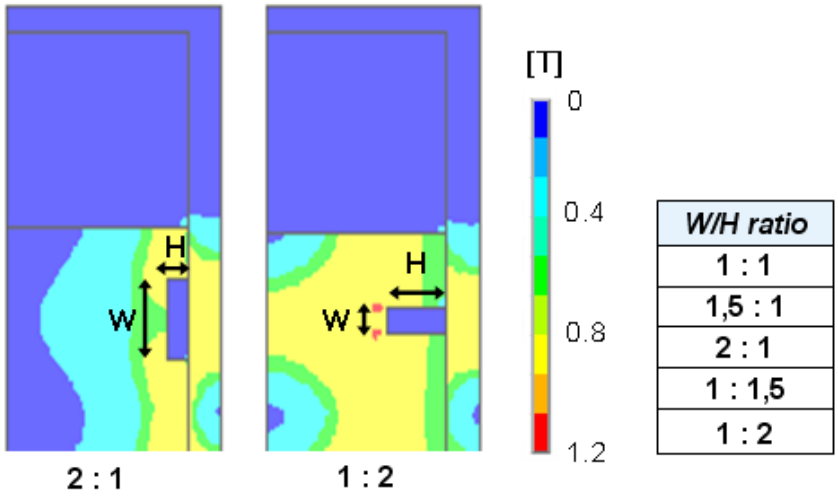

Figure 3.10 – Magnetic induction in the damper piston at different height-width coil couples (in the table on the right the valued ratio)

Better configuration, in term of distribution of magnetic flux, resulted where coil height was greater than width.
Magneto-static simulation gave in each nodes of the numerical model the magnetic induction value used in (Eq. 3.1 to define viscosity for coupled analysis. Figure 2.19 resumes an example of magnetic isoflux lines defined into the device gap.

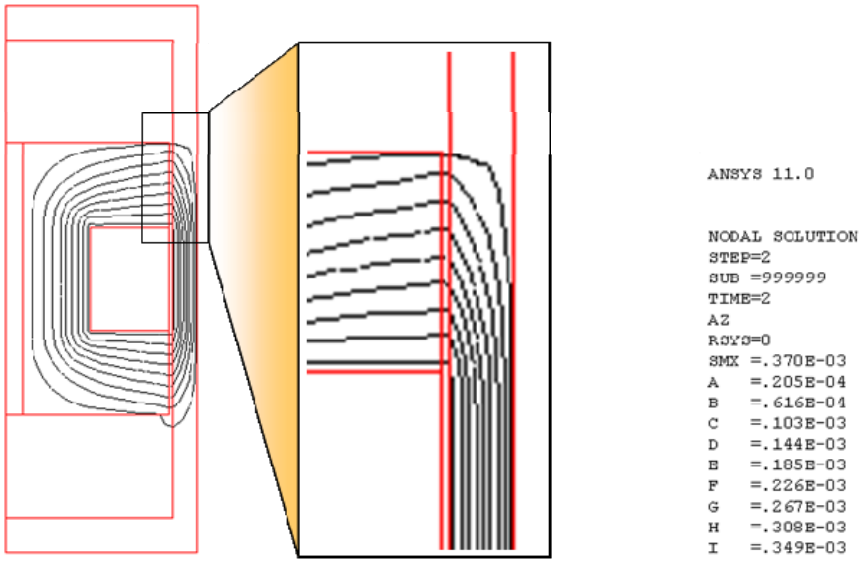

Figure 3.11 – Magnetic isoflux lines in the piston – cylinder gap.

3.4.2 Thermal-structural-fluid coupled analysis

The thermal and fluid dynamic behaviour of the damper device were analyzed in five impulsive sequential loads in the activation time of the device at different piston speed and exit pressures of the MR fluid (see Table 3.2).

Table 3.2 – Simulative coupled analysis plan.

	Velocity [mm/s]	Pressure [MPa]	Input current [A]
(a)	10	0÷10	0÷3
(b)	20	0÷10	0÷3
(c)	60	0÷10	0÷3
(d)	80	0÷10	0÷3
(e)	100	0÷10	0÷3
(f)	600	0÷10	0÷3
(g)	1000	0÷10	0÷3
(h)	2500	0÷10	0÷3

Axial and radial lines, as shown in Figure 3.12, were chosen as analysis lines, where evaluate the main thermal and dynamic parameters.

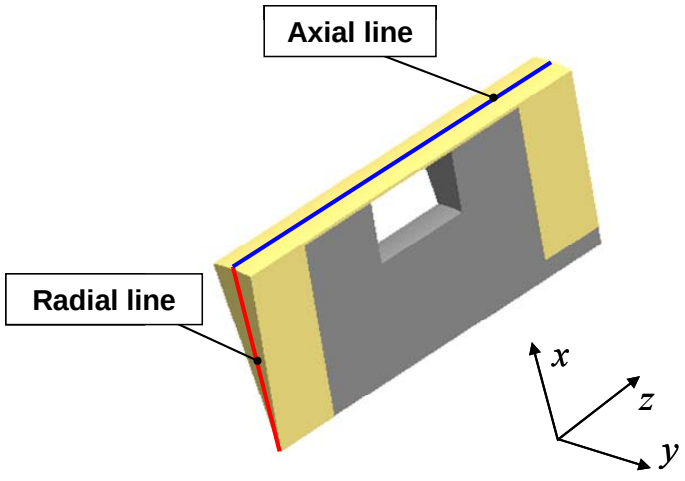

Figure 3.12 – Axial line and radial line in the numeric models.

Considering temperature increase, linked to the viscous works into the MR fluids, numerical simulation gave the temperature profile in the models (Figure 3.13). It

could be observed that maximum increase of temperature was localized in the gap exit, where the fluid flow had the main changes of direction, then the maximum work of viscous forces.

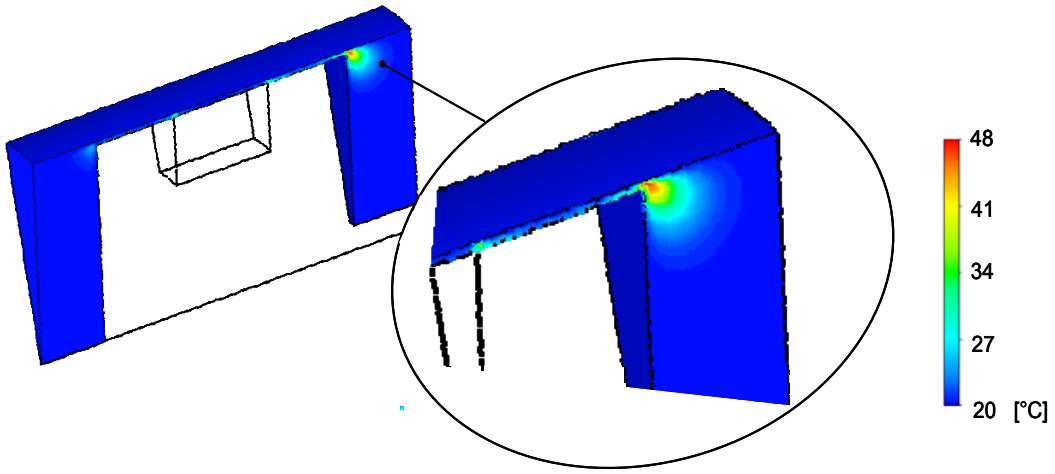

Figure 3.13 – Temperature profile in the models. It is underlined the thermal concentration in the gap.

The temperature variation along the radius (radial line) are presented in following Figure 3.14.

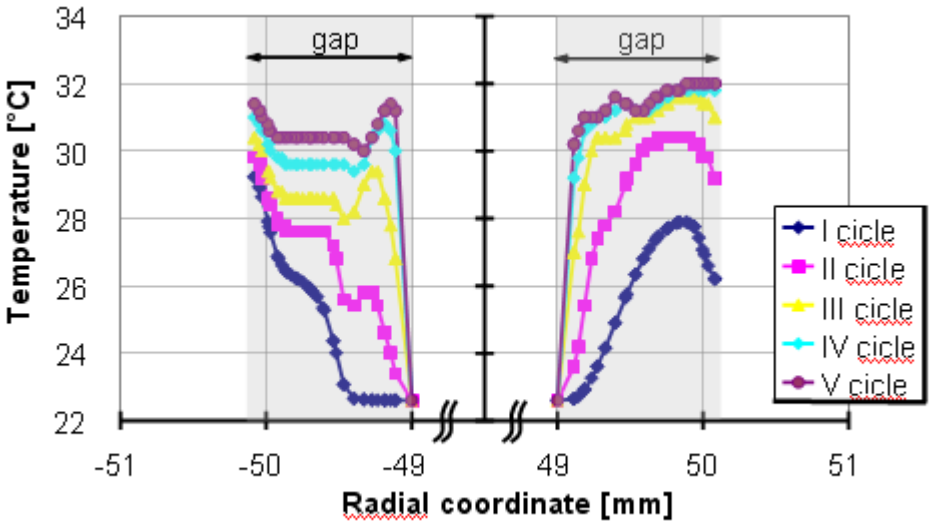

Figure 3.14 – Temperature values predicted along model radial line.

It can be observed that, on the one hand, expected temperature increased at maxima values at the end of the impulsive cycles, and theses values tended to maintain constant in the last impulse load, when thermal exchange reached the equilibrium

with structural domain. On the other hand, maxima values were with the maximum activation of the MR fluid, i.e. a current of 3 A in the electric coil. Figure 3.15 summarize the predicted maximum temperature values considering a piston speed of 20 mm/s. Temperature increase in last three impulse was less than 3° C at 10 MPa exit pressure. The results were validated by the experimental measurements monitored in the laboratory prototype, as shown in following Chapter 4.

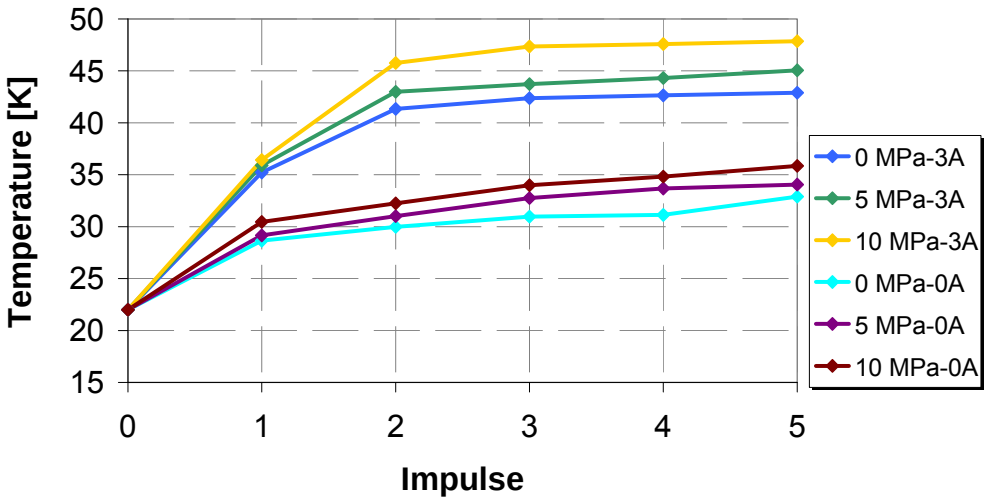

Figure 3.15 – Predicted maximum temperature values considering a piston speed of 20 mm/s.

In all the cases studied, it was verified that this temperature do not exceed the operating range of the MR fluid (see section 4.3.1), in order to prevent possible negative effect on the final working performances of the materials.
Any load condition have provided particular problems about the temperature working range of the material. Table 3.3 resumes the maxima temperature values in the last impulsive load predicted by simulations in the case of 10-20-60-100 mm/s.

Table 3.3 – Maxima temperature values predicted in the case of 10-20-60-100 mm/s.

	Velocity [mm/s]	Pressure [MPa]	Input current [A]	Max Temperature [°C]
(a)	10	0	3	36,92
	10	10	3	40,66
(b)	20	0	3	42,89
	20	10	3	47,85
(c)	60	0	3	43,77
	60	10	3	49,12
(e)	100	0	3	44,36
	100	10	3	51,29

Monitoring of fluid velocity during simulative piston movement was possible. Perturbed relative flux lines from the entry surface to the exit surface showed that in the central movement of the piston, no turbulent regime started. Figure 3.16 presented the velocity configuration in the case of piston speed of 100 mm/s. It can be noted that the maxima values of velocity could be found in the gap space where velocity of the fluid in the annular gap reached 2 m/s, because the available section is smaller.

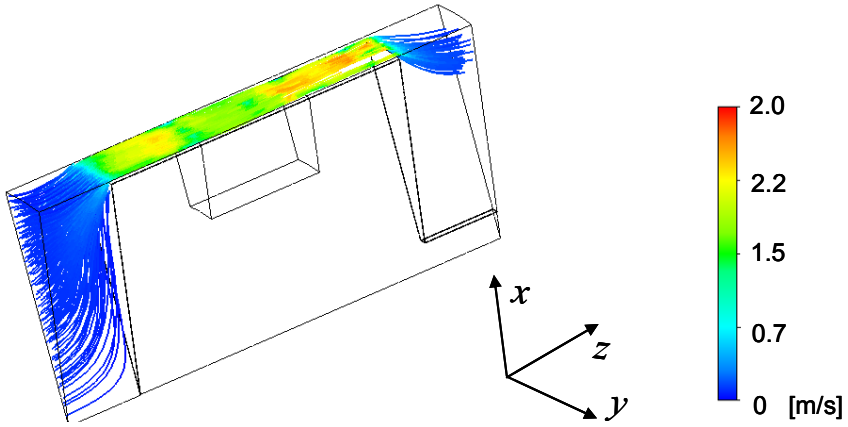

Figure 3.16 – Velocity lines distribution in the fluid volume (v=100 mm/s).

Pressure parameters in the damper inner chamber was fundamental, in order to evaluate possible conditions of cavitation problems in the structural part of the model. Coupled analysis detected pressure both along the axial line and along the radial one, in order to predict the global distribution. Considering the simulation case previously described, no particular singularities were presented (Figure 3.17).
Graph in Figure 2.25 summarizes the pressure values along the axial line of the model in every load condition simulated.
Axial direction presented the main changes of pressure, considering the boundary conditions and the geometries of models. Maximum value could be found at the maximum piston speed, in agreement with [28].

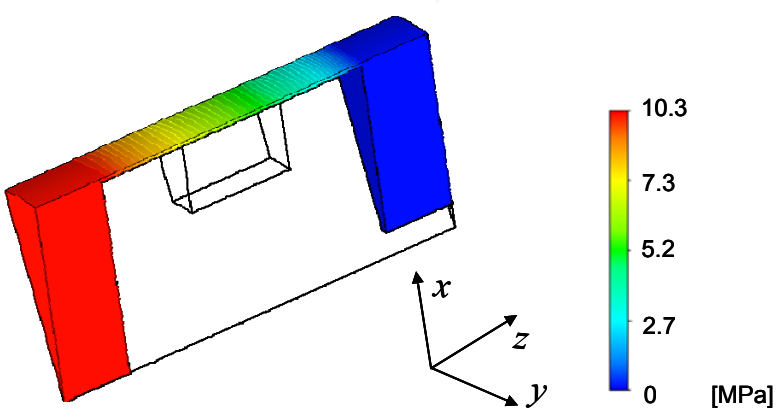

Figure 3.17 – Pressure distribution in the fluid volume (v=100 mm/s)

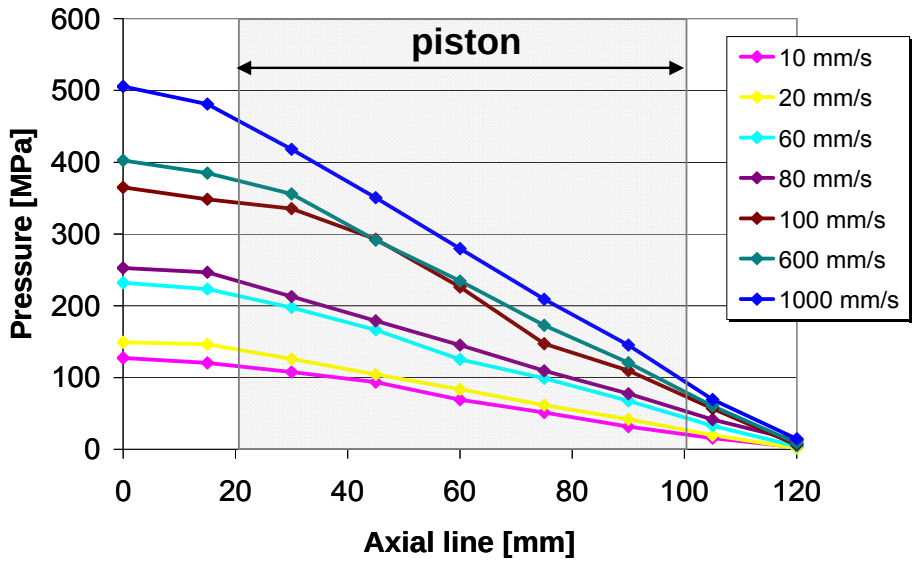

Figure 3.18 – Pressure values in the axial line of the model

Coupled analysis allowed to study the influence of the fluid dynamics in the structural domain. Since the temperature of the structure increases, due to the frictional phenomena at interfaces between the fluid and the structure, the dimensional changes of the piston and the cylinder may affect the gap distance and, consequently, the magnetic response of the MR fluid.

Stresses and strains in the device have been analyzed by the coupled structural analysis, in order to investigate their influence on the magnetic field during the device functioning (Figure 3.19).
The results of the numerical simulations, in terms of radial deformations, are shown in Table 3.4 for different working speed. Maximum radial deformation is negligible in the working conditions by the fluid pressure and velocity. It has been verified that the damping response of the device in the range of process parameters examined is quite stable.

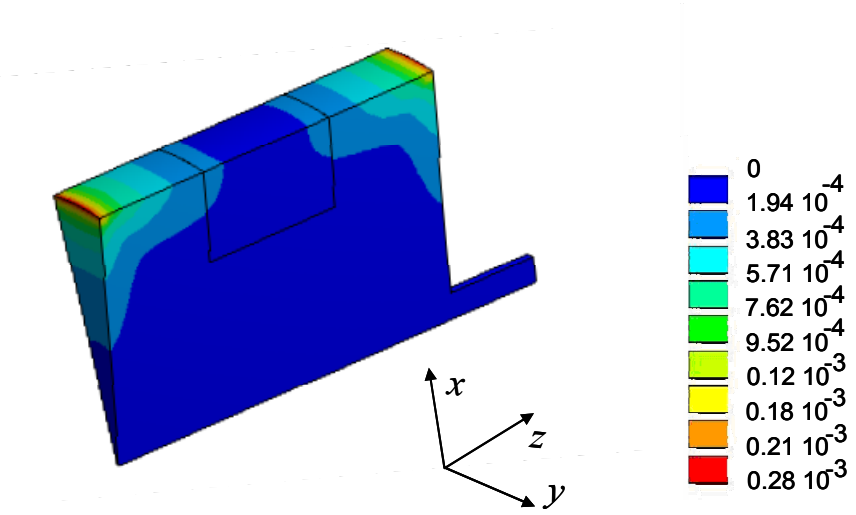

Figure 3.19 – Radial deformation of the structural model

Table 3.4 – Maximum radial strain predicted with multi-physics simulation

Piston speed [mm/s]	Maximum radial deformation [mm]	Von Mises stress [MPa]
20	$0{,}28\ 10^{-3}$	52
60	$0{,}95\ 10^{-3}$	78
80	$1{,}28\ 10^{-3}$	162
1000	$8{,}19\ 10^{-3}$	256

3.5 CONCLUSIONS

A coupled multi physics finite element analysis has been define in order to develop an innovative solution for the industrial problem of reverse load vibrations.
Single analysis allowed to evaluate the effect of thermal, structural, fluid fields and the effects of their mutual interaction in each field and in the global system.
A hydraulic damper configuration was modified in order to house inside magneto-rheological fluid.
A magneto-static simulation was performed in order to study magnetic induction distribution in the models and to achieve inputs for the coupled analysis.
Both fluid dynamics and structural domains have been studied. It can be noted that:

- Temperature increase, due to the dynamics and the changes in MR fluid viscosity determined by the applied magnetic field, do not exceed the operating range of the MR fluid;
- Velocity and pressure in the fluid volume are not critical for cavitation effects in the device;
- Stress and deformation of the components do not influence working and performances of the device.

CHAPTER 4

MR DAMPER TESTING

4.1 INTRODUCTION

Rheological behaviour of MR fluid can be useful to develop innovative systems for the vibration dissipation. Thanks to an external controlled activation, a yield stress characterizes the materials and it has to be won in order to ensure relative every movements to the sliding bodies.
In this chapter, design and manufacturing procedure of two magneto-rheological testing devices is presented. These prototypes are fundamentals for the validation of the numerical model and that allow investigations about damping performances, working temperatures and pressure of materials.

4.2 THE APPROACH

In order to study the rheological capabilities of the magneto-rheological fluid, it was necessary to develop and manufacture prototypes. The design was based on the mechanical model proposed by the authors in literature. Device developments took into account architectural configurations, available in technical reports, and original ad hoc solutions to optimize the structure, its performances and its use.
First prototype (20 kN) was developed in a single ended design with an external reservoir. This configuration allowed a study of the influence of the reservoir in the damping performances. Second prototype (10 kN), on the contrary, is based on double ended structure, where no influence of auxiliary equipment is present, allowing a better detection of the temperature evolution occurring.
On these bases, once obtained the prototypes, an experimental campaign needed, in order to test the device during its working conditions, and detect the behaviour of the fluid, considering:

- the influence of the input current on the final damping results;
- the influence of external factors;
- the working temperature and pressure.

4.3 DESIGN

Initial design phase of the structure of the magneto-rheological damper started from the relations of parallel-plate Bingham theory, as presented in Section 2.3.1. When an external magnetic field is generated, the fluid in response changes its rheology in a semi-solid state, characterized by a yield strength, derived by magnetic induction of the magnetic field. The rheology is governed by Bingham's equation (Section 2.1.3).
Architectural configuration of flow mode fluid working has been taken to account. According as presented in Section 2.3.3, final damping load was the results of the sum of three different contributions: one component controlled by the magnetic properties of fluid F_τ and two others, F_f and F_η, not directly controllable, connected to the friction generated at the interface liquid-steel and the viscous force of the carrier fluid. Both controllable and non controllable forces have been written in Section 2.3.2 as:

$$F_\tau = \frac{\tau_0 L A_p}{h} \operatorname{sgn}\left(v_0\right) \qquad \text{(Eq. 2.27)}$$

$$F_\eta = \left(1 + \frac{wh}{2A_p}\right)\frac{12\eta L A_p}{wh^3} A_p v_0 \qquad \text{(Eq. 2.28)}$$

As it could be seen, previous relations linked geometrical quantities of the damper with process parameter and fluid proprieties but they often do not provide the best insight into the significance of the various parameters.

A first key parameter (Eq. 4.1) for the design and the evaluation of the performance of the damper device is the ratio of controllable force to non controllable force, as known as Dynamic range *D* [54]:

$$D = \frac{F_\tau}{F_\eta + F_f} \qquad \text{(Eq. 4.1)}$$

A maximized dynamic range allows to optimize the damping capabilities of the damper. Linked to the geometrical parameters, it influences the architecture of the single parts. It can be noted that both controllable and non controllable force are inversely related to the gap h between piston and cylinder, where MR fluid flows. However, visco-plastic component varies two orders of magnitude higher than controllable one. Friction force usually is considered constant [54].
High values of *h* means that both two forces are quite low, so the need of create small activated cavities for the fluid flow.
However, while a progressive decrease in the gap size leads to an increase of the damping effect of the device, too small values, on the other hand, produce decrease of *D*, that tends to zero in the conditions of magnetic saturation of materials, usual limits at witch the magneto-rheological actuators are designed for the generation of its maximum yield stress.
So, considering the geometry requirement and the desired damping performances, dynamic range value has to be maximized, in order to ensure optimal behaviour of fluid and device. It is important to underline that although *D* is defined as function of the viscous properties of the MR fluid, it can be significantly influenced by other factors, such as friction and sealing on the devices.
A second key parameter for the damping design (Eq. 4.2), that provide information in the significance of the main parameters, is the Minimum Active Fluid *V* [64]. It corresponds to the minimum volume of MR fluid that is activated when an external magnetic field is applied.

$$V = Lwh = \frac{12k}{c^2}\left(\frac{\eta}{{\tau_0}^2}\right)\left(\frac{F_\tau}{F_\eta}\right) Q\Delta p_\tau \qquad \text{(Eq. 4.2)}$$

where:

k = geometrical constant (≈ 1 cause in most cases $whv_0 \ll Q$);

$Q\Delta p =$ mechanical power required.

The volume V is always directly proportional to a factor linked to fluid proprieties (η/τ_0^2), to the dynamic range and to the mechanical power required.

Parallel to the working mode of MR fluid, the realization of a suitable magnetic circuit in the device is fundamental, because the final load damping performances depends on fluid activated shear stress τ, that depends on magnetic field $\vec{B}$ produced.

Several considerations has to be considered in order to optimize the circuit design [82]:

- The uniformity of the magnetic field that active MR fluid in the at the gap between the cylinder and piston;
- Magnetic flux lines have to be most normal considering both the cross-sections of piston and cylinder. This means considering negligible the losses through the steel parts and the areas of fluid non-activation;
- The non linearity of magnetic proprieties of both fluid and metal elements (B-H curves);
- The expansion of magnetic flux along the gap h;
- The leakage on the edges and in the seals;
- Limits in terms of voltage, current and inductance in the coils;
- Possibility of eddy current effects.

The main objective of circuit design, once chosen the maximum current intensity i for the working condition of the device, was to calculate the necessary number of coils N that allowed to generate the desired magnetic field, according with the limits on the geometry and on safety.

According to this [83], principal steps used in the design of the devices objective of this work can be summarized:

- determination, once chosen the objective yield stress of the activated fluid τ_0, of magnetic induction H_f in the MR material;
- detection of the magnetic field of the fluid B_f, considering B–H curves;
- calculation of the magnetic field of the steel B_s, according to the hypothesis of continuity of magnetic flux Φ (Eq. 4.3) [82]:

$$\Phi_{FLUID} = \Phi_{STEEL1} = \Phi_{STEEL2} = \ldots \qquad \text{(Eq. 4.3)}$$

- detection of the magnetic induction in the metal H_s ;
- determination of the coil number, using Kirchoff's law of magnetic circuit (Eq. 4.4):

$$NI = \oint H \cdot dl = \sum H_i L_i = H_f \cdot g + H_s \cdot L \qquad \text{(Eq. 4.4)}$$

Figure 4.1 presents a sketch of the magnetic circuit where are highlight the main parameter previously discussed.

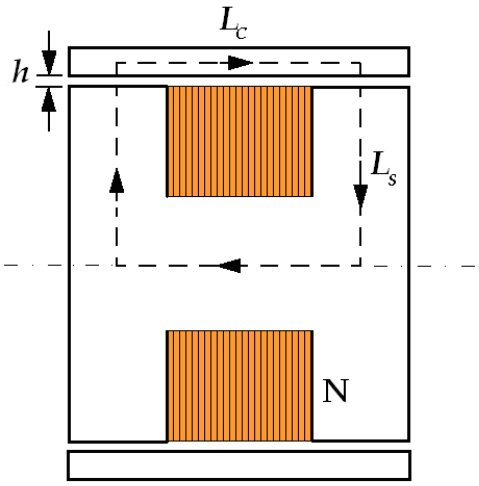

Figure 4.1 – Sketch of magnetic circuit in the MR damper (the dotted line shows a generic magnetic flux line).

Circuit design had to be optimized and integrated considering structural prototype design. Magnetic activation of the MR fluid had to be maximized in order to gain high performances, according to the magnetic limits of the materials, while losses in metal had to be reduced in order to minimized the power and supply required.

4.4 EXPERIMENTAL APPARATUS

On the basis of previous consideration of Sections 2.3.3 and 4.2, different magneto-rheological prototypes were developed and manufactured at the Chair of Manufacturing Technology, University of Padova, within the PhD period.
These devices were sensorized in order to study MR fluid behaviours and their implementation in the blanking process conditions.

4.4.1 Magneto–Rheological fluid

The magneto rheological fluid used was LORD MRF-132DG [77]. It was a hydrocarbon-based fluid formulated for general use in controllable energy-dissipating applications. Magnetic proprieties were evaluated according to H $-\tau$ and shear stress vs. shear rate curves (respectively resumed in Figure 4.2 and Figure 3.3) The most relevant properties were resumed in Table 4.1.

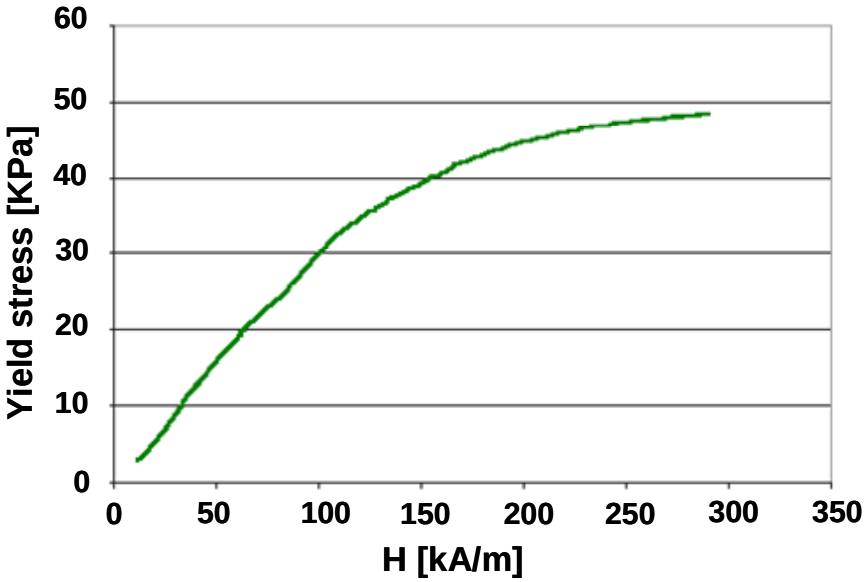

Figure 4.2 – Yield stress vs. magnetic inductance of MRF132DG.

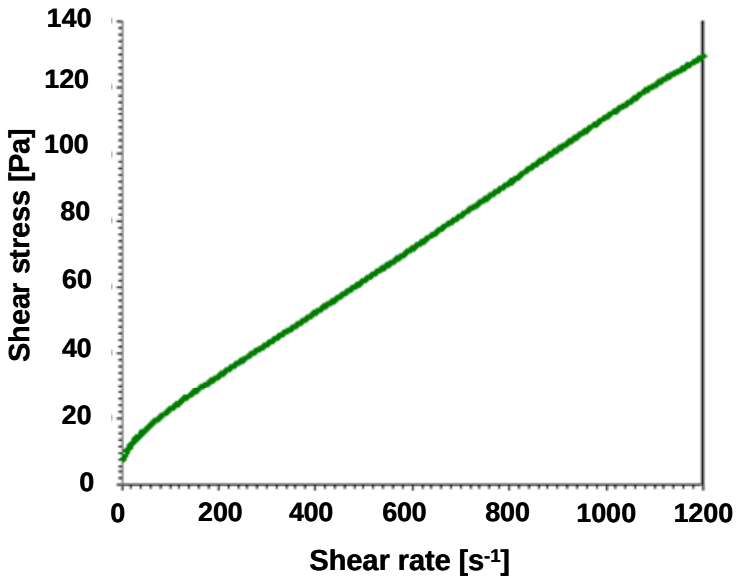

Figure 4.3 – Shear stress vs. shear rate of MRF132DG.

Table 4.1 – Properties of LORD MRF-132DG

Viscosity, Pa (at 40°C) Calculated as slope 800 – 1200 s^{-1}	0.092 ± 0.015
Density, g/cm^3	2.98 – 3.18
Solids content by weight, %	80.98
Flash point, °C	>150
Operating temperature, °C	40 to +130

4.4.2 Single ended damper 20 kN

In order to evaluate magneto – rheological fluid performance in damping problems, at first, a single hand damper was designed, developed and manufactured. The prototype is shown in Figure 4.4a.

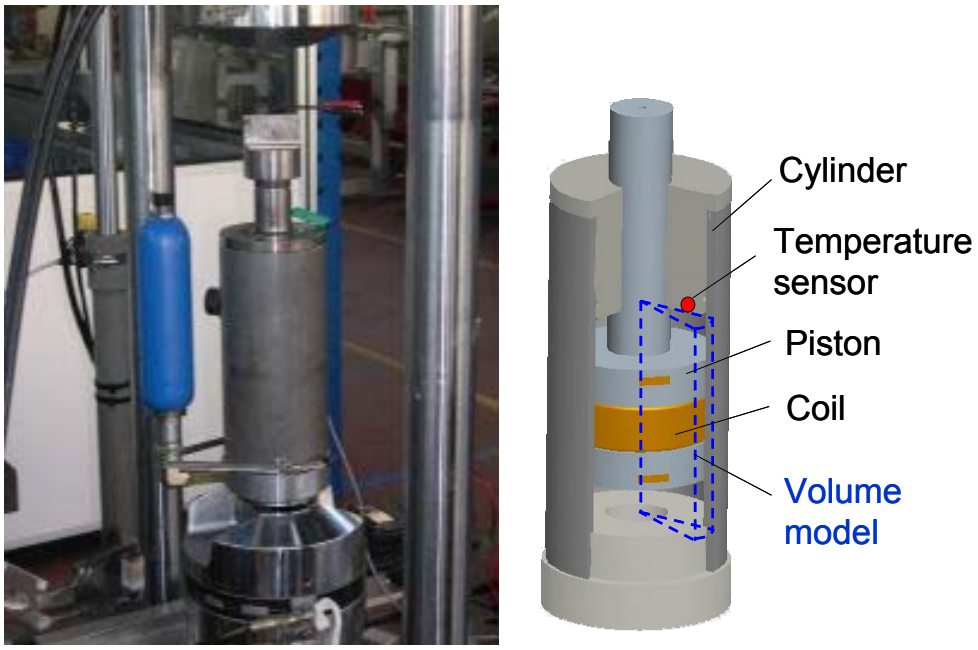

Figure 4.4 – a) MR vibration damper prototype; b) device CAD model (the dotted line shows the volume model under investigation).

It consisted of a single hand damper architecture in a monotube configuration (see Section 2.3.3), where a piston 80 mm long was connected to the press ram and a cylinder 300 mm long was fixed to the press bed.
The maximum project damping force, basis for the structural design, was 20000 N.
The prototype based on flow mode operation of MR fluid: MRF132DG fluid was sandwiched between the magnetic surfaces of piston and cylinder, with a fixed distance gap of 1 mm. The relative pressurized flow of MR fluid moved between them, due to the relative movement during the functioning of the device. The change in viscosity determined a shear resistance to the rod stroke, depending on the magnetic field applied. As the field intensity increased, the MR fluid's resistance to shearing increased. The total fluid used was equal to 0,56 litre. In Figure 4.4b could be identified the main components and the volume model under investigation of the device.
The main geometrical parameters are resumed in Figure 4.5, where is shown a sketch of the device.

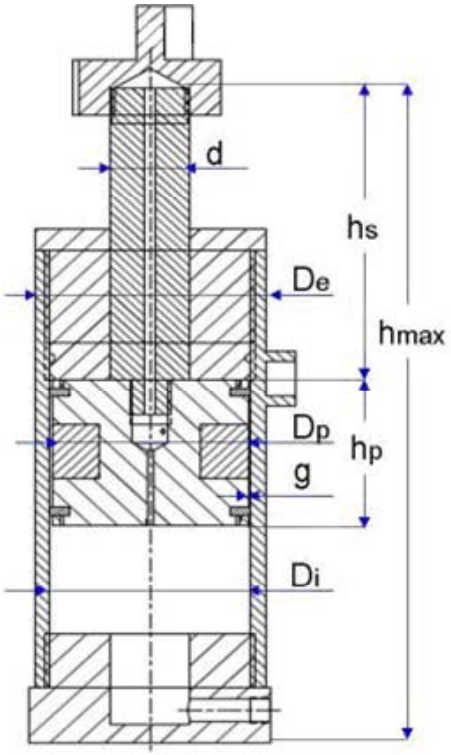

Dimension	
H_{max}	412 mm
H_{min}	357 mm
stroke	60 mm
D_e	115 mm
D_i	100 mm
D_p	98 mm
h_p	80 mm
d	40 mm
g	1 mm
mass	19,6 kg

Figure 4.5 – Sketch of 20 kN single ended damper. In the table are reported the main geometrical parameters values.

According to magnetic requirements, structural parts were manufactured using AISI 1040 steel.

The electrical circuit that allowed reproducing the required magnetic field was embedded in the piston architecture. Coils were housed in a single central groove (Figure 4.6). A 1.6 mm diameter copper wire was used for the realization of the circuit that was powered by an input current varying from 0 A to 3 A.
In order to assure maxima insulation and safety, a thermosetting coating was applied to the electrical coil and to the wire connections.
Magnetic flux generated was equal to Φ = 0,00722 T m^2 and provided a maximum magnetic field in the fluid of 0, 4692 T.
The damper operated along a ± 30 mm stroke, in continuous or discontinuous mode, depending on the applications.

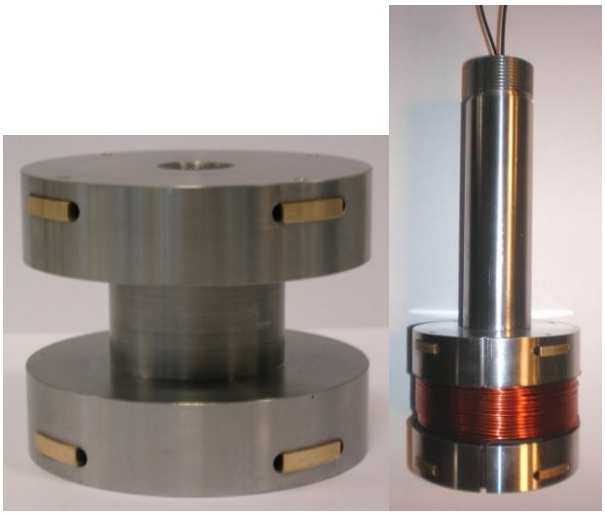

Figure 4.6 – Details of the damper piston part.

As shown in the Figure 4.6, on the lateral surface of the piston were placed the bearings, which have the task of maintaining constant the radial distance between the piston and cylinder.
They also avoid contact steel–steel during working operations. Even if they influenced the fluid motion to annular gap, bearings had dispensed with the presence of a guide attached to the bottom part of the piston, otherwise essential to ensure the concentricity between the moving parts [68].
V parameter was calculated as 1,55509 E-05 m^3, according to the magnetically polarized length of the piston.
The structural analysis has been performed by using the multi-physics approach previously presented in section 3.2. For each parts out of the coupled domains, an independent structural analysis was carried out by using the FEM code ANSYS.
Design had taken to account the evaluation of the Dynamic range and the minimum actived fluid parameters. Thanks to recursive iterations, dynamic range was set equal to 8,28. It was not the maximum available value because of geometrical limits, which required gap length unacceptably too small.

Figure 4.7 summarizes the dynamic range trend, as function of gap to piston radius ratio.

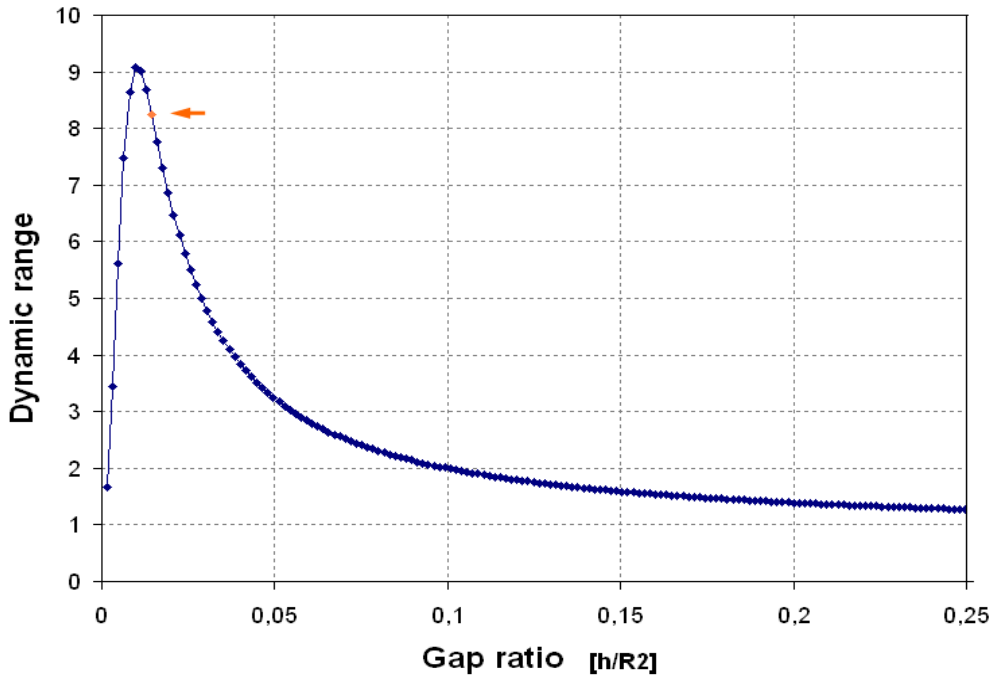

Figure 4.7 – Dynamic range trend of the damper. The orange arrow indicate the D valued set in the design.

Because of its configuration, a separate accumulator was used to compensate the volume change of the fluid during its testing (see Figure 4.8). It was also useful for any change in volume due to thermal expansion of fluid.
The reservoir target data are reported in Figure 4.9.

Figure 4.8 – Hydraulic reservoir of the damper for the volume change compensation.

Dimension	
Total mass	2,1 kg
Diameter	58 mm
Height	266 mm
Maximum pressure	350 bar
Gas volume	0,17 l
Volume	0,2 l

Figure 4.9 – Reservoir data target.

This reservoir, thanks to a membrane that separated the MR fluid and a nitrogen gas volume, ensured a pressure to the fluid when the piston moved in the opposite direction, in order to reintroduce it (with the appropriate velocity) in the cylinder chamber.
Pre-charge pressure was fundamental. If too high, the reservoir played an active role in the damping and its effects were not negligible (as it should), depending on the direction of piston displacement.
Otherwise, if too low, the reservoir received fluid without offering an adequate strength. So the fluid first filled the reservoir without passing through the annular conduit. This caused a considerable drop in performance, according to the volume of the void that arises to inside of the cylinder [54].
After a series of preliminary tests, pre-charge pressure was chosen in order to maintain the pressure constant in the cylinder chambers at the level of 10 bar. The pressure was monitored by a manometer placed between the cylinder and the accumulator.
The upper cylinder head was equipped with a temperature sensor for the monitoring of the fluid temperature in the inner camera (Figure 4.4b). The sensor was built with a k-thermocouple that was spot welded at a distance of 0.5 mm from the sensor surface.

4.4.3 Double ended damper 10 kN

Double ended damper, realized in the labs of University of Padua, is presented in Figure 4.10.

Figure 4.10 – Double ended 10 KN MR damper. (Photo by FIERA LAMIERA 2010).

This second prototype was based on double ended architecture, such as it provided with two piston rod of equal diameter and length at both the side of the inner piston. This configuration, unlike 20 kN damper, allowed to delete the influence of external auxiliary equipment (reservoir effects previously described).
Maximum stroke has been chosen of 250 mm, in order to activate the MR fluid along a long displacement. The maximum project damping force, basis for the structural design, was set as 10000 N.
The structural design has been performed by using the multi-physics approach and design theory previously presented respectively in section 3.2 and section 4.2. It was based on flow mode operation and MR fluid flowed in a annular gap of 0,8 mm.
Dynamic range parameter was optimized considering geometrical limits and damping forces required. As shown in Figure 4.11, *D* parameter was identified as 33,96.

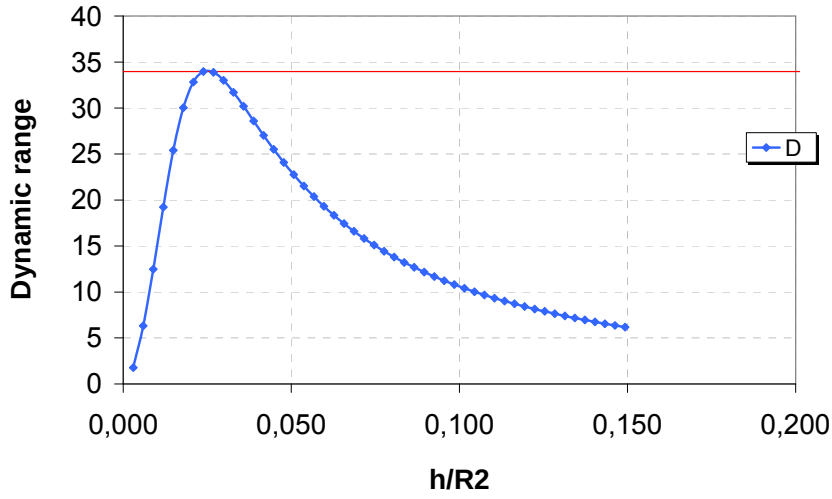

Figure 4.11 – Dynamic range trend of the damper. The orange line indicate the maximum D valued set in the design.

The piston has been manufactured by modular part, in order create two grooves to better housing the coils and for possible changes of the gap width in the same device. According to magnetic requirements, structural parts were manufactured using AISI 1040 steel, while the total fluid MRF132DG used is equal to 0,78 litre..
Electrical circuit has been compound of two independent windings powered in series. Electric copper wire had a diameter of 0,8 mm. Input current objective varied from 0 A to 2 A. Design was possible according to the theory presented in section 4.2 and it was verified and optimized by magneto-statics analysis, as presented in section 3.31. Figure 4.12 resumes the main geometrical information of the damper.
Magnetic flux generated was equal to Φ = 0,00238 T m^2 and provided a maximum magnetic field in the fluid of 0,4347 T.
On the cylinder lateral surface (Figure 4.13), a series of cavities at 1 mm from the inner chamber has been provided, in order to housing k-thermocouple temperature sensors.

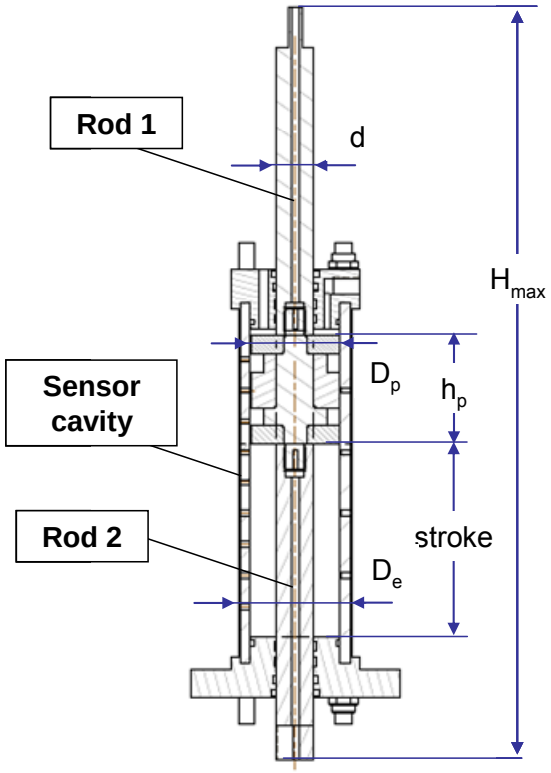

Dimension	
H_{max}	412 mm
stroke	250 mm
D_e	82 mm
D_p	65,4 mm
h_p	81 mm
d	28 mm
g	0,8 mm
mass	13,1 kg

Figure 4.12 – Sketch of 10 KN double ended damper. In the table on the right are reported the main geometrical parameter values.

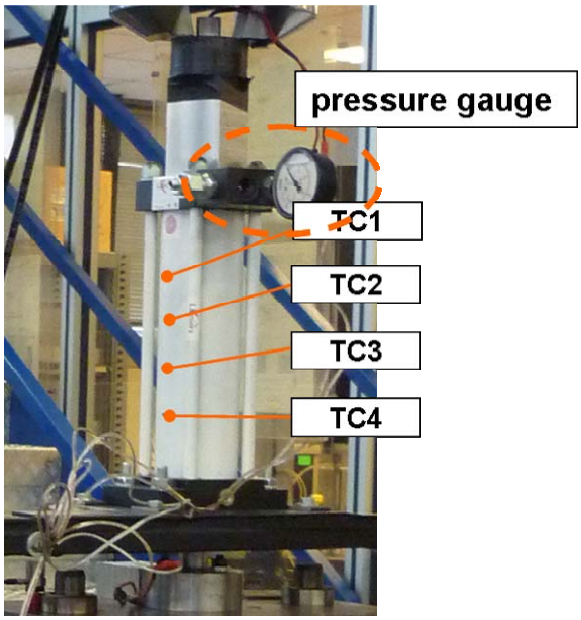

Figure 4.13 – Double ended damper in the testing press: k-thermocouple temperature sensor positioning and pressure gauge.

4.4.4 Electric auxiliary equipment

In order to provide magnetic fields required for the magneto rheological fluid work, an electric laboratory equipment was necessary to supply the relative current intensity and to link to the inner electric coils of the devices.
This equipment was made of following main components:

- Power pack
- Resistor
- TVS

Power Pack

Figure 4.14 – Kert Cosmo 3000 power pack

Kert cosmo 3000 power pack was the most suitable one both in terms of control and current supplied (Figure 4.14). The control could be made manually (above all in setting steps) and externally by computer control. The available current was into the range 0÷10 A. Shift between voltage and current were available.
The supply pack target data are reported in Table 4.2.

Table 4.2 – Kert Cosmo 3000 target data

Voltage supply [Vac]	230 (48÷63 Hz)
Output voltage [Vdc]	0÷30 ±1%
Output current [A]	0÷10
Ripple [mV]	15 RMS
Protection	Electronic-fuse
Measure intruments	Digital Volt/Ampermeter

Resistor

A resistor was necessary in order to increase the total resistance of the piston coils (see Figure 4.15). This provided heat sinking, better control of the current supplied to the dampers and better protection of the electric circuit, avoiding possible short circuit.
The resistor ARCOL HS100 target data are reported in Table 4.3.

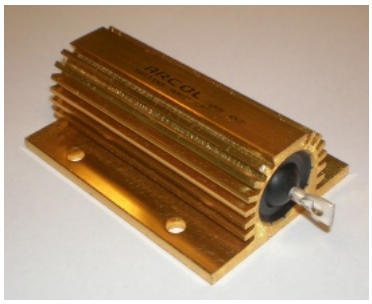

Figure 4.15 – ARCOL HS100 4R7 resistor

Table 4.3 – ARCOL HS100 4R7 target data

power rating [W]	100
electric resistance [Ω]	4.7
voltage proof ac peak [A]	6363
voltage proof ac rms	4500
core	ceramic- steatite

TVS

The electric coils of the damper can be supplied both by voltage and current source. However, it is suitable to avoid any abrupt interruption of the power. Observing Faraday's law:

$$V(t) = -L\frac{di}{dt} \qquad (2.1)$$

with a magnetic induction, if a abrupt variation of current happens, a peak voltage that opposes to the change appears. This is what happens when a failure occurs in electrical system [82]

The peak of tension that arises can damage the insulation and cause short circuits. If this happens, the magnetic field which affects the fluid decreases inevitably and therefore the performance of the damper.

A bidirectional transient voltage suppressor was introduced in parallel to the damper (Figure 4.16a), in order to protect the coil from such voltage surges.

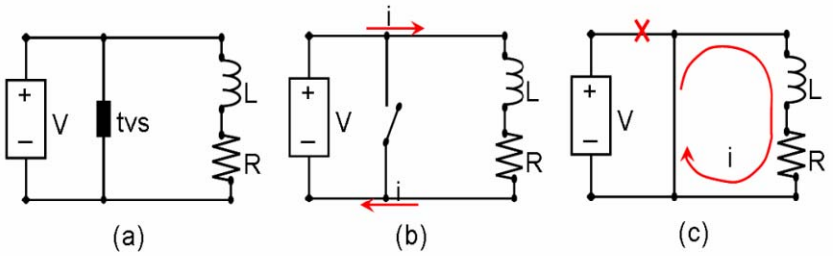

Figure 4.16 – Bidirectional transient voltage suppressor (TVS) configuration

As long as the voltage remains below a certain threshold, called breakdown voltage, the TVS has a high electrical resistance. So only a small fraction of the current (few microamperes) flow through it (i.e. TVS do not exist, as shown in Figure 4.16b). Otherwise, when the voltage exceeds the threshold value, the TVS begins to conduct, thus bringing down the tension at the heads of the coil (Figure 4.16c).

The TVS ST 1.5KE30CA target data are reported in Table 4.4.

Table 4.4 – TVS ST 1.5KE30CA target data

Peak pulse power dissipation [W]	1500
leakage current [μA]	1
stand-off voltage [V]	6363
break down voltage [V]	30
clamping voltage [V]	41,5 (10/1000μs)
peak pulse current [A]	36 A (10/1000μs)

4.5 RESULTS

In the following sections the experimental results concerning the magneto-rheological behaviour of damper prototypes, previously described, will be presented and analyzed. Load-stroke performances, the influence of geometrical configurations and the working temperatures according to the main critical process parameters will be presented and discussed. In section 4.5.1 are resumed 20 KN damper results, while in section 4.5.2 are reported 10 KN damper ones.

4.5.1 Single ended damper results

4.5.1.1 Load-stroke performances

Table 4.5 summarizes the experiments carried out at different ram speed and in different magnetic conditions. For every couple of factors, both triangular (i.e. constant speed during stroke) and sinusoidal (i.e. variable speed with a minimum in the peak of the sinusoid curve) displacement excitations was tested on MTS 322 T-slot 50 kN load machine.

Table 4.5 – Tested values of speed piston and current coil.

Speed (mm/s)	2.5	5	10	20	30	40	50	60	70	80
Current (A)	0	0.25	0.5	1	1.5	2	2.5	3		

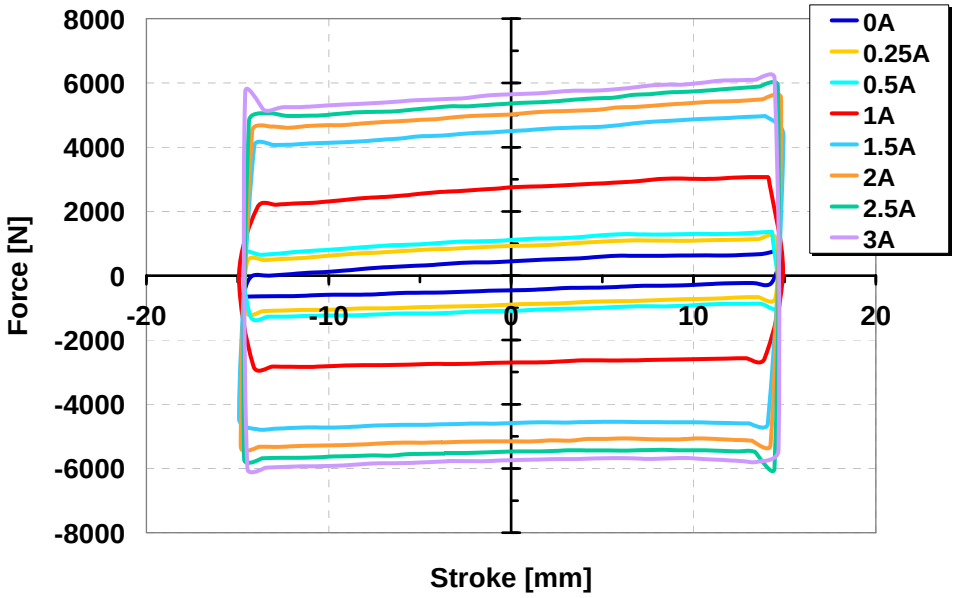

Figure 4.17– Load vs. stroke performances (v=10 mm/s)

In Figure 4.17, the behaviour of the damping force vs. piston displacement for a piston speed of 10 mm/s was presented. All the values at different current densities were reported. The uncertainty calculation allowed an estimated range of ± 230 N at each test.
The significant increase in damping force, which is done by passing from the minimum to the maximum current density, gave to the damper controllability and flexibility.
Because of the stroke was constant during every test, when the current increased also the enclosed area in every cycle enlarged. This meant that the damper absorbed a greater amount of vibration energy.
It was noticed a non-linear correlation between the increase in damping force and the electrical current of the magnetic circuit.
The best range that allowed great improvement in the damper performance it was noted that corresponded to 0 ÷ 1,5 A (i.e. the objective current value in the design).
For both speed profiles that were tested, the increase of load is less important for values of current intensities greater than 1.5A, while under this value the force trend is almost linear. This meant the approaching the limit of magnetic saturation of the materials.
A quasi-symmetric behaviour is verified in both tensile and compressive mode. For current intensities larger than 3 A, the performances of the damper do not increase because of the magnetic saturation is reached, as magneto-static simulation anticipated.
It is important to underlines that force values obtained in every tests are about 12% lower than theoretical value because losses in magnetic circuits takes place. Interfaces between parts, isolation of the electric circuit and spaces are not taken in account by numerical model. Table 4.6 shows, for example, experimental and theoretical results in force calculation with a piston speed of 10 mm/s.

Table 4.6 – Experimental and theoretical forces (v=10 mm/s).

	Force [N]	
current [A]	**experimental**	**theoretical**
0	694	705
0,5	998	1189
1	2821	3391
1,5	4517	5314
2	5125	5835
2,5	5678	6074
3	5688	6419

In Figure 4.18, it can be noted the cyclical of the test, and the force peak when velocity change direction.

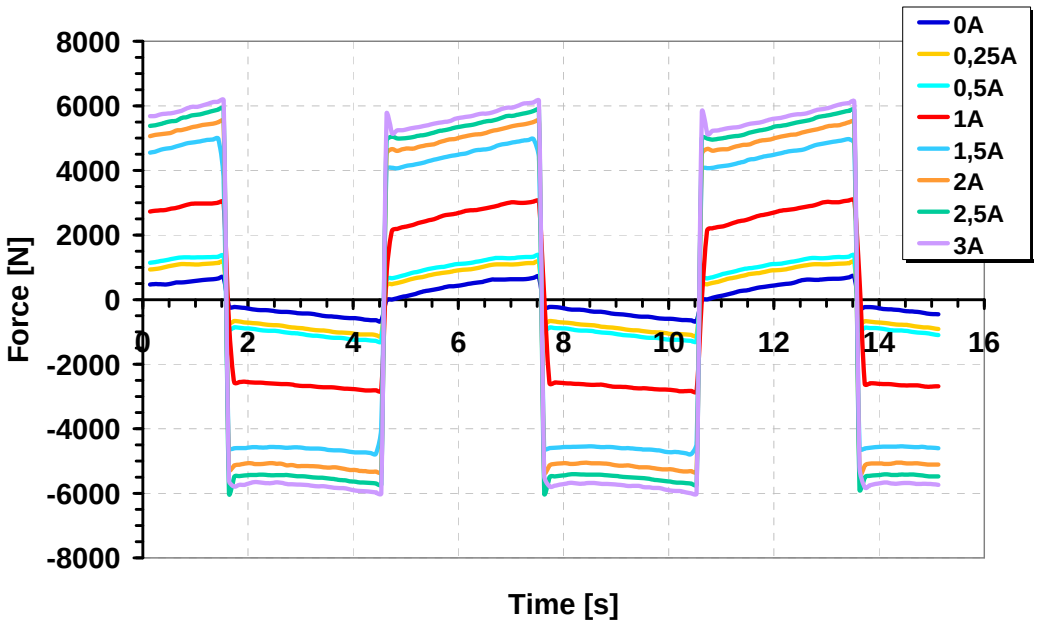

Figure 4.18 – Load vs. time performances (v=10 mm/s)

Force peaks, when piston damper change of direction, could be linked to inertial effects but, first of all, to stiction phenomenon [38] in the MR fluid.
Stiction is a particle jamming or a mechanical restriction to flow that is dependent upon both particle size and shape, as well as magnetic field an flow history of the material [84]. Figure 4.19 presents a peak force in a test with 10 mm/s of speed and 1,5 A current intensity.
Stiction causes striction of the material flow, that generates an elastic energy that is stored and released when velocity change of direction. However the amount of this peak (about 350 N in every tests) can be considered negligible in the evaluation of damper behaviour

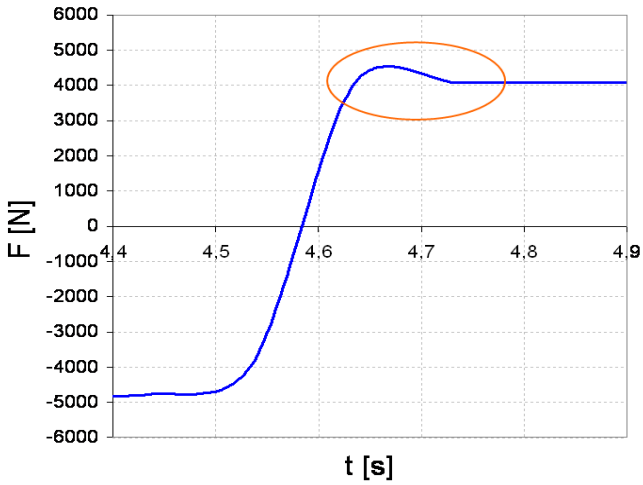

Figure 4.19 – Striction effect: particolar of peak force.

Following Figure 4.20, Figure 4.21, Figure 4.22 and Figure 4.23 present the load - stroke performances in the tests with respectively 40 mm/s e 80 mm/s velocity of piston. It can be remarke the same considerations of 10 mm/s test.

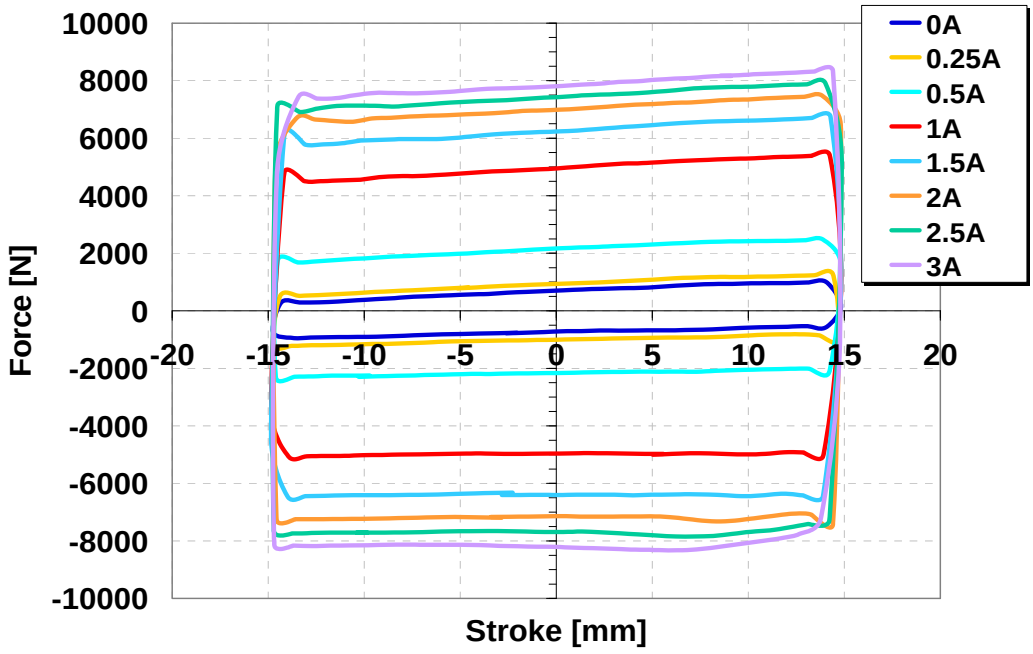

Figure 4.20 – Load vs. stroke performances (v=40 mm/s)

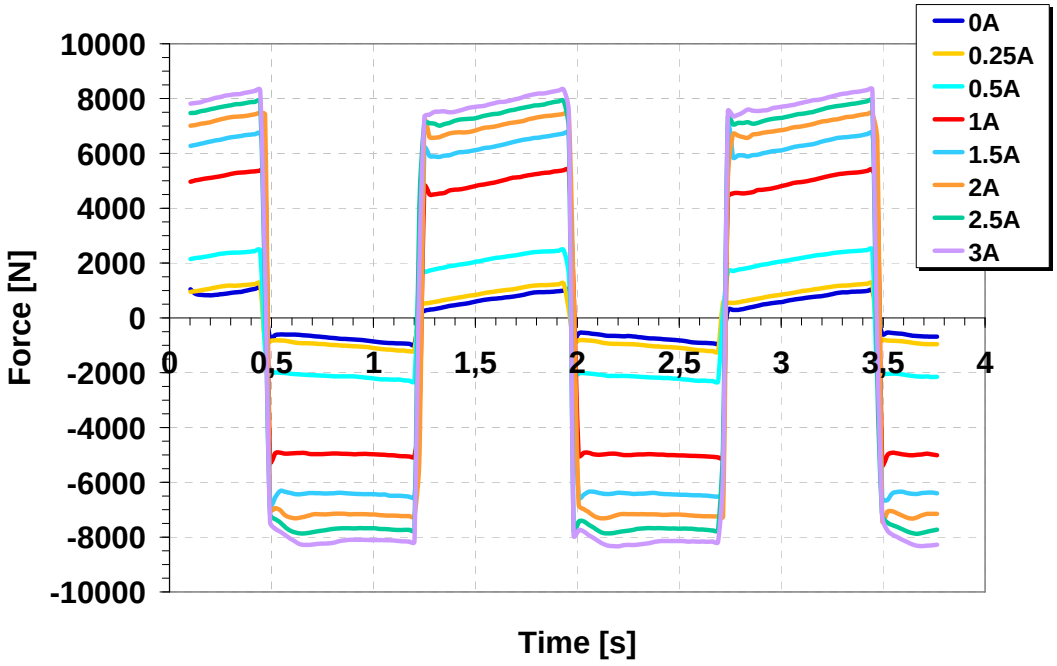

Figure 4.21 – Load vs. time performances (v=40 mm/s)

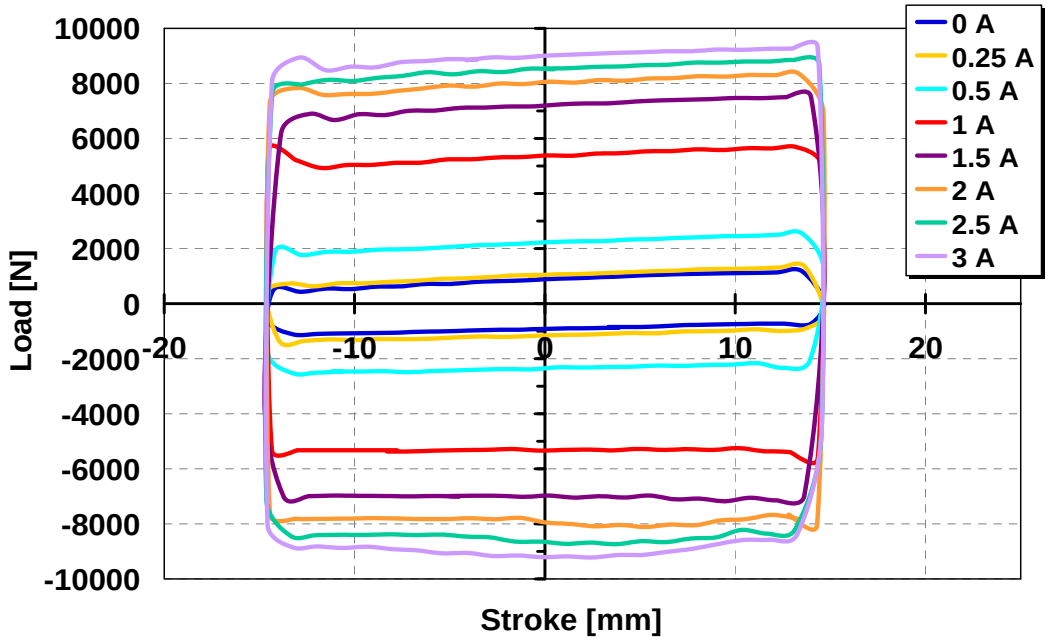

Figure 4.22 – Load vs. stroke performances (v=80 mm/s)

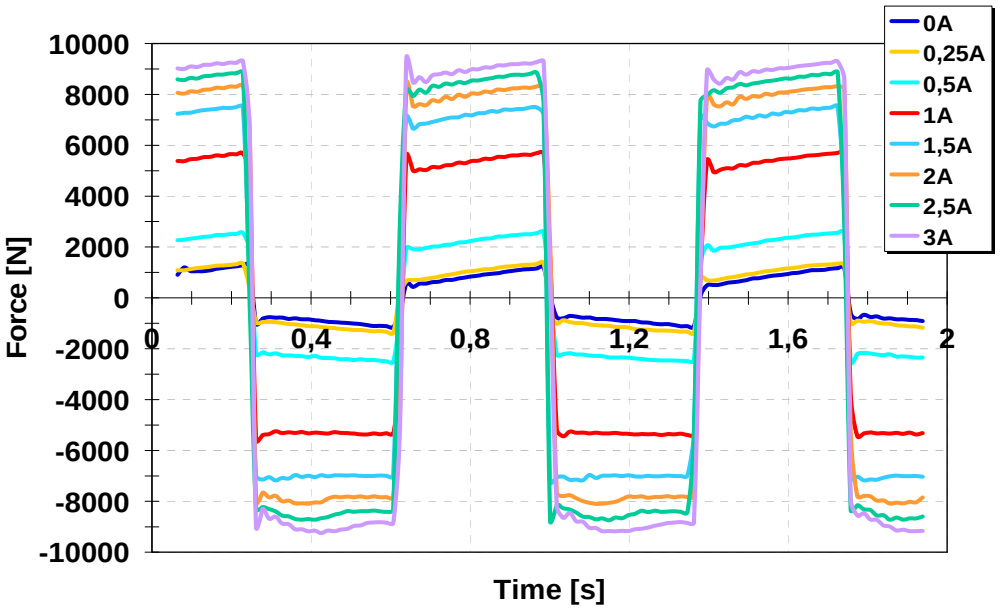

Figure 4.23 – Load vs. time performances (v=80 mm/s)

An increase in the piston speed meant a change in the force damped, that became greater. This effect was more clear at elevates current intensity, where MR fluid were characterized by particle chains with higher shear stress. So the viscosity was more influent.

Figure 4.24 shows the effects of piston speed and current intensity in the damping forces.

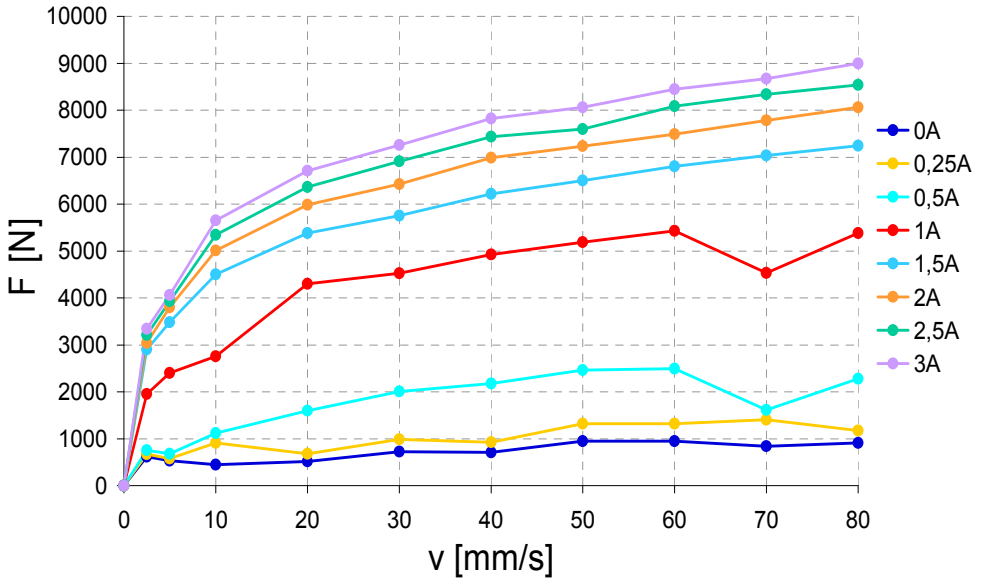

Figure 4.24 – Velocity of damper excitation in the damping load at different input current.

However the effect of the velocity change in the force was lower than the influence of a different current intensity, above all if low values of magnetic field were considered.
Figure 4.25 shows the influence that the supplied intensity current exerts on the damping force. The results reported in the figure show three relevant zones of the curves: the first part (values of current intensity in the range 0-0.3 A) represents values of current intensity too small for the activation of MR fluid; the second zone (values of current intensity in the range 0.5-1.5 A) represents the area in which the damping load can be controlled during the process and the last zone (values of current intensity in the range 1.5-3 A) where the MR fluid approaches the saturation values and no significant increase of lad can be obtained.

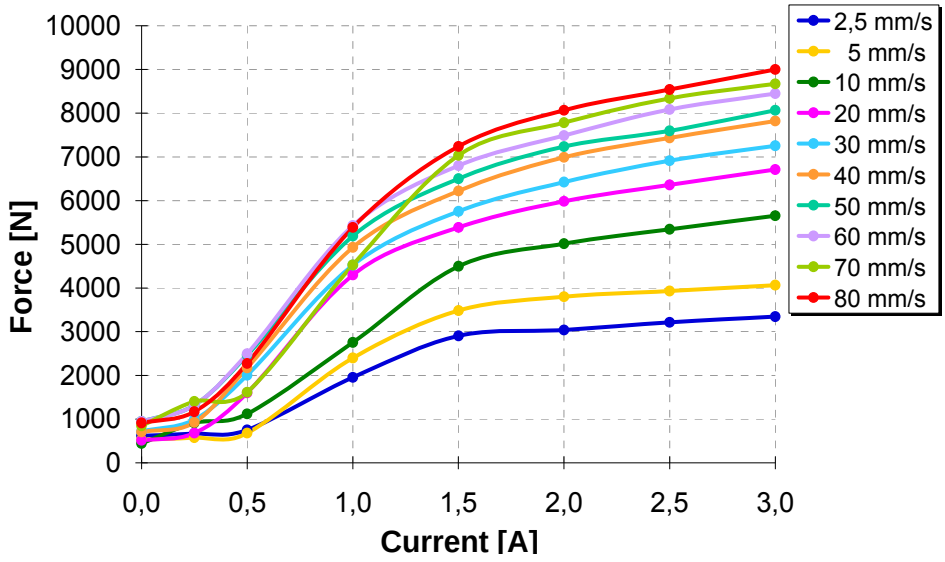

Figure 4.25 – Influence of current on damping force of device.

Pressure influence of the external reservoir was analysed. In both displacement directions of the piston along its stroke, reservoir both realised or housed fluid by its pre-charged chamber. Pressure chamber increased as well as the fluid was stored inside.
As shown in Figure 4.26, reservoir provides a negative load (i.e. compression) that become greater as the piston reaches the bottom dead centre of the damper (PMI). In this point, the pressure is at the maximum value, and all the MR fluid that have to flow in the annular gap is passed. When the piston changes the displacement direction, the fluid in the upper part of the cylinder chamber fill through the gap and MR fluid in the reservoir come back in the chamber, because the piston rod goes out. At the damper top dead centre (PMS), all the fluid is inside the damper and the reservoir is empty.

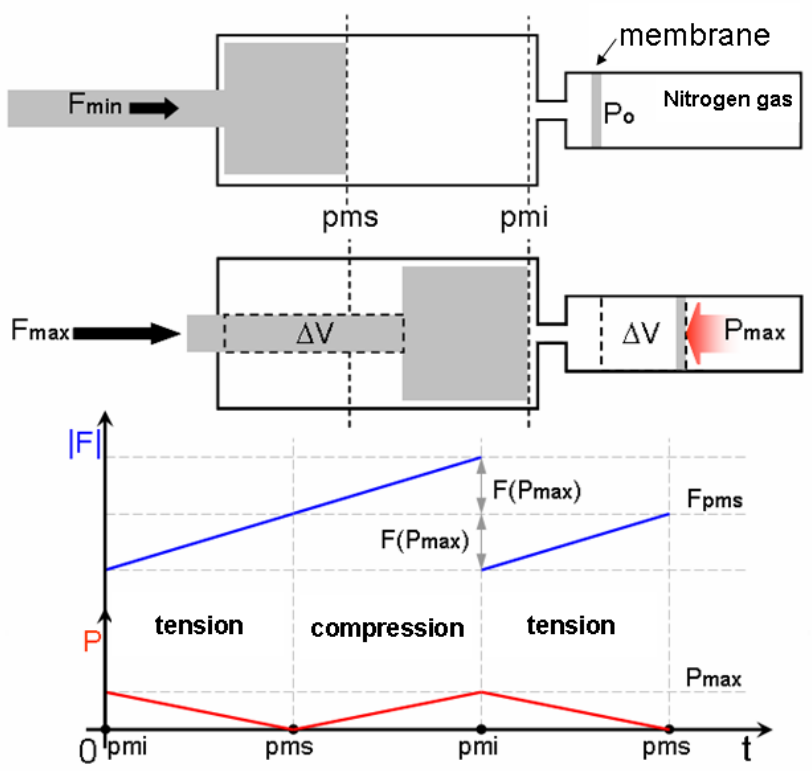

Figure 4.26 – Hydraulic reservoir pressure effects: qualitative behaviour.

Optimization of the pre-charge pressure values was fundamental in order to consider the reservoir effect. If the reservoir pressure was not sufficient to provide a right resistance to the flow, the fluid flowed easier in the reservoir chamber rather than filling through the annular gap. So possibility of vacuum condition, that reduced damping forces, could appear. However at this stage, the reservoir pressure was always increasing: as soon as it reached a value greater than the pressure in the damper chamber, the fluid returned to flow through the annular conduit, restoring the proper functioning of the damper.
An example of this behaviour is shown in Figure 4.27, where the results obtained in a test at a piston speed of 10 mm/s are presented.

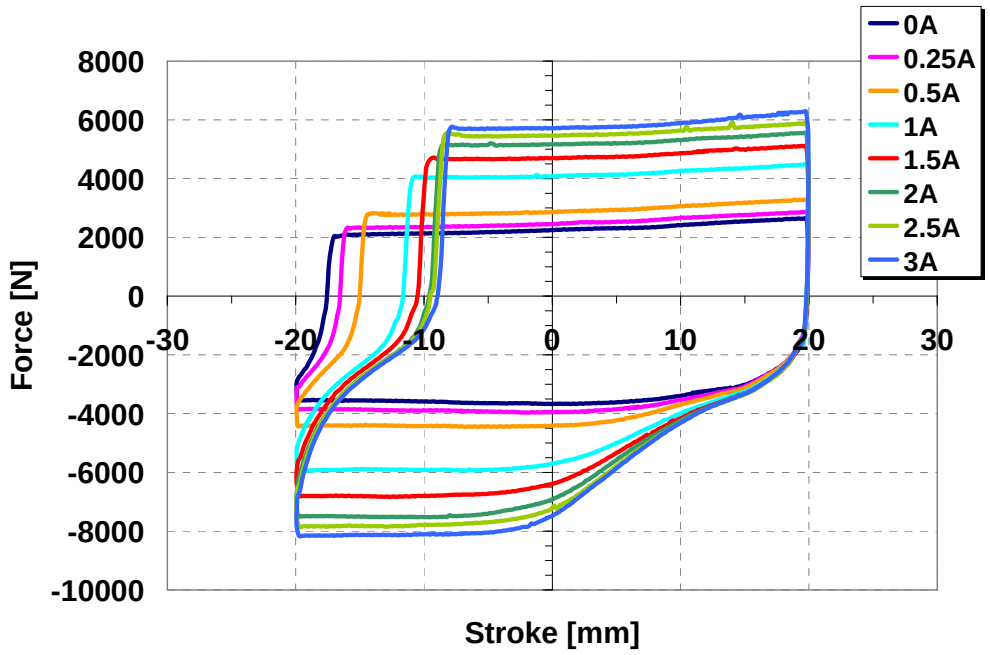

Figure 4.27 – Load vs. stroke performances (v=10 mm/s) with a non optimal precharge pressure in the hydraulic reservoir of the damper

In effect, initially, the reservoir connected to the damper was preloaded with a pressure of 1.5 bar.

It can be noted a non-linear behaviour of damper. Force values were low along a great amount of stroke, considering each current intensity tested. In particularly, also for the current of 3 A (maximum magnetization), the force didn't exceed 2000N, that is one quarter of the maximum forces awaited. This because fluid was filling up in the reservoir rather than flowing through the gap and providing the required force.

On the other end, if the pressure is too high, reservoir works as a gas spring, that has to be avoided.

By experimental test, pre-charge reservoir pressure was set equal to 10 bar.

Air presence in the cylinder chamber has to be absolutely avoided. Improvement in the damper performances can be noted in Figure 4.28, that represents a preliminary load cycle test at a velocity of 20 mm/s, with no activation of MR fluid. Red line corresponds to the presence of volume of air in the damper chamber, while in green line there is the same cycle but with total absence of it. In the former case, the force fell down completely in the first part of the compression stroke, i.e. when air was pushed through the annular conduit, without generating resistance (about 500 N instead of 2000N.

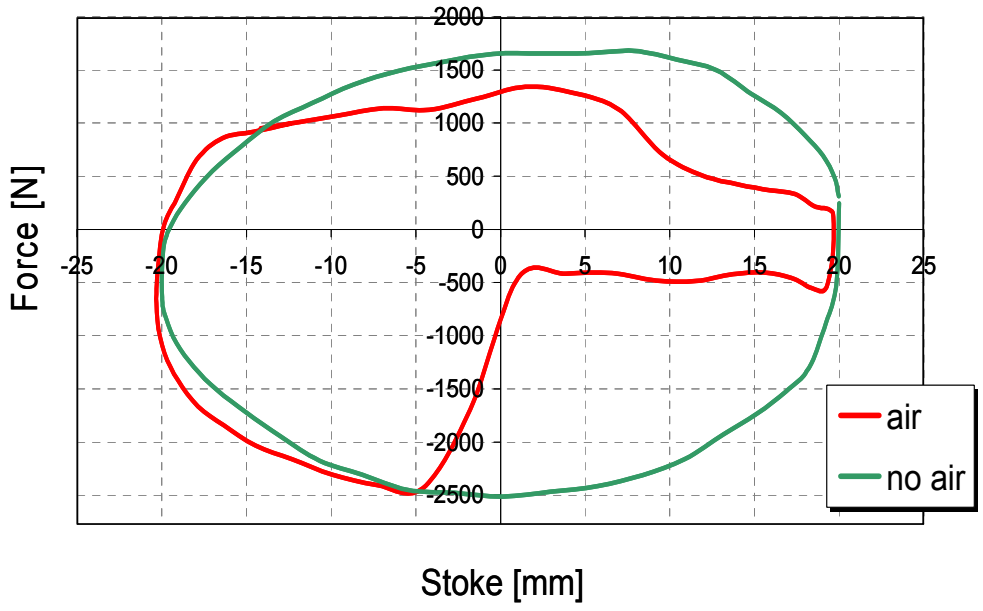

Figure 4.28 – Load vs. stroke performances (v=20 mm/s): effect of air presence in the cylinder chamber

Sinusoidal displacement of the piston (i.e. variable speed with a minimum in the peak of the sinusoid curve) has been tested in the same experiments previously carried out.

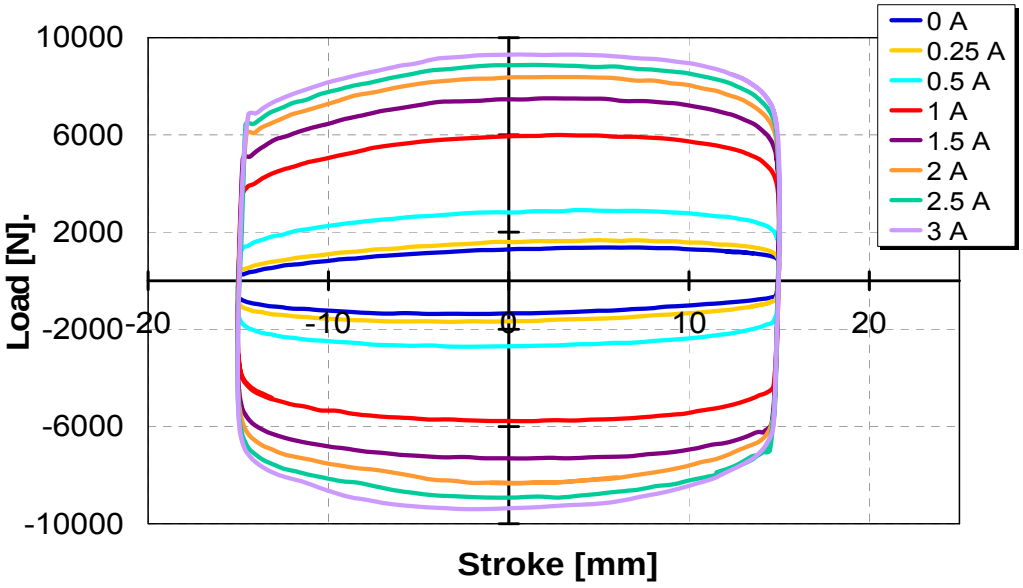

Figure 4.29 – Force vs. stroke curves with sinusoidal displacement excitation (speed 80 mm/s)

In Figure 4.29 is shown force vs. stroke curves with a sinusoidal displacement excitation with a piston speed of 80 mm/s, that is a sinusoidal frequency of 1 Hz.

It can be noted that the increase of the damping force until the objective values, passing from zero current, at which there is a purely viscous force, to the maximum current of 3 A. The uncertainty calculation allowed an estimated range of ± 315 N at each tests.
Unlike triangular tests, speed now is not constant; so the damping force receives a viscous effect variable. This contribution is maximal in the central part of the curves, where project values has been reached, and it reduces at least on its ends. At the same time peak force, where piston displacements change, tends to disappear.
Moreover, the viscous contribution in the total force become smaller at the increase of excitation current.
Figure 4.30 presents a comparison between tests with different sinusoidal frequency (0.5, 1 e 1.5 Hz) at constant stroke and current (respectively 20 mm and 3 A), while, in Figure 4.31, three different strokes (10-20-30 mm) at the same frequency (1 Hz) are reported.

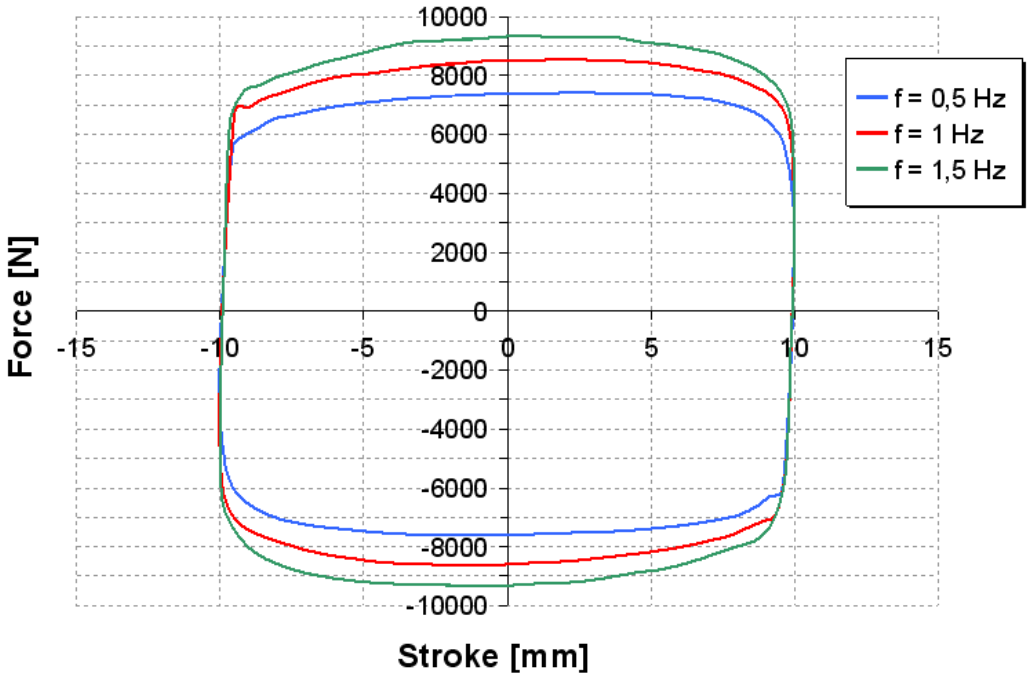

Figure 4.30 – Load vs. stroke performances with different sinusoidal frequency (0.5, 1 e 1.5 Hz).

As the stroke was maintained on a constant value, at the increase in the frequency corresponded a greater velocity. The resulting in total damping force was allowed by the viscous force. In fact, at the extremes of the curves, where velocity is common in all three tests, force values are almost identical.

Similarly to the previous case, in Figure 4.31 the viscous contribution, and therefore the force, increases with the stroke because of, at constant frequency, the velocity increases.

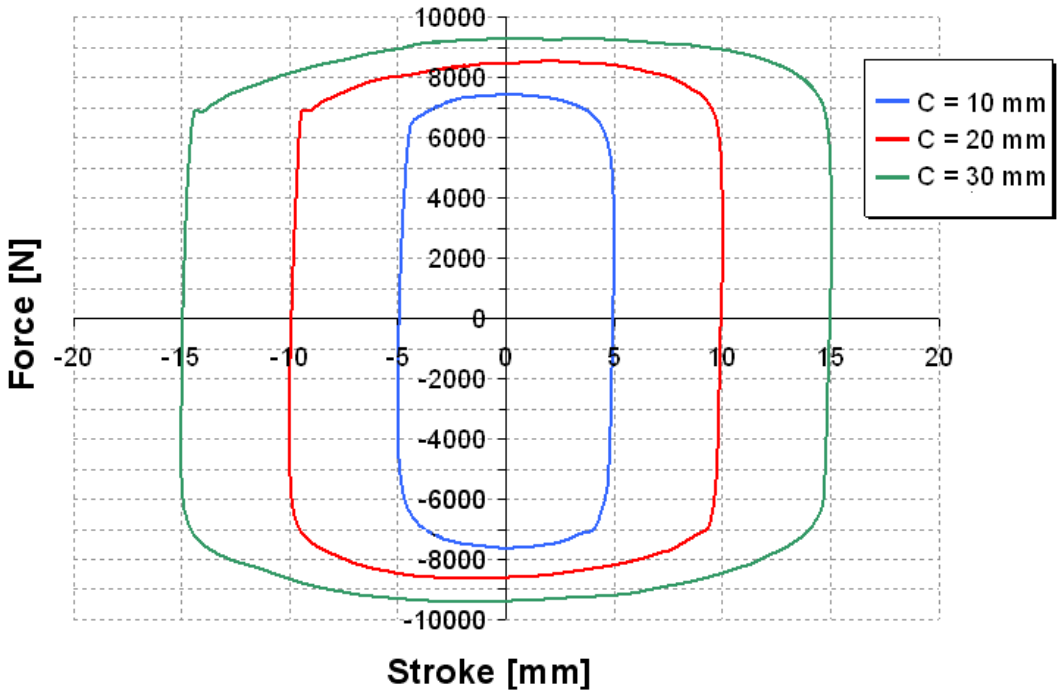

Figure 4.31 – Load vs. stroke performances with 10-20-30 mm of stroke at constant sinusoidal frequencies

4.5.2 Double ended damper results

Double ended damper presented in Section 4.3.3 has been tested, first of all, at the experiments carried out for the single ended damper summarized in Tables 6. Both triangular and sinusoidal displacement excitations was tested on MTS 322 T-slot 50 kN load machine.
Figure 4.32 presents the results of triangular test at piston velocity of 20 mm/s.

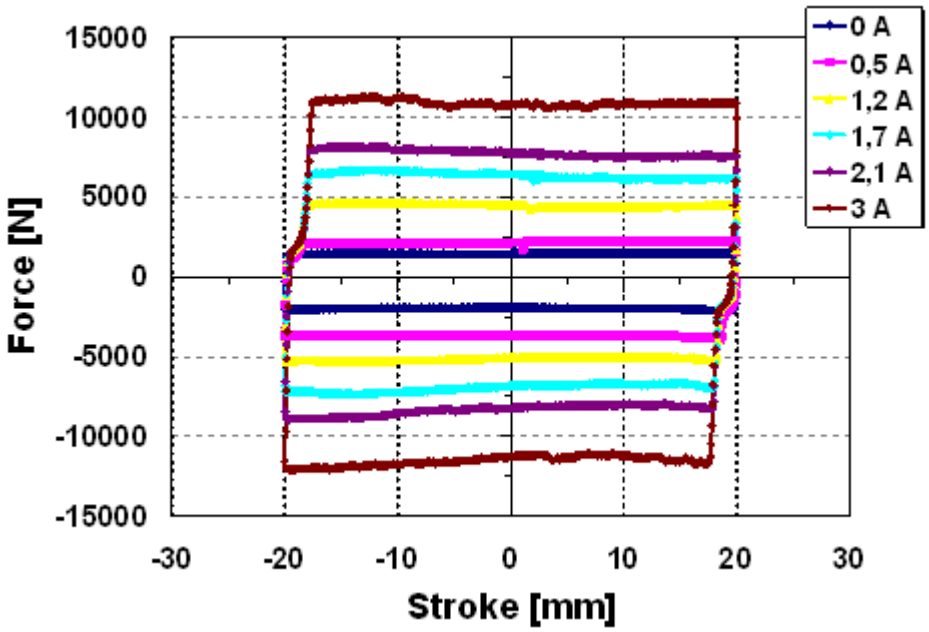

Figure 4.32 – Load vs. stroke performances (v=20 mm/s)

Magneto–rheological fluid performances depend on fluid rheological proprieties (see Section 2.3), but also on driving electric parts that regulate MR yield stress. Response time of the MR damper has been investigated.
Experimental tests, in order to study the velocity at witch damper provided a satisfactory response, have been carried out. The procedure consisted on the time measurements from the off-state to the on-state of the damper at different current intensity.

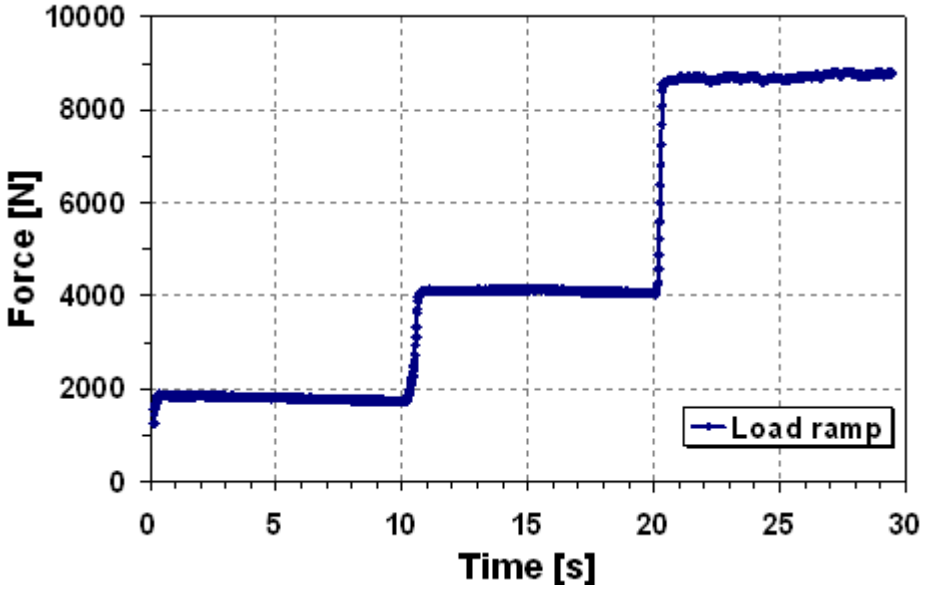

Figure 4.33 – Evaluation of response time in 60 mm stroke displacement in 0-1-2A drop.

Figure 4.33 shows the time that the damper spent to reach, starting from off-state, the target damping force at 1A and from this one to the target force of 2 A. Strokes were in a displacement ramp of 60 mm at a piston speed of 20 mm/s.

Response time in the 0-1 A shift was measured as 0,36 s, while 1-2 A shift was considered equal to 0,29 s. It can be noted that in both cases it is higher than the time of rheological fluid change (i.e. 20 ms as presented in Section 2.3).
Moreover, considering the 0-1 A shift and the 0-2 A shift, the response of the device was proportional to the input current in the electric coil (Figure 4.34): 0,36 for the former and 0,69 for the latter shift.

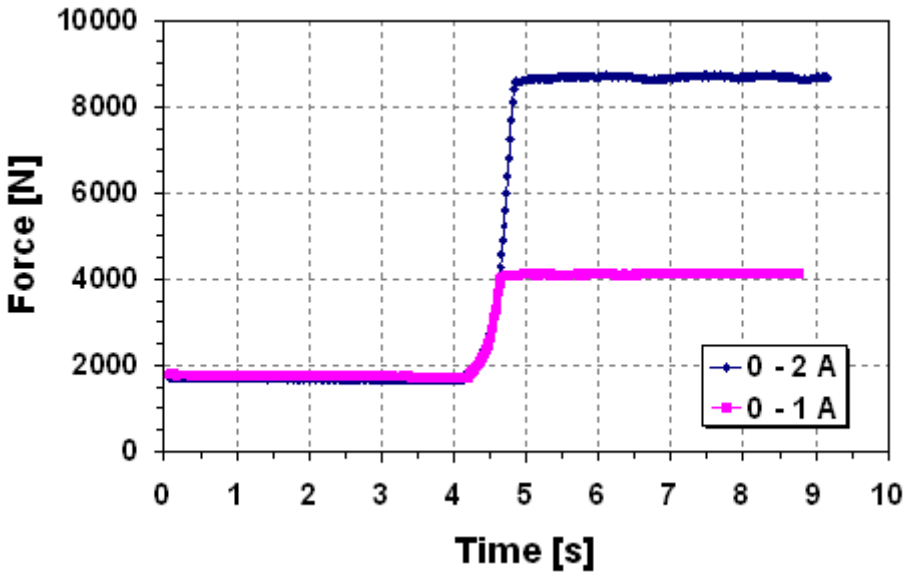

Figure 4.34 – Evaluation of response time in 60 mm stroke displacement in 0-1A and 0-2 A drop.

Evaluations of the velocity influence in the time response of the damper have been conducted.
The activation time of the damper by a 0-2 A shift of the input current has been studied, at a piston speeds of 10 - 20 - 40 and 80 mm/s.
As shown in Table 4.7, where it is reported the input time of activation and the time where the target force has been reached, the velocity of piston displacement was not strongly influent on the time of the activation of the damper performances.

Table 4.7 – Response time of MR device at given working velocity

velocity [mm/s]	response time [s]	time constant
0	0,837	286
10	0,903	301
20	0,896	299
40	0,915	395
80	0,851	284

As expected, response times are different if compared with the rheological change of the MR fluid.
The electric circuit of the damper can be simplified in a RL circuit diagram (see Figure 4.35), where *L* is the inductance and *R* is the resistance of the inner coil and the connections of damper.
According to [85], the time constant of the circuit can be calculate as:

$$T = \frac{L}{R} \qquad \text{(Eq. 4.5)}$$

If a current intensity *i* is applied, the performance of the temporal response is described by the following relation:

$$i(t) = I\left(1 - e^{-t/T}\right) \qquad \text{(Eq. 4.6)}$$

where *i* is the current intensity constant in the circuit and *t* is the time spent reaching the desired *i.*
This means that the current circulating in the coils, i.e. the damping force, takes time to reach the desired value. The duration of the transition does not depend on current intensity applied, but only by the time constant.

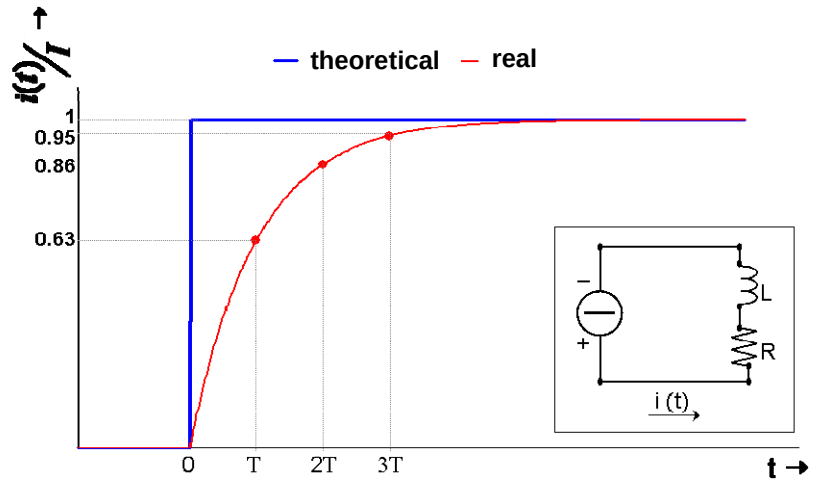

Figure 4.35 – Theoretical and real damper response trend. In the box is presented a simplified RL circuit of the MR damper.

Considering acceptable the device performances equal to the 95% of its maximum designed value, time constant can be calculated as

$$T = -t / \ln(1 - 0,95) = 0,3338 \cdot t \qquad \text{(Eq. 4.7)}$$

In the Table 4.7 are reported also the time constant for the 4 cases of study previously described. It can be noted that constant values were quite high and this suggest that circuit inductance should be reduced in order to maximize the response time of the damping system.
In Table 4.8 are resumed time constant values for several time targets :

Table 4.8: Time constants for time objective.

Time objective [ms]	200	100	50	20	10	5
Time constant [ms]	66,8	33,4	16,7	6,7	3,5	1,7

Finally, it was verified that MR fluid device response is not limited by the MR fluid but by the inductance and the resistance of electric circuit, such as output impedance of the driving system.
Fundamental in the device design is considerer the time constant of the electric circuit. The delay due to the inductance of the system has to be considered at the

moment of the activation of the fluid, in order to allow a better and efficient active response to the vibration load.

4.5.1.2 MR Damper temperature behaviour

As presented in Section 4.4.3, on the cylinder lateral surface of the device k-thermocouple sensors have been spot welded in order to study MR damper temperature behaviours. They were placed along the axial line identified in section (see Section 3.3.3), uniformly spaced at 45 mm. Measurement point was placed at 1 mm from the inner surface of the cylinder, in order to detect real fluid temperature during tests, without substantial losses due to thermal conduction effects in the metal. Table 4.9 summarizes the experiments carried out at different ram speed and in different magnetic conditions.
Triangular displacement excitations was tested, as seen in previous sections be more significant for the damper working. Evaluation time stopped as soon as temperature trend detected became constant. Acquisition frequency of temperature sensor was set equal to 10 Hz.

Table 4.9: Tested values of speed piston and current coil

Speed (mm/s)	5	10	20	
Current (A)	0	0.5	1	1.5

Figure 4.36 shows results in the case of damper piston that moved at velocity of 5 mm/s with 1 A of current intensity supplied.

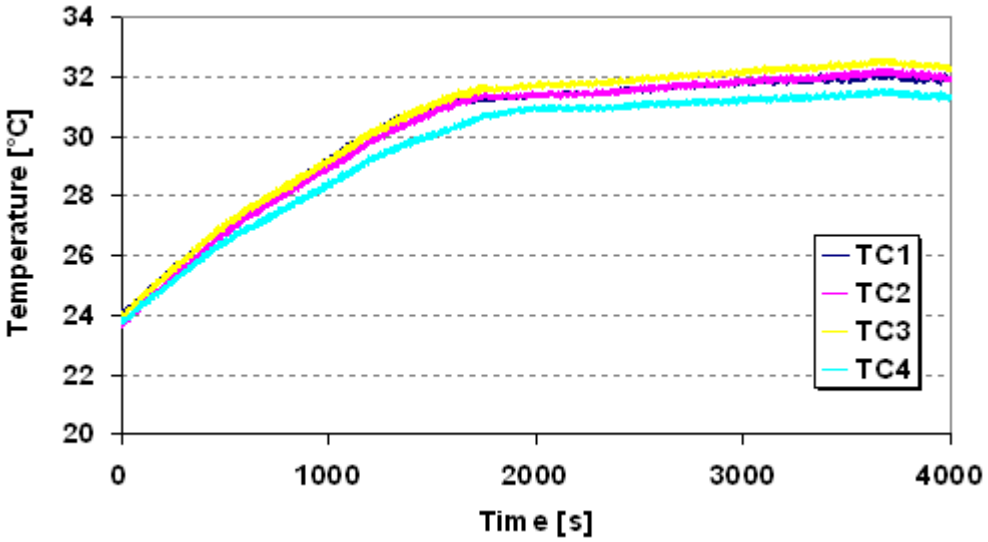

Figure 4.36 – Temperature behaviour evaluation (v = 5 mm/s; current intensity = 1A)

It can be noted that each thermocouple, starting from room temperature, after an initial drop where there was the maximum increase, reached a constant value where equilibrium between fluid temperature increase and thermal exchange took place. After about 1500 s temperatures were quite stable. Maximum temperature increase was usually between 7 and 9 °C and higher values were reached in the central thermocouples, TC2 and TC3, during the entire test.
More interesting results could be observed when the velocity of the piston and the magnetization increase.
Figure 4.37 shows results in the case of damper piston that moved at velocity of 10 mm/s with 1 A of current intensity supplied.

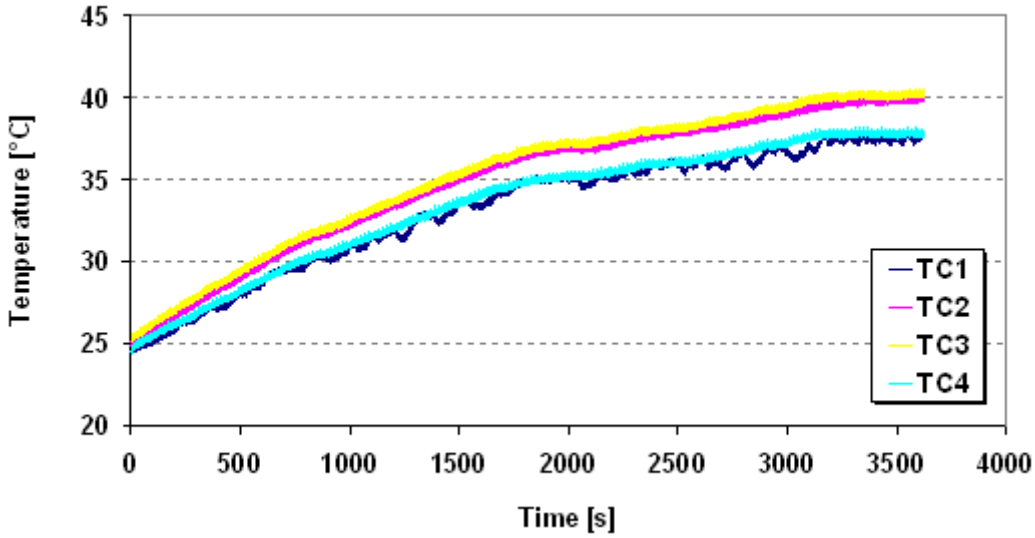

Figure 4.37 – Temperature behaviour evaluation (v = 10 mm/s; current intensity = 1A)

Doubling in piston speed, maximum temperature increased until values of 40,5±0,6 that is +25% higher compared with previous 5 mm/s test.
Also the drop of temperature increase change: after 1500 s temperature ramp is not ended and average constant values are obtained after about 3000s.
The same difference between thermocouples are maintained: central TC2 and TC3 reached values about 3°C higher than lateral ones. This can be explained considering that, next to the aluminium heads of damper, in both compressive and tensile piston displacements, there are the accumulation of the MR fluid that filled out of the annular gap. So higher mass can dissipate better the heat generated by friction and viscous forces during fluid rheological activation. Moreover this amounts of fluid are in contact with higher surfaces (cylindrical but also the sides of the aluminium damper heads) that provide to conductive effects and a quicker thermal exchange with the external.

Similar temperature behaviour can be reached by increase of the current intensity of the MR fluid.
Considering the average temperature values at a constant triangular displacement at 10 mm/s, graph in Figure 4.38 can be drawn. Temperature, as expected, tended to increase with the input current in the electric coils. That aspect can be explained thinking about the magnetic field. In effect, when magnetization was low (i.e 0,25 A) chain generation was not so strong and the viscosity of fluid was not sufficient to allow friction force work. The fluid flowed in the damper gap still in its original liquid state and only on piston and cylinder coupled surfaces fluid increased locally its viscosity. When the fluid was more strongly activated, and flux lines of magnetic field increased in magnetic inductance, chains became more resistant and viscosity increased. If, on the one hand, this required more applied load (i.e the vibration damping performance increased), on the other hand allowed higher friction and viscous works, that converted itself in heat that had to be dissipated by the device.
With 1,5 A it was obtained a value of 43,9± 0,8 °C, that represented the maximum value in the tests performed.
The same behaviour could be found analysing results at 20 mm/s velocity (Figure 4.39). Now maxima values of temperature increase were equal to 58,3±0,7 °C

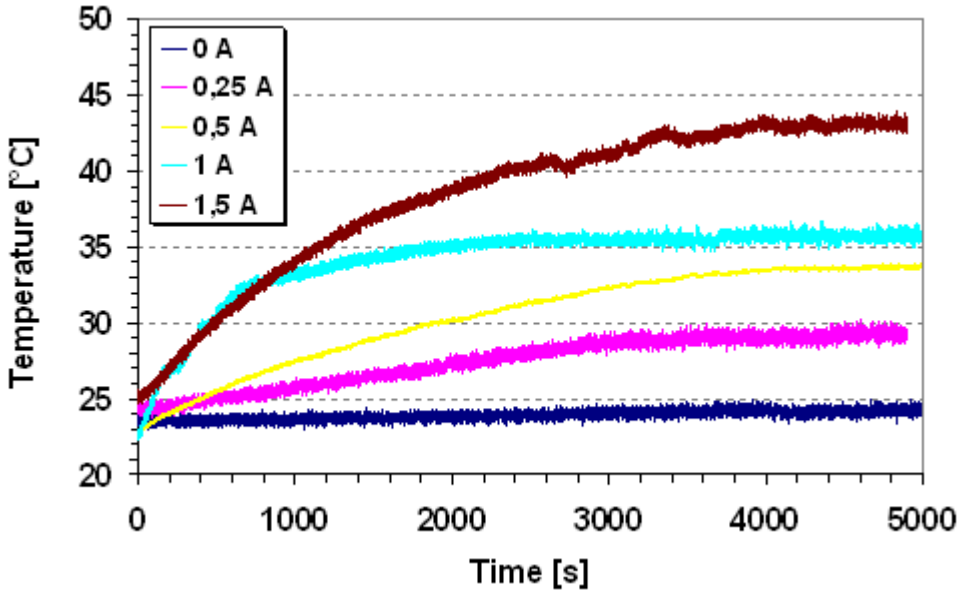

Figure 4.38 – Temperature vs. time evaluation at several input current values (v = 10 mm/s).

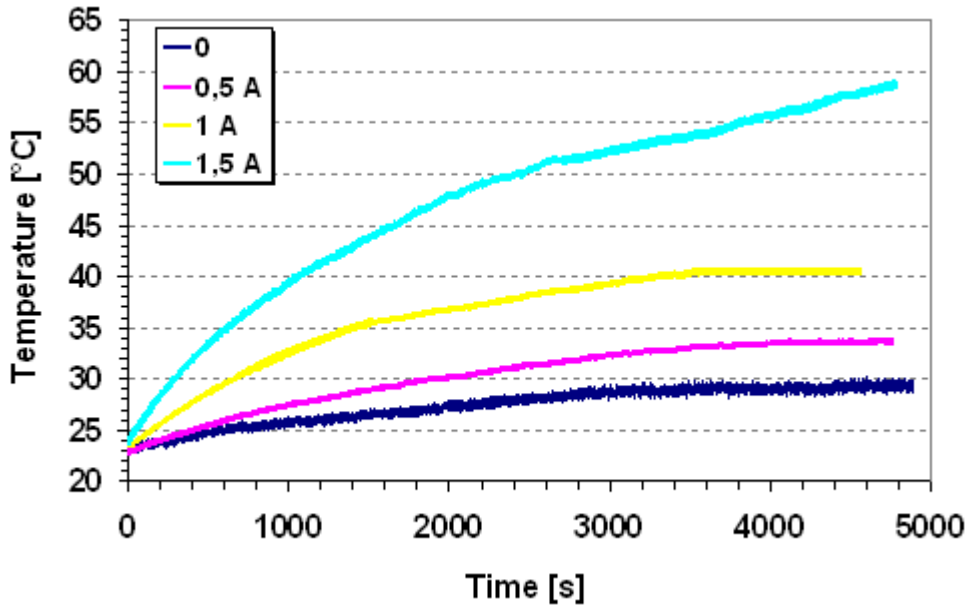

Figure 4.39 – Temperature vs. time evaluation at several input current values (v = 20 mm/s).

Ultimately, temperatures were quite affect by both the speed witch characterized the damper movement and the input current used to generate the magnetic field (Figure 4.40). In the case of lower currents (until 1 A) velocity of displacement was more influent on temperature increase, while the trend changed in the range of optimal activation of the MR fluid.

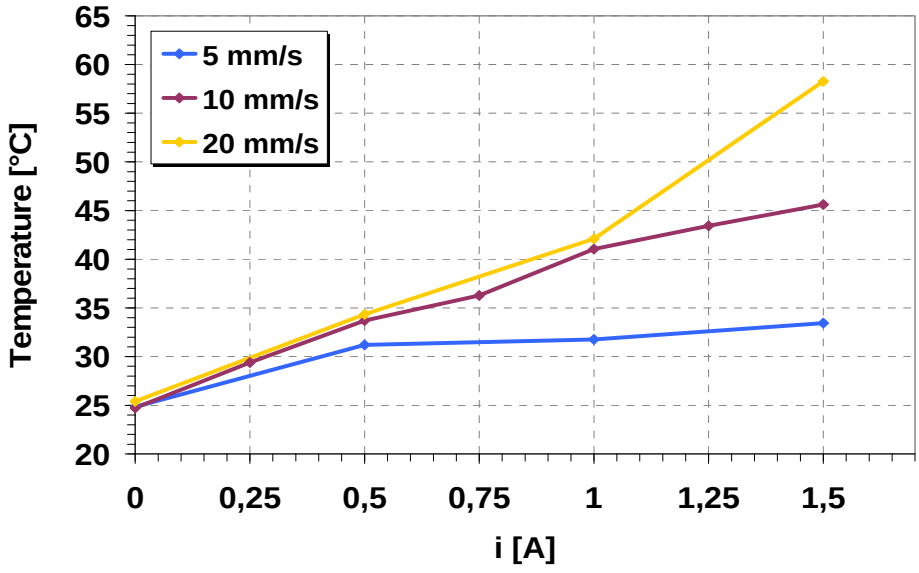

Figure 4.40 – Temperature vs. current intensity values at speed piston of 5- 10- 20 mm/s

The influence of temperature increase on MR fluid properties has been investigated (Figure 4.41). Considering the same operating time of 60 minutes, a piston speed of 10 mm/s and a current of 1,5 A in each test, average value of load has been calculated at every step of 0,5 °C.

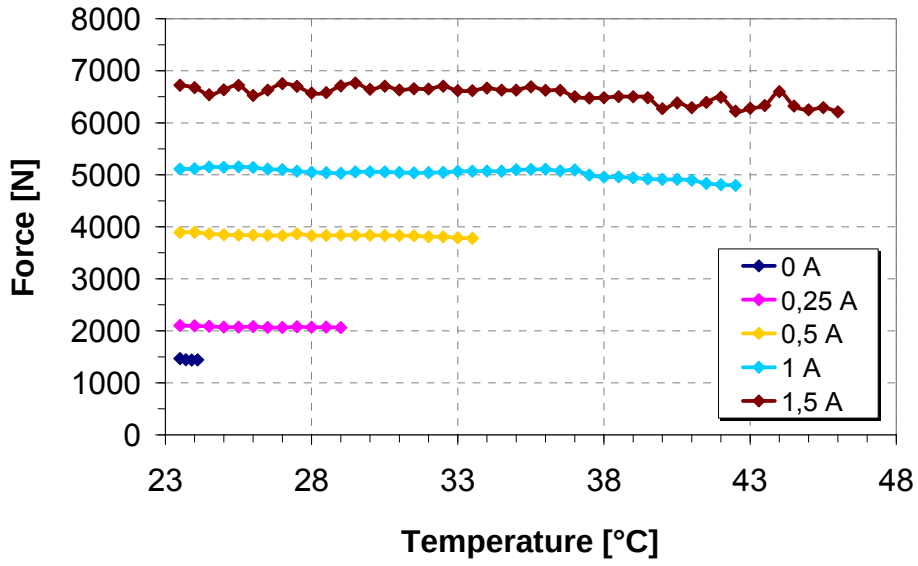

Figure 4.41 – Temperature effect on damping force at different input current (v=10 mm/s).

It can be noted value of load quite constant at temperature increase. A slight decrease in damping force was present with higher temperature values, according to plastic viscosity decrease [54].
Furthermore, at the same time, a dependence between the heating rate of the fluid and the piston speed can be observed (Figure 4.42). At low speed, it has been observed a slight increase of temperature, due to the viscosity of the activated fluid with respect to the greater working speed, where internal friction effect become significant.
A remarkable effect on device performances, in terms of maximum damping force, has been found. With a piston speed of 80 mm/s the force drop amounts to 27% (see Table 4.10).

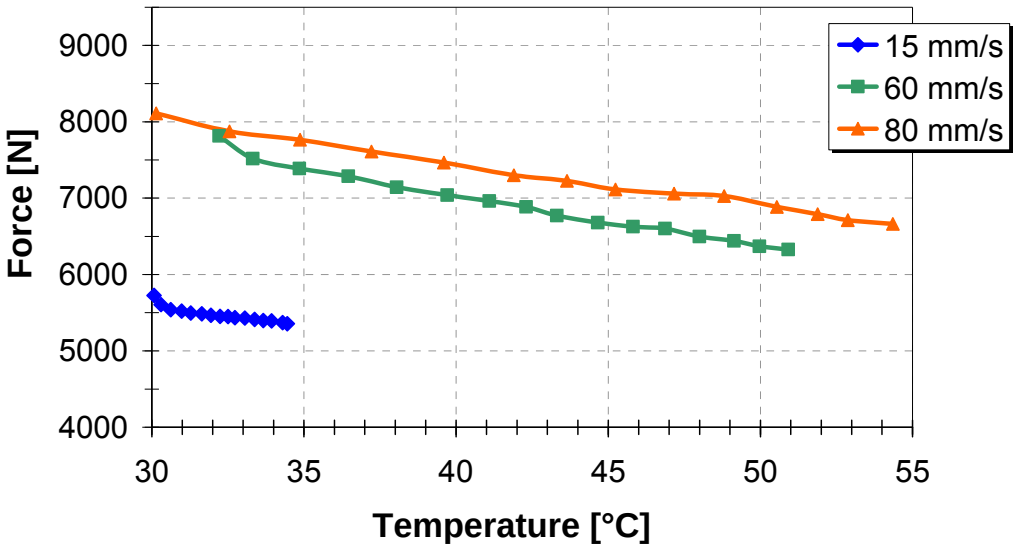

Figure 4.42 – Temperature effect on damping force.

Table 4.10 – Damping force drop with fluid temperature increase

	Piston speed (mm/s)		
	15	60	80
Initial temperature (°C)	30,1	30,2	30,1
Final temperature (°C)	34,4	50,9	54,4
Initial damping force (N)	5726	7815	9136
Final damping force (N)	5355	6328	6663
Force drop (%)	6,5	19	27

4.5.1.3 MR Damper inner pressure

Qualitative pressure detection has been allowed by the pressure manometer positioned in the aluminium head of the device (see Figure 4.13). In following Table 4.11 are reported the pressure values registered at different velocity of the damper piston (5-10-20 mm/s) evaluated in the range of input current of 0 ÷ 1,5 A:

Table 4.11 – Pressure values measured at different input fluid activation and piston speed

current [A]	V= 5 mm/s	V= 10 mm/s	V= 20 mm/s
0	4,3	5,1	9,8
0,25	-	7,0	-
0,5	7,3	10,9	11,8
0,75	-	13	-
1	17,1	19,8	23,1
1,25	-	25,0	-
1,5	22,4	29,2	38,3

As can be noted, pressure increased both with the velocity of the damper and with the change of the current *i*. As soon as the viscosity of the fluid increase, thanks to the current change, the forces became higher and this resulted in an increase of the pressure detected in the cylinder chamber. These values were in line with analytical expectation linked to the constructive calculations (as shown in Chapter 3) and showed that not particular pressure condition were reached thanks to the working mode of the damper.

4.6 CONCLUSIONS

Information about the influence of current in the load damping performances are needed to optimized dampers behaviour in the working process conditions.
In this chapter experimental devices completely developed at The Chair of Manufacturing University of Padova are fully described as well as the tests performed to study magneto-rheological device working and performances.
First prototype (20 kN) was developed in a single ended design to study the influence of the reservoir in the damping performances. Second prototype (10 kN), was based on double ended structure, where no influence of auxiliary equipment was present.
The effects of the input current on the final performances were studied, as well as the influence of noise factors and choices in the set-up.
Temperature an pressure of fluid during the work of the device has been also investigated.
Different tests were performed in order to value predicted and experimental result, obtaining a confirmation, in term of values of temperature and magnetic flux.

CHAPTER 5

MR DAMPER INDUSTRIAL IMPLEMENTATION

5.1 INTRODUCTION

Compared to most conventional dampers, which are passive hydraulic devices, MR dampers are semi-active devices where the damping capacity can be modulated either gradually or in real time based on the system response.
Thanks to this feature, MR dampers are expected to offer effective performance over wide ranges of amplitude and frequency, as demonstrated most notably for applications to control the low-frequency and large-amplitude vibrations of civil structures.
In the present chapter the industrial implementation of MR dampers will be introduced.

These devices were characterized by an elevate damping force (400 kN) along a considerable stroke.
An innovative solution to the volume compensation of fluids characterize their work.
The experiments were carried out on a four-column double-effect 2500kN hydraulic press manufactured by Omera Srl. Full-scale experiments set up to investigate feasibility and practicability of MR dampers and to understand the potential benefits (in comparison with conventional dampers) will be described and analysed

5.2 THE APPROACH

Although the working principle does not change, the characteristics of MR dampers for metalworking presses are quite different from those that are used for civil structures. The vibrations of metalworking presses caused by break through shocks are high-frequency and small-amplitude vibrations. Furthermore, long working strokes can be required, especially for hydraulic presses, which are equipped to carry out in one stroke a set of sheet metal working operations including blanking.
The design and construction of MR dampers has to be focused on realize devices suitable to hydraulic high tonnage presses. These were based on numerical and experimental know how obtained within the PhD period.
In order to evaluate the press system response to the break through shocks generated during blanking operations, through full-scale experiments has to be performed with the principal aim of evaluating the feasibility and practicability of implementing MR dampers. Potential benefits when they are used in a semi-active manner in comparison with conventional dampers needed to be studied.
The performances of the press equipped with the MR dampers in the time and the frequency domains were contrasted also with those achieved with the same press equipped with conventional hydraulic cushions and hydraulic shock dampers.

5.3 EXPERIMENTAL APPARATUS

5.3.1 MR dampers 400 kN

The MR dampers 400 kN developed to withstand the break through shock generated during blanking in a long-stroke hydraulic press are based on single end dampers architecture, as the laboratory prototypes shown in Chapter 3. A schematic section of the MR dampers is given in Figure 5.1.
A 1 mm thick annular orifice between the piston rod and the liner allows the fluid to flow through the entire annular region as the piston moves.
Four electromagnetic coils are seated in dedicated sections on the piston, using a 0.87 mm diameter copper wire. These electrical coils, embedded into the piston, generate

a uniform magnetic field across the gap and perpendicularly to the direction of the MR fluid flow.
The design of the actuator has involved the layout of the magnetic circuit. According with the procedures presented in Chapter 3 and Chapter 4, considerable effort has been put for the optimization of geometry components, in order to maximize the magnetic flux density in MR fluid without reaching the limit conditions that could affect the final performances during the current range of working. The circuit is powered by an input current varying from 0 A to 3 A.
During the blanking operation (at or just before the immediate release of the stored up energy) the coils may be activated, generating a shear resistance to the rod stroke in the axial active length of 240 mm.
The main characteristic of the devices developed for the implementation in the industrial context is the ad hoc solution designed for solving the problem of the volume fluid compensation during the piston rod displacements [87].
Because of space limitations in the blanking machine and in order to avoid the use of an external reservoir, an inner shaft, positioned in the cylinder housing, was designed in order to grant the alignment of the piston during the entire ram stroke (Figure 5.1).

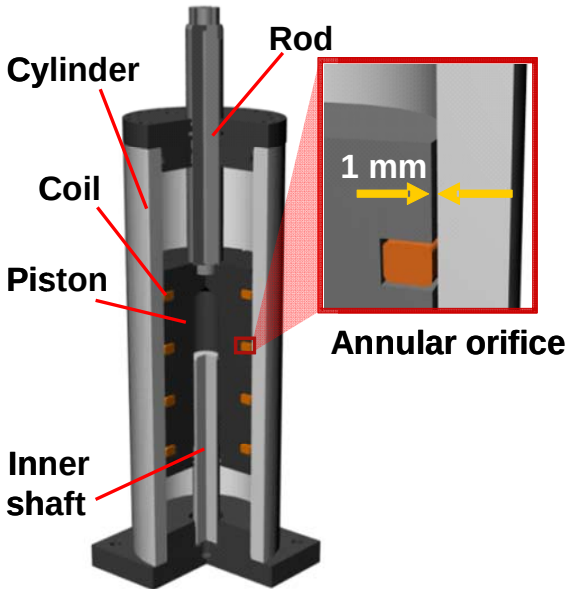

Figure 5.1 – Sketch of the MR damper. It can be noted the innovative solution of inner shaft for the volume fluid compensation problem.

The shaft has the equal diameter of the piston rod, as double ended solution, but without the geometrical problem of this last. It is coupled with the piston of the damper and it disappears, entering in the provided dead hole manufactured in the centre of the moving part.

An inner channel allows to a mineral oil flow, provided by the hydraulic unity of the press; this flow, activated when the piston is at the end of its stroke, allow to it to return in the target process position after each blanking steps.
This innovative solution allows to prevent any misalignment due to the high frequency vibrations that arise during the reverse load, and it solves smartly the use of a volume compensator to balance the volume change due to the rod stroke.
Figure 5.2 shows the four dampers in the working area of the press used for the experiments. The main mechanical and electrical features of the MR dampers are given in Table 5.1.

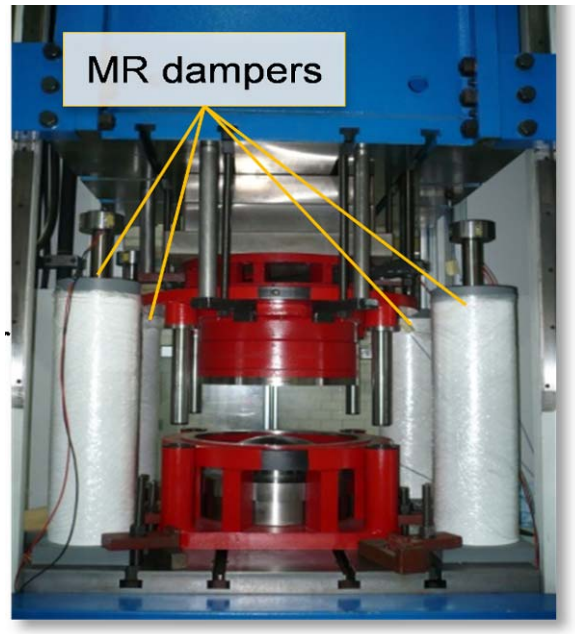

Figure 5.2 – The 4 MR Damper housed in the 2500kN hydraulic press bed for the experiments

Table 5.1 – MR dampers specifications.

MR DEVICE		
Nominal damping force	400	kN
Stroke	± 125	Mm
Cylinder bore	178	Mm
Inner annular orifice	1	Mm
Axial active length	240	Mm
Coil resistance	15	Ω
Coil inductance	0,34	H
Copper wire diameter	0,87	Mm
Current intensity range	0 ÷ 3	A

The experimental apparatus consists of a long-stroke hydraulic press equipped with a die set, dampers and a data acquisition system.

5.3.2 Hydraulic press and die set

The experiments were carried out on a four-column double-effect 2500kN hydraulic press manufactured by Omera Srl, presented in following Figure 5.3a.
The press has a four columns O-type frame, in order to grant high stiffness and small deflections during the forming operations, like drawing, redrawing, and coining. The machine specifications are reported in Table 5.2.

Table 5.2 – Hydraulic press specifications.

Capacity (adjustable) [kN]	2500
Stroke length [mm]	800
Speed range [mm/s]	1-52
Table dimensions [mm]	1200 x 1100
Total dimensions [mm]	2280 x 2321 x 5370
Point gap frame	2

The used tooling device was a double action die, in which the blank is first separated from the straightened strip and then deformed to obtain a hemispherical shape. The sheet metal is blanked between the upper annular punch and the die plate at first, and then deep drawn by the spherical lower punch, housed in the machine bed. Both the upper punch and die plate are flat, in order to enhance the blanking force peak and the break through shock.
The blanking operation was performed by the slide, which descended and gripped the blank. Figure 5.3b and Figure 5.3c show a picture and a sketch of the die set. In the tests, only the first part of the process, related to the blanking operation, was monitored.

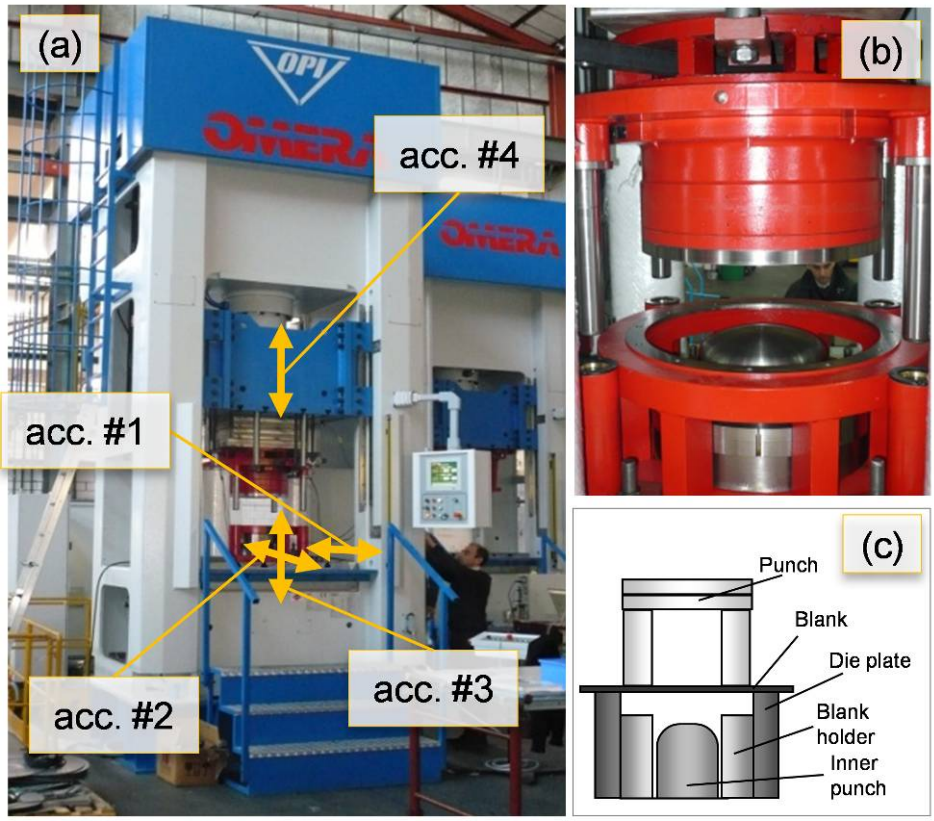

Figure 5.3 – The 2500kN hydraulic press with indication of the accelerometers, (left). Detail view and sketch of the tooling (right).

Damping devices

The experiments were carried out with three different kinds of damping systems. In addition to the MR dampers described in Section 5.2.1, conventional hydraulic cushions and hydraulic dampers were utilized.

The former system, shown in Figure 5.4 (right top), belonging to Type I hydraulic dampers described in Section 2.3.1, consisted of four cylindrical dampers, whose chambers were connected in parallel to a common oil manifold. . The working stroke and maximum counter force were 40 mm and 80 kN, respectively. The hydraulic circuit allowed calibrating the initial inner pressure in the four chambers according to the power required by the process. This device may provide an upward counter-force only through the compression of the oil inside the chambers.

The second system is composed by four dissipative dampers belonging to Type II hydraulic devices described in Chapter 2. They provide the counter upward pressure force by governing the oil flow through valves and a fixed orifice in a reservoir. An external hydraulic power unit is necessary to control the oil pressure of each damper and the valves of the hydraulic circuit. The working stroke and maximum counter force were 20 mm and 200 kN, respectively. These dampers are shown in Figure 5.4 (right bottom).

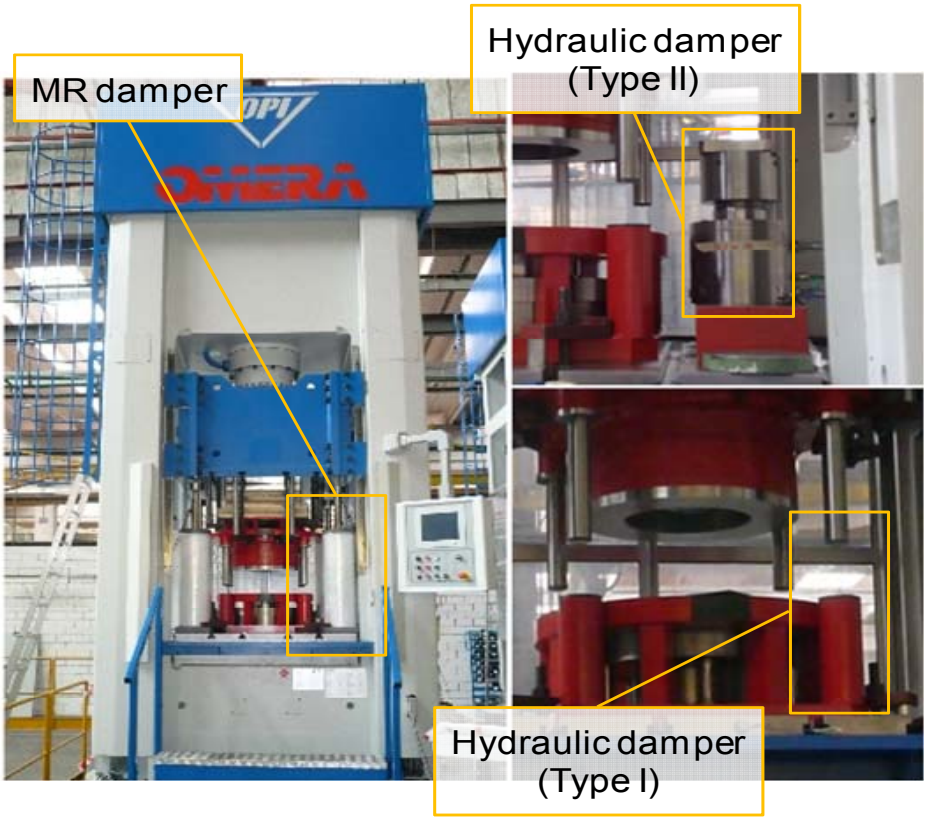

Figure 5.4 – Mr damper in the press on the left; on the right, details of Type I hydraulic dampers (top) and detail of the Type II hydraulic dampers(bottom).

Data acquisition system

During the blanking experiments, the data regarding the pressure and acceleration were acquired by using an acquisition system capable of real time monitoring up to 100kHz, which consisted of a PC equipped with a National Instruments™ acquisition board and LabView™ software.

In order to compare the performances of the tested devices, the pressure of the press manifold and the vibrations arising during the reverse load were measured during the experiments. Accordingly, the press system was equipped with the following sensors, resumed below:

- *pressure measurement sensor* (Hydac HDA4400), mounted on the manifold of the upper actuator, which governs the downward motion of the slide. The sensor target data, used to monitor the pressure applied during the blanking operation, are reported in Figure 5.6;
- *accelerometers* (Kistler® 8704 B 500 M1), to measure the machine vibrations under the different testing conditions. Four single axis piezoelectric

accelerometers were used to monitor the vibrations in different directions. The positions and the directions of acceleration measurements are specified in Figure 5.4. The accelerometers target data are reported in Figure 5.5

Measuring ranges	bar	16 ÷ 600
Rise time	ms	2
Operating temperature range	°C	- 40 ÷ 100
Accuracy	≤ ±0.5 %FS	
Hysteresis	≤ ±0.4 %FS	
Linearity (DIN 16086)	≤ ±0.3 %FS max	

Figure 5.5 – Hydac HDA4400 sensor target data

Measuring ranges	g	± 500
Sensitivity	mV/g	10
Frequency Range	Hz	1 ÷ 10000
Resolution, Threshold	mgrms	10
Shock	g	5000
Operating temperature range	°C	-55 ÷ 120

Figure 5.6 – Kistler® 8704 B 500 M1 accelerometer target data

5.4 EXPERIMENTS

5.4.1 Experimental plan

The blanking experiments were conducted on 2 and 3 mm thick C40 steel sheets with a constant punch-die clearance of 0.2 mm. All the tests were performed at room temperature, with a constant slide speed of 20 mm/s; a constant amount of lubricant was applied on the metal blank by a roller lubricator.
Tools with flat surfaces of the punch tip and the die were used, in order to obtain a rapid force built up during shearing. The symmetric shape of the component prevented lateral deflections induced by the geometry of the blanked part. The experiments were repeated for four different configurations of the press: with no

damping device, with MR dampers, with hydraulic cushions and hydraulic dampers. The experiments with the MR dampers were carried out using four levels of current intensity: 0.4, 0.6, 1.1 and 2 A. To assure the repeatability of results, all the experiments were replicated at least twice.

5.4.2 Damping force of the MR dampers

The damping force of the four MR dampers for different values of the current intensity and the punch speed were measured through experiments carried out on a 1000kN servo-hydraulic INSTRON testing machine. Figure 5.7 shows the curves of the force vs. current intensity of the MR dampers for a fixed value of the punch speed.

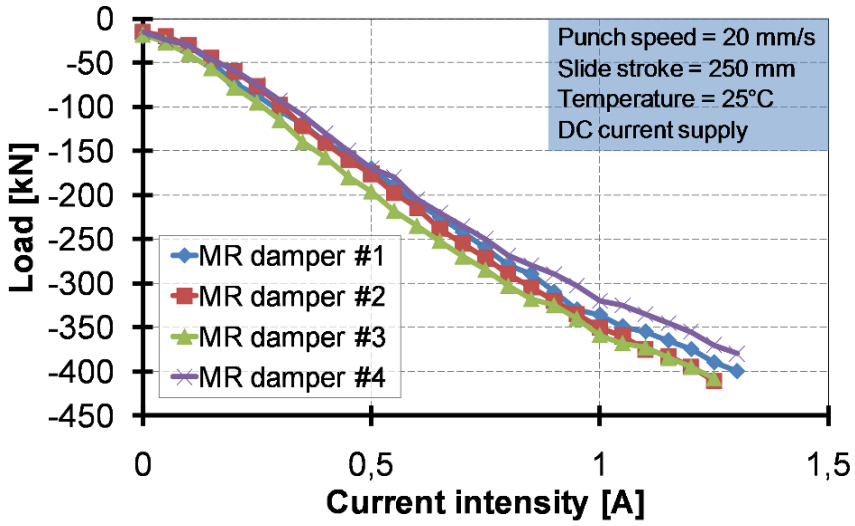

Figure 5.7 – Force vs. current intensity curves of the MR dampers for a fixed value of the punch speed.

The speed used was the same of the blanking process and the devices were tested along the entire stroke. For the four dampers, the damping characteristics are very similar: the damping force is constant along the entire testing stroke and presents a good linearity with the current intensity.
These features make the dampers suitable to be easily controlled during the entire stroke of the press.

5.5 RESULTS

5.5.1 Vibration analysis

At first, the optimization of the moment when activate the damper was fundamental, in order to provide an optimal damping effect without negative upward counter–forces. Several tests had be performed to identify the right moment, considering the response time of the devices (see section 4.4) and the dynamic of the specific blanking process.
Figure 5.8 shows the results of the optimization of the damper activation. Referring to the press stroke, several efforts were carried out activating the MR fluid before or just after the break through of the material. On the one hand, if too early, damping is not efficient and rather negatively affects the machine power required. On the other hand, if the dampers were activated too late, reverse load had already happened and the ram oscillation were remarkable.
Optimal moment was identified when the punch was at 5 mm above the blanking of the part.

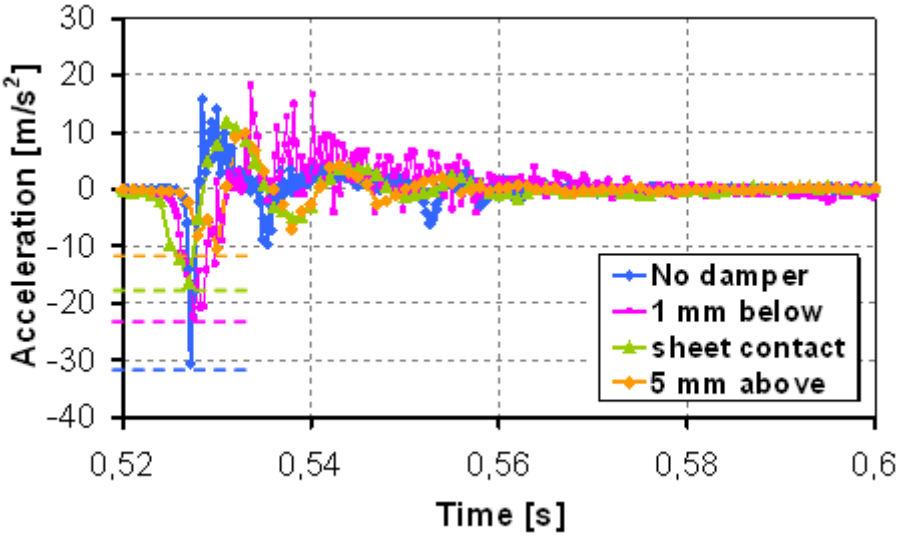

Figure 5.8 – Acceleration measurement at different damper activation referring to press stroke, according with the position of the sheet plate.

Figure 5.9 shows in the time domain the effect of the current intensity in the MR damper circuits on the response of the press system to the break through shocks. Damping performance increases with the current intensity until a critical value of 3 A generates the saturation of the magnetic circuit and the permanent magnetization of the particles in the MR fluid. A value of 1.1 A proved to be an appropriate compromise between damping performance and system stability.

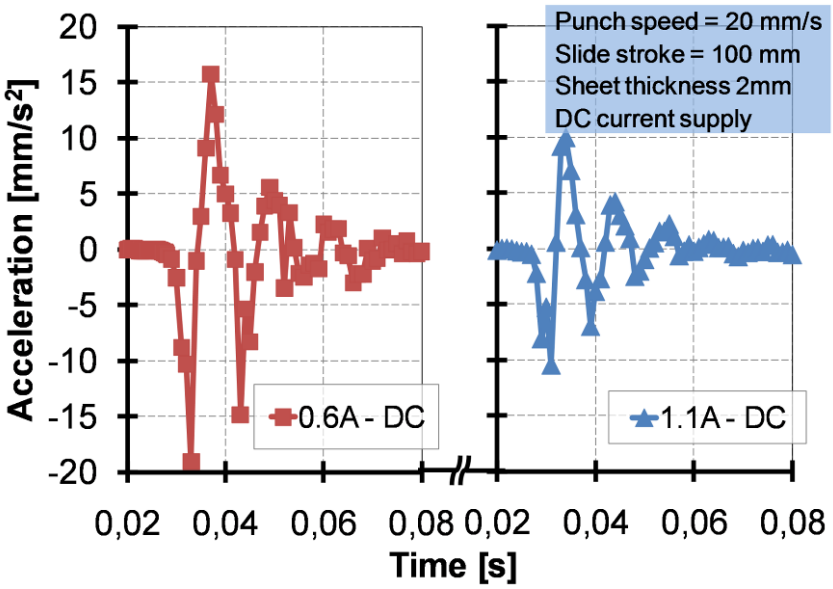

Figure 5.9 – Accelerations measured at press ram for different electrical currents with the MR shock dampers

Following Figure 5.10, Figure 5.11 and Figure 5.12 show the acceleration-time response over the duration of the break through vibration when the press system is equipped respectively with the hydraulic cushions (Type I), the hydraulic dampers (Type II) and the MR dampers. Each of the three responses is compared to the one measured on the press without any damper device.

Reductions in the peak acceleration are achieved by using both the hydraulic cushions and the MR dampers.

The accelerations measured using Type I hydraulic dampers presented lower peaks than the ones obtained with the other shock absorbers, but this typology of devices had poor damping properties compared to the un-damped machine, since the blanking vibrations decayed with the same time and the same frequency.

Vibrations measured with Type II hydraulic dampers presented the largest amplitude, and high frequency vibrations continued to propagate in the press frame after blanking.

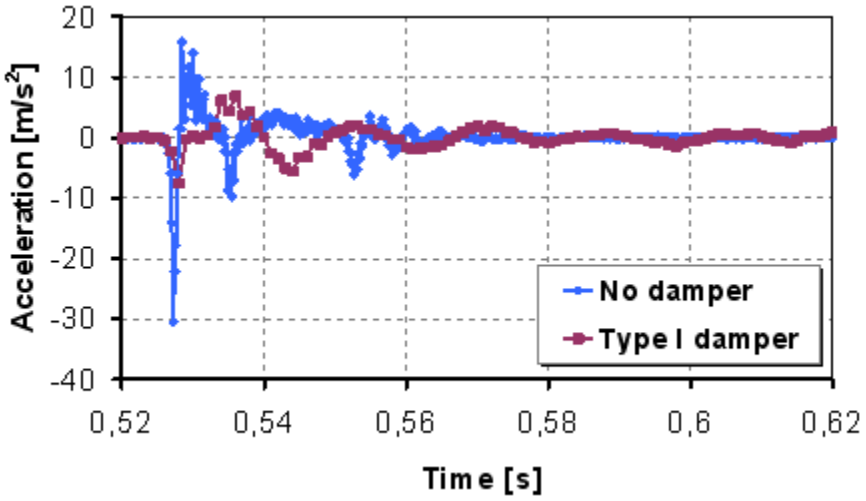

Figure 5.10 – Accelerations measured with the Type I cushion system (2 mm)

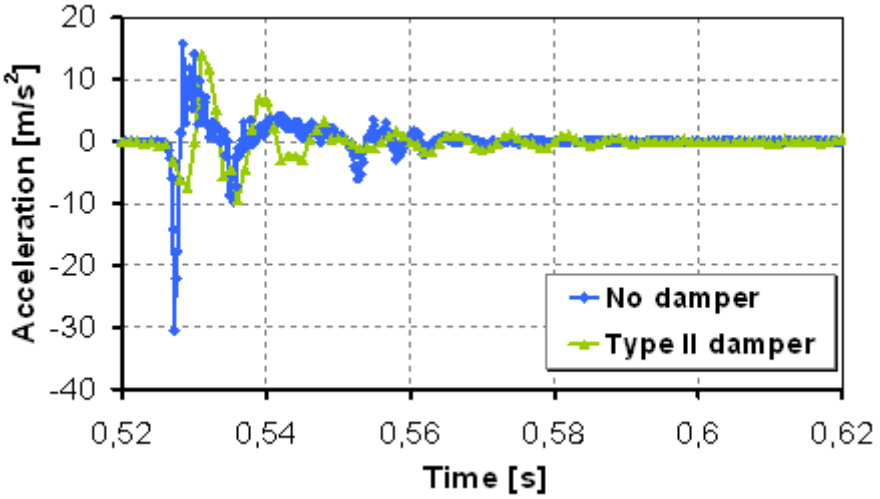

Figure 5.11 – Accelerations measured with the Type II hydraulic shock dampers (2 mm)

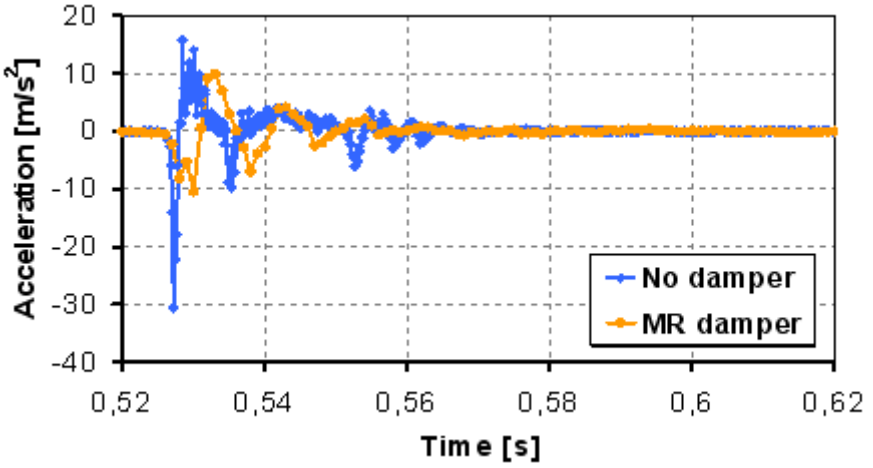

Figure 5.12 – Accelerations measured at the press ram with the MR shock dampers (2 mm).

Compared to the response of the system equipped with the conventional dampers, the decay of residual vibrations that was observed with the MR dampers was significantly faster. Approximately the reduction found reach the value of 30% if they are compared with Type I and 10% if compared with Type II system. This is because the damping effect of the highly viscous MR fluid (when the magnetic field is activated) predominates over the unavoidable elasticity of the fluid pressurized in the conventional dampers.
Analysing the acceleration results in term of frequency of damped system ω_d [81] it can be observed, as shown in Table 5.3, that MR damper allowed a reduction of the 10% compared to the Type II hydraulic dampers. This decrease in the frequency of damped vibration means an increase of amount of total damping.

Table 5.3 – Frequency of damped system ω_d of the tested conditions.

DAMPERS	ω_d [rad/s]
no damper	~ 800
Tipe I	~ 400
Tipe II	~ 800
MR	~ 700

Figure 5.13, Figure 5.14 and Figure 5.15 show the amplitude spectrum of the ram acceleration in the domain of frequency for the press system equipped respectively with the hydraulic cushions (Type I), the hydraulic dampers (Type II) and the MR dampers. FFt analysis consider values from the punch – sheet contact until material fracture, in order to delete noise errors.
Each of the three spectra is compared to the one measured on the press without any damper device. As expected, the spectrum diagrams for the press machine without any damper shows a high number of excited frequencies, with the highest values close to 25Hz
Moreover, the spectrum shows that also the frequencies excited can be significantly reduced by using the developed MR prototypes, thus reducing significantly the risk of resonance (under 100 Hz) for the press structure and the tooling.

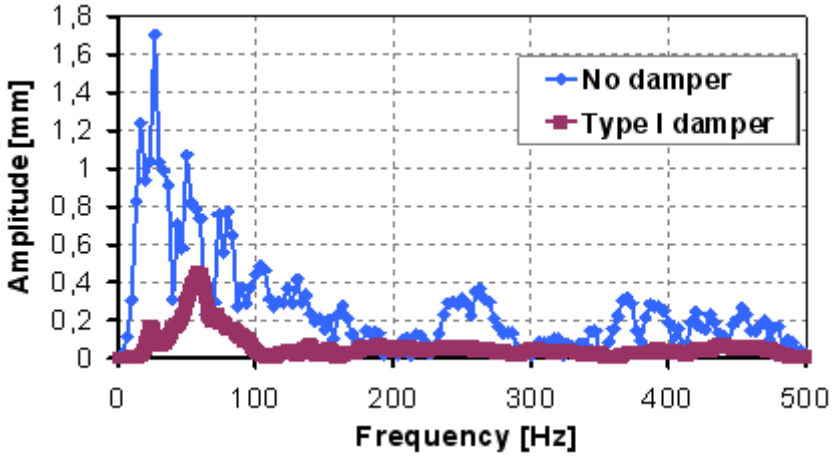

Figure 5.13 – Amplitude spectra of accelerations with the Type I cushion system(2 mm)

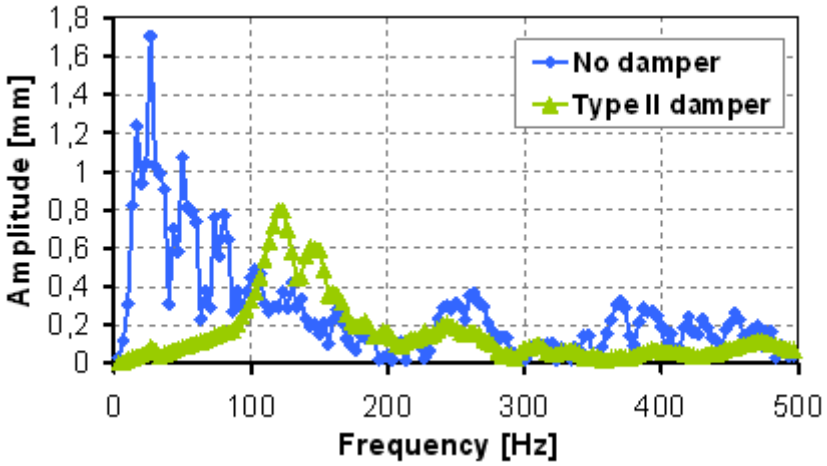

Figure 5.14 – Amplitude spectra of accelerations with the Type II hydraulic dampers (2 mm)

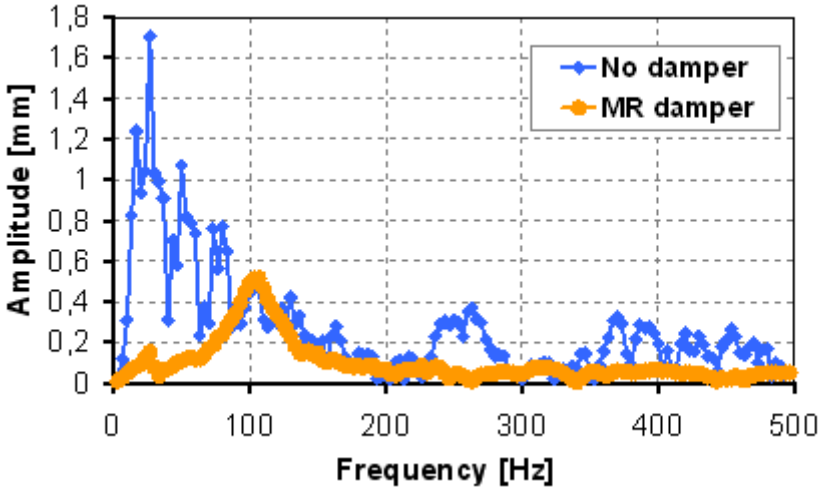

Figure 5.15 – Amplitude spectra of accelerations with the MR shock dampers (2 mm)

Significant reductions of the number of the excited frequencies and the acceleration amplitudes are observed for the three kinds of dampers. However, the hydraulic cushions behave worse than the other two shock dampers typologies since they are not able to damp the low frequencies vibrations that are typical of the tested hydraulic press.
Among the latter, the amplitude of vibrations measured with the MR dampers is approximately 40% less than the one obtained with the hydraulic dampers.

Considering results for the tests with 3 mm plate, similar considerations can be found. As it can be noted in following Figure 5.16, Figure 5.17 and Figure 5.18, accelerations are in general greater than 2 mm plate: 33,8 m/s^2 and 19,2 m/s^2 peaks are reached respectively in the no damping and with hydraulic cushion damper conditions. Moreover, as expected, the blanking vibrations of un-damped machine decayed with a time longer than 2 mm case (on the average 0,2 s more that previous case) due to the different thickness of the sheet.
Type I hydraulic dampers confirmed their lower damping properties compared to the other three kinds of dampers and no-damped condition (Figure 5.17). Decay time of the vibration is reduced but acceleration peaks are remarkable.
Type II hydraulic dampers and MR damper presented similar behaviour considering acceleration range, but decay time of MR damper is lower (about 40 %).

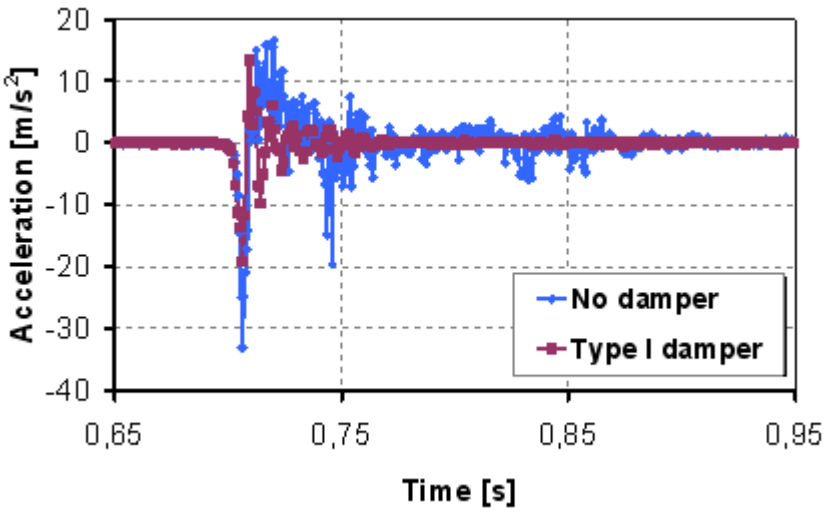

Figure 5.16 – Accelerations measured with the Type I cushion system (3 mm)

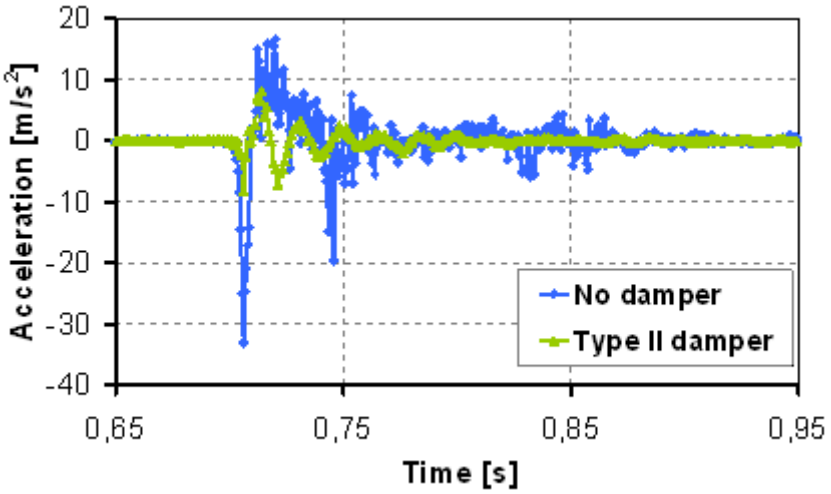

Figure 5.17 – Accelerations measured with the Type II hydraulic shock dampers (3 mm)

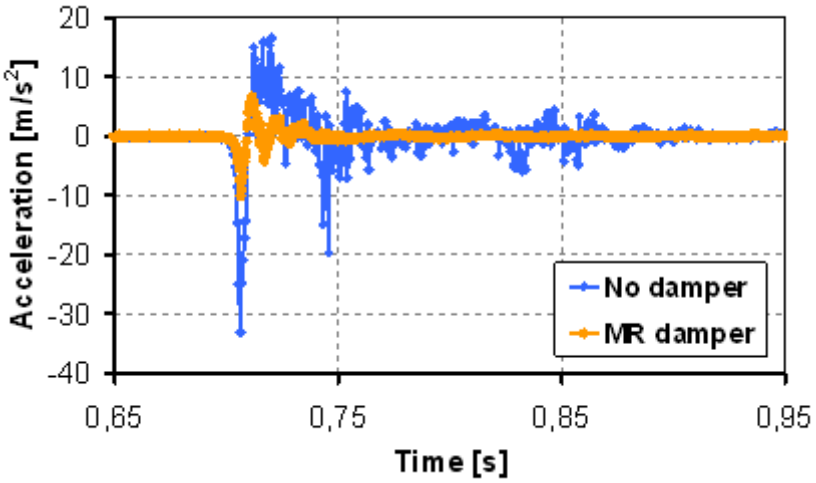

Figure 5.18 – Accelerations measured at the press ram with the MR shock dampers (3 mm).

The analysis of the amplitude spectrum in the domain of frequency for three damping system, presented in Figure 5.19, Figure 5.20 and Figure 5.21, shows that MR damper allowed a reduction of the amplitude peaks (that are, with both hydraulic solutions, closes to the un-damped machine vibration) and a shift towards high frequency of the critic value, that is out of the range of risk of resonance.

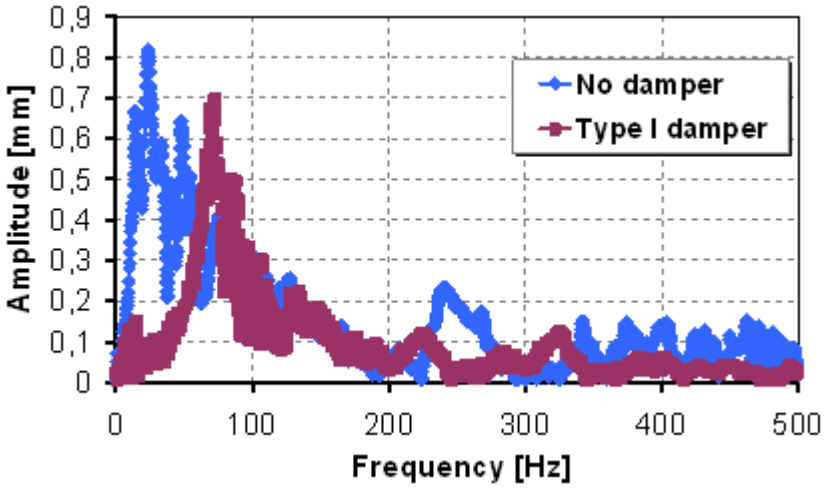

Figure 5.19 – Amplitude spectra of accelerations with the Type I cushion system(2 mm)

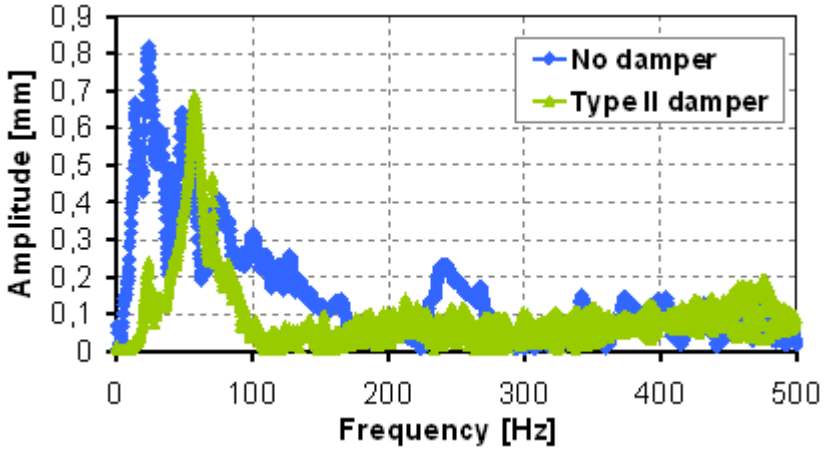

Figure 5.20 – Amplitude spectra of accelerations with the Type II hydraulic dampers (2 mm)

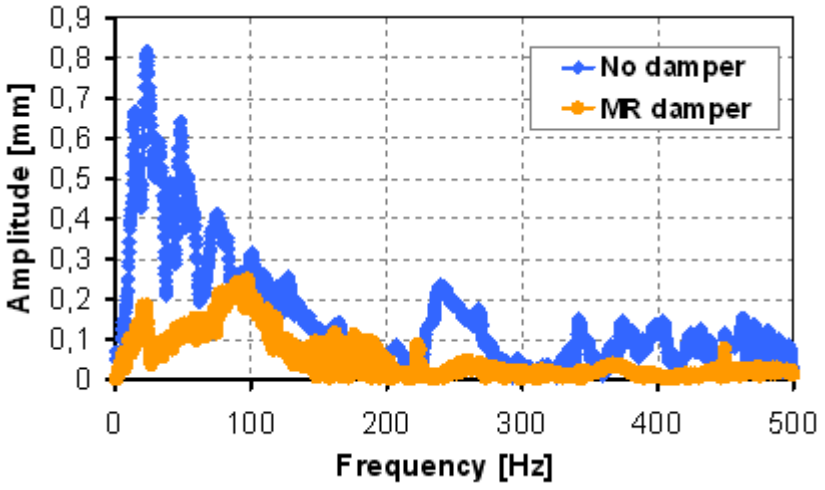

Figure 5.21 – Amplitude spectra of accelerations with the MR shock dampers (2 mm)

5.5.2 Press power analysis

Figure 5.22 resumes the pressure measured at the manifold of the slide actuator in the experiments with the 2 mm thick sheets. The blue curve, obtained without using any damping device, shows the typical steps of the theoretical blanking process. After the metal sheet fractured, pressure decreased from 100 bar to 0 bar in about 0.03 s. Some pressure variations are due to wave propagation monitored in the hydraulic circuit.

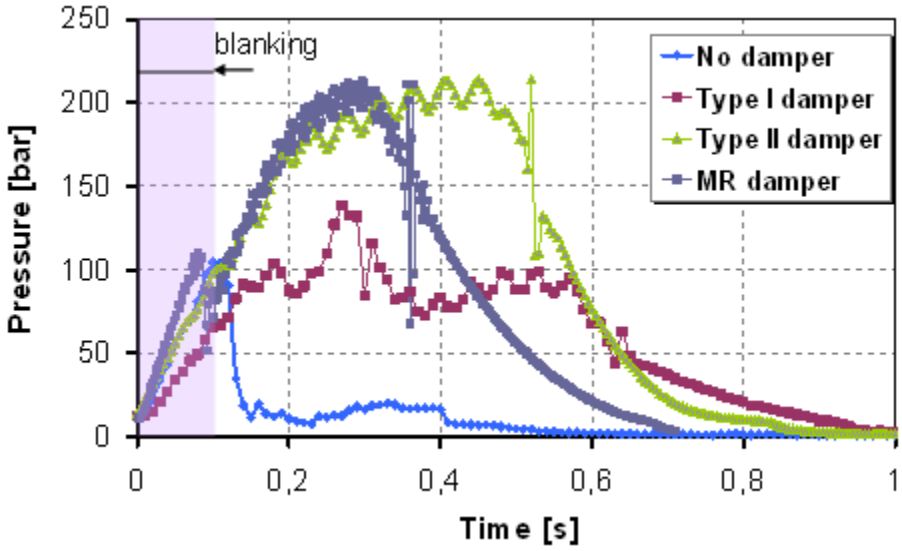

Figure 5.22 – Pressures measured at the manifold of the slide actuator during the tests

The use of the tested shock dampers causes an increase of pressure at the manifold of the slide actuator, due to the upward counter-force applied by the damping devices just before the material shearing took place. Thanks to the active behaviour of the magneto-rheological fluid, the MR dampers (violet curve in Figure 5.22) exercise a variable upward counter-force that can be switched off just after the sheet metal blanking, thus reducing the cycle time of the total process. On the contrary, both Type I and Type II hydraulic devices tested, could not be switch off after the blanking operation and continue to apply an upward counter-force up to the end of the slide stroke, increasing the power energy used. The total load required by the process in case of using hydraulic dampers increase significantly, exceeding the one requested for the sole blanking operation.

5.5.3 Fracture surface analysis

The fractured surfaces of the sheet, after the blanking process describer in section 5.2, were qualitatively analyzed, using laboratory microscope 10x. Quality, roughness and extension were investigated for every case of vibration damping.
According to Figure 5.23, fractured surfaces could be divided in two main zone, as defined: shear zone and fracture zone, both results of fracture process [15].

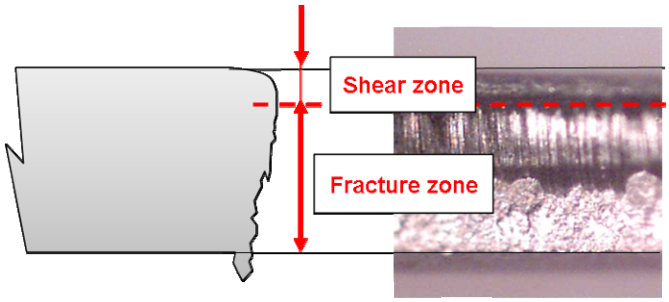

Figure 5.23 – fractured surface: shear zone and fracture zone distinction.

Figure 5.24 shows the fractured surface of 2 mm sheet resulting after each blanking process. It can be noted that width of both surface changed considering the typology of damping. In particular, between shear and fracture zone, a third area could be observed, highlighted in the orange dotted line in the pictures. This surface appeared scratched and quite polish; then it was called *scratch zone*. Its amplitude decreased in the sheet results of blank with damping systems. A possible explanation was principally linked to the oscillation of the press ram after fracture of the material and during reverse load effect (Section 2.2). When the storage energy dissipated as ram oscillation, machine punch scrubbed and scratched at the fracture interface. An improve of the damping meant a reduction of the oscillations, of relative amplitude and therefore a reduction of scratched area.
Minima values could be found with blanking damped by MR damper (Table 5.4), that suggested that these systems could reduce the influence of tool vibrations due to the blanking shock, allowing, as the other systems, an increase of shear zone compared to the fractured thickness.
Figure 5.25 shows the fractured surface of 3 mm sheets. It can be noted that scratch zone again reduced in width, passing from the un-damped to the damped cases. Moreover, in MR damper case shear zone was maximum and it was about 20% more that hydraulic Type II dampers.

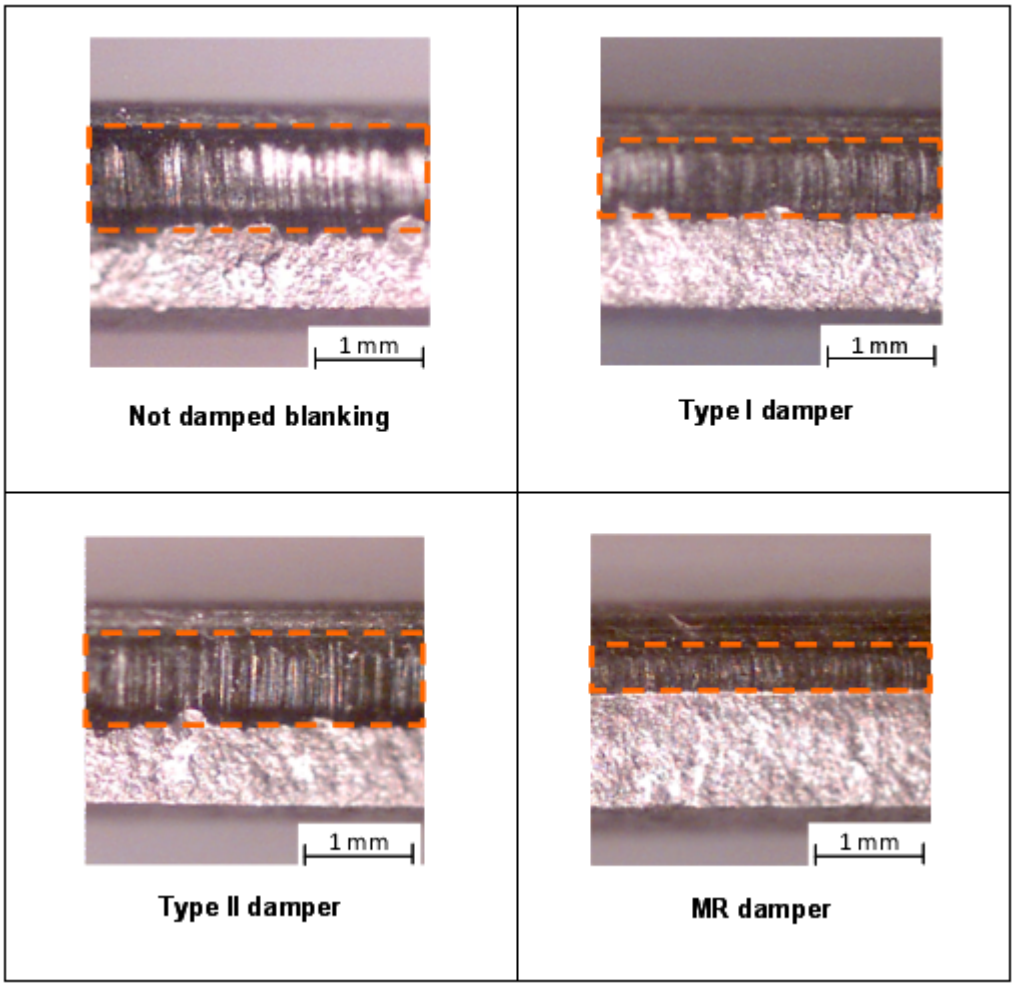

Figure 5.24 – Fractured surfaces of 2 mm sheet in the cases studied.

Table 5.4 – Shear, fracture and scratch surface width of 2 mm sheet**.**

2 mm sheet	**fratured surface [mm]**		
	shear	**fracture**	**scratch**
no damping	0,234	0,780	0,942
Type I	0,325	1,096	0,580
Tipe II	0,324	0,978	0,698
MR	0,354	1,129	0,516

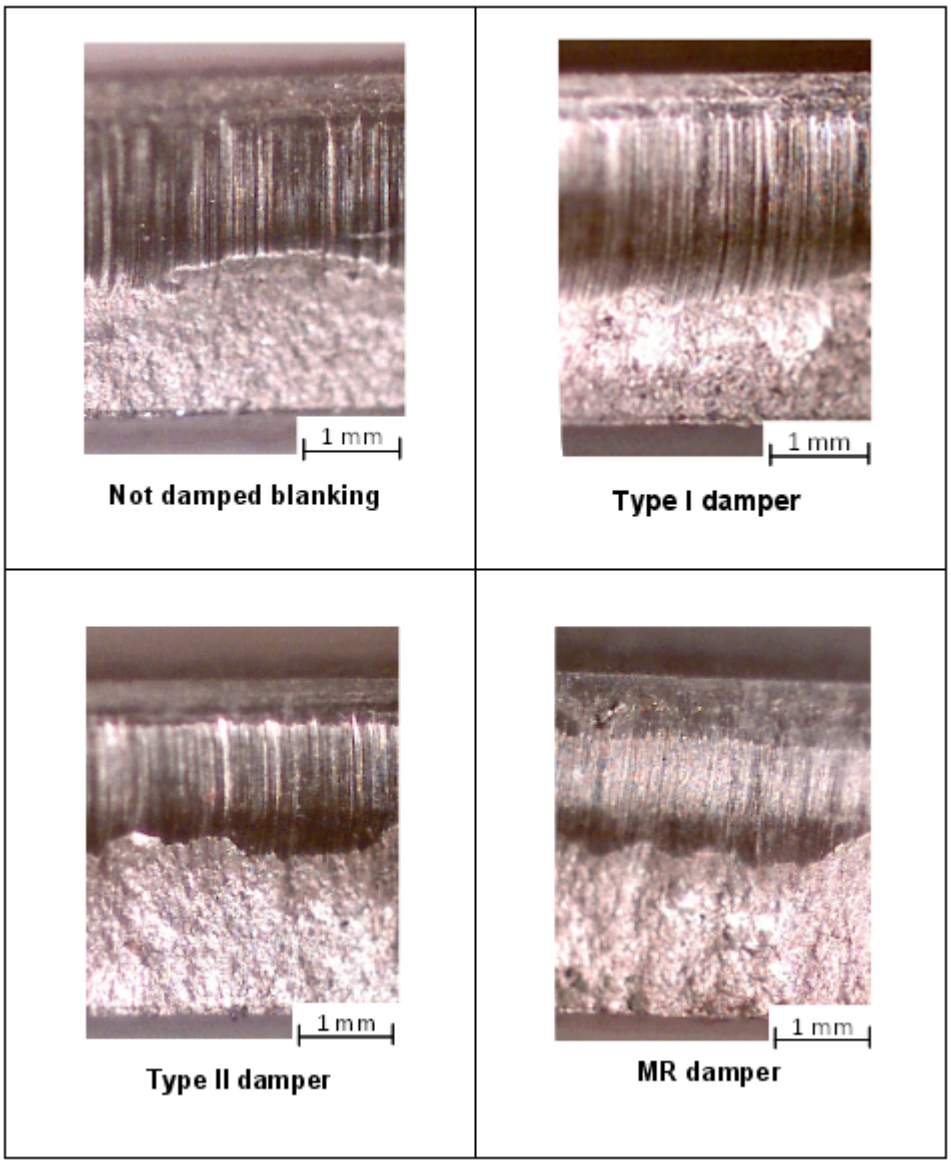

Figure 5.25 – Fractured surface of 3 mm sheet in the cases studied.

Table 5.5 – Shear, fracture and scratch surface width of 3 mm sheet

3 mm sheet	**fratured surface [mm]**		
	shear	**fracture**	**scratch**
no damping	0,134	1,46	1,404
Type I	0,282	1,256	1,471
Tipe II	0,406	1,53	1,06
MR	0,498	1,527	0,975

The average values of roughness (in terms of Ra) of several zones, for 2 mm and 3 mm the case studied, are respectively reported in Table 5.6 and Table 5.7. Typical roughness of shear and fractured surfaces [86] are measured.

Table 5.6 – Shear, fracture and scratch surface Ra values in 2 mm sheet metal.

2 mm sheet	**Roughness Ra [µm]**		
	shear	**fracture**	**scratch**
no damping	0,06	6,17	1,26
Type I	0,07	5,93	0,34
Tipe II	0,08	7,63	0,74
MR	0,06	6,92	0,19

Table 5.7 – Shear, fracture and scratch surface Ra values in 3 mm sheet metal.

3 mm sheet	**Roughness Ra [µm]**		
	shear	**fracture**	**scratch**
no damping	0,71	4,82	0,13
Type I	0,05	11,15	0,44
Tipe II	0,08	9,54	0,71
MR	0,06	9,12	0,19

5.6 CONCLUSIONS

The present chapter focuses on the study of the application of innovative damping systems to control vibration in shearing operations. These devices, based on MR fluids, allowed a controllable and reversible change of damping characteristics when an external magnetic field is applied. The experimental campaign conducted on an hydraulic press using both commercially available hydraulic dampers and MR dampers has shown that:

- the total process load is lower when using MR dampers;
- vibration frequencies during blanking and force oscillations after break through can be significantly decreased with MR dampers, reducing the impact of vibrations for the press structure and the tooling.

Effects on the fractured surfaces has been investigated and a reduction of scratched zone has been found with MR device damping.
Considering an assessment of production costs of the devices, mainly cost items can be distinguished (Table 5.8):

Table 5.8 – Cost assessment of a MR device

Cost item	Cost incidence [%]
Coil	10 %
Fluid	45 %
Raw material	5 %
Manufacturing	30 %
Control	10 %
Total	**100 %**

It can be noted that fluid is the main factor that influences the final cost; secondly the manufacturing. Thence, greater efforts have to be addressed in order to reduce to the minimum the magneto-rheological fluid used, to ensure the damping performances, as well as an economy of scale can optimize the manufacturing item.
The final expense of a single MR damper is comparable with the cost, for example, of hydraulic devices commercially available: about 10 % greater cost can be noted.
This difference can be justified for a possible industrial investment by the higher versatility and flexibility of MR devices in setting up new processes than a proven technology currently available.

CONCLUSIONS

The present work aimed at developing innovative technology for the process control in sheet metal forming operation, with particular interest to the proprieties of innovative magneto–rheological (MR) fluids. Among various forming operation, blanking and, more generally, shearing operations are the most common operations in the process chains for sheet metal parts. No application of magneto–rheological devices could be found in technical literature in the sheet metal context.

An innovative coupled multi-physics analysis has been defined, able to give an evaluation of thermal, structural and fluid dynamic fields and the effects of their mutual interaction in each field and in the global system. Finite elements analysis has been performed, according a preliminary damper model.

In the specific, results show that the prediction of the temperature increase, due to the dynamics and the changes in MR fluid viscosity determined by the applied magnetic field, do not exceed the operating range of the MR fluid.
Velocity and pressure distribution in the fluid volume are not critical for cavitation effects in the traditional range of use of the device. Moreover, stress and radial deformation of the moving components do not influence working and performances of the damper.
A magneto-static simulation was performed in order to study magnetic induction distribution in the models and to achieve inputs for the coupled analysis. The analysis of the influence of architectural configurations and the effects of the design solution, for particular requirements, on the magnetic field distribution were also possible.

Once developed the numerical model, useful for the design steps, MR damping proprieties have been studied by means of ad hoc experimental devices completely design and set up at DIMEG, University of Padova within the Phd period.
Deep experimental investigations on magneto-rheological fluids behaviour during devices working were performed, thanks to the development of two prototypes.
Damping response, linked to the input intensity currents and influence of noise factor and reservoir effects were investigated through the first device, showing good load performances with small power supplied.
Temperature evolution in the device during its work was investigated thanks to the second one. Temperature increase, due to the friction and viscous works when the MR fluid was activated, shows that maxima values are always under the critical fluid conditions and do not influence remarkably the damping performances of the device.

Main efforts were focused on optimizing the reverse load solution in metal blanking presses. MR damper characterized by high damping load (400 kN) has been developed. An original design solution has been studied in order to solve the problem of the fluid volume compensation, allowing an improvement in the centring of the moving parts and in the space placement on the press.
Through full-scale experiments, the feasibility and practicability of implementing MR dampers in an industrial context on an hydraulic press have been valued.
The potential benefits, when they are used in a semi-active manner in comparison with conventional dampers, have been studied. Analysis in time and frequency domains show that vibration frequencies during blanking and force oscillations after blanking can be significantly decreased with MR dampers, reducing the impact of vibrations for the press structure and the tooling. Moreover, magneto-rheological dampers allow to obtain a better control on the fractured surfaces, reducing the influence of tool vibrations due to the blanking shock

REFERENCES

[1]. R. Hambli, "Comparison between Lemaitre and Gurson damage models in crack growth simulation during blanking process", International Journal of Mechanical Sciences 43 (2001) 2769-2790.

[2]. G. Fang, P. Zeng, L. Lou, "Finite element simulation of the effect of clearance on the forming quality in the blanking process", Journal of Materials Processing Technology 122 (2002) 249–254.

[3]. B.A. Behrens, O. Marthiens, M. Werbs, "Electro-magnetic dampening of the cutting shock on sheet metal presses", Proceedings of the 8th International Conference on Technology of Plasticity 112/2-3 (2005) 379–380.

[4]. M. Otsu, C. Yamagata, K. Osakada, "Reduction of blanking noise by controlling press motion", CIRP Annals 52/1(2003) 245-248.

[5]. B. Guo, W.M. Chen, Z.R. Wang, "Analysis of blanking vibration with consideration of the break-through state", Journal of Materials Processing Technology 75/1-3 (1998) 117-121.

[6]. C. Brecher, M. Esser, S. Witt, "Interaction of manufacturing process and machine tool", CIRP Annals 58/2 (2009) 588-607.

[7]. J. Breitling, B. Pfeiffer, T. Altan, K. Siegert, "Process control in blanking", Journal of Materials Processing Technology, vol. 71/1, pp 187-192.

[8]. M. Farzin, H.R. Javani, M. Mashayekhi, R. Hambli, "Analysis of blanking process using various damage criteria", Journal of Materials Processing Technology 177 (2006) 287-290.

[9]. Y.W. Stegeman, A.M. Goijaerts, D. Brokken, W.A.M. Brekelmans, L.E. Govaert, F.P.T. Baaijens, "An experimental and numerical study of a planar blanking process", Journal of Materials Processing Technology 87/ 1-3 (1999) 266-276.

[10]. M. Murakawa, J. Mo, Y. Wakatsuki, N. Koga, "Investigation of blanking noise reduction using a hydraulic inertia damper", Journal of Materials Processing Technology 112/2-3 (2001) 205-213.

[11]. R.L. Wonsetler, M. White, "The use of hydraulic shock dampers to arrest the reverse load of blanking in presses".

[12]. AIDA-Tech, “Reverse Tonnage”, Volume Nine.

[13]. Metal Forming Handbook”, Schuler GmbH.

[14]. C.W. De Silva, “Vibration: Fundamentals and Practice”, CRC Press (1999)

[15]. S. Kalpakjian, “Manufacturing Processes For Engineering Material”, Pearson Education Inc. (2003).

[16]. D. A Smith, “Cutting force reduction and snap through energy reduction principles and techniques” (2006).

[17]. D. A Smith, “Die design handbook”, Technology & Engineering (1990)

[18]. E. Doege, H. J. Seidel, “Noise Reduction on Mechanical Punch Presses”, CIRP Annals, 34/1 (1985) 507-509.

[19]. A.M. Bassiuny, X. Li, “Fault diagnosis of stamping process based on empirical mode decomposition and learning vector quantization”, Int. J. Mach. Tools and Manuf. 47/15 (2007) 2298-2306.

[20]. J. Lai “Metal-cutting machinery noise and vibration prediction and control”, Handbook Of Noise And Vibration Control (2007).

[21]. O. Shinaishin, “Impact-Induced industrial noise”, Proceedings of International Conference on noise control Engineering, Washington (1972).

[22]. VIBROSTOP, website.

[23]. Ro-Dam, “Mechanische schnittschlagdmpfer technische beschreibung”, technical manual.

[24]. W-TECHNOLOGIES, website.

[25]. HYLATECHNICK, “Blanking stroke damper for presses”, technical manual.

[26]. C.M. Oldenburg, G.J. Moridis, “Ferrofluid flow for tough2”, LBL-41608 (1998).

[27]. P. Phulé, “Magnetorheological (MR) fluids: Principles and applications”, Smart Materials bulletin (2001).

[28]. G. Yang, B.F. Spencer, J.D. Carlson, M. Sain, “Large-scale MR fluid dampers: modelling and dynamic performance considerations”, Engineering Structures 24 (2002) 309-323.

[29]. G. Bossisa, S. Lacisb, A. Meuniera, O. Volkovaa, “Magnetorheological fluids”, Journal of Magnetism and Magnetic Materials 252 (2002).

[30]. J. D Carlson, M. R. Jolly, “MR fluid, foam and elastomer devices”, Mechatronics 10 (2000) 555-569.

[31]. LORD CORPORATION, "Materials Data", website.

[32]. F.D. Goncalves, J.H. Koo, M. Ahmadian, "A Review of the State of the Art in Magnetorheological Fluid Technologies – Part I: MR fluid and MR fluid models", The Shock and Vibration Diges (2006), Sage Publications.

[33]. J. D. Carlson "What makes a good mr fluid?", 8th International Conference on Electrorheological (ER) Fluids and Magneto-rheological (MR) Suspensions, Nice (2001).

[34]. A. Ashfak, K.K. Saheed, A. Rasheed, J.A. Jaleel, "Design, Fabrication and Evaluation of MR Damper", International Journal of Aerospace and Mechanical Engineering (2001).

[35]. LORD corporation, MRF 132 DG Technical data.

[36]. M.R. Jolly, J.W. Bender, J.D. Carlson, "Properties and Applications of Commercial Magnetorheological Fluids", SPIE 5th Annual Int. Symposium on Smart Structures and Materials, San Diego (1998).

[37]. M.R. Jolly, J.D. Carlson and B.C. Muñoz, "A Model of the Behaviour of Magnetorheological Materials", Smart Mater. Struct. 5 (1996) 607-614.

[38]. B.F. Spencer, S.J. Dyke, M.K. Sain, J.D. Carlson, "Phenomenological Model of a Magnetorheological Damper", Journal of Engineering Mechanics, March 10 (1996).

[39]. R.W. Phillips, "Engineering Applications of Fluids with a Variable Yield Stress," Ph.D. Dissertation, University of California (1969).

[40]. P.C. Murphy, E. Adalsteinsson, M. Zahn, "Numerical Simulations of Magnetic Nanoparticle Suspensions as Interactive MRI Contrast Agents", Comsol Conference Boston (2007)

[41]. D.R. Gamota, F.E Filisko, "Dynamic Mechanical Studies of Electrorheological Materials: Moderate Frequencies." Journal of Rheology 35 (1991) 399–425.

[42]. C. Namuduri, M. Golden, J. Praeckel, "Concurrent Research and Development of a Magnetic Ride Control System", US Patent (2000).

[43]. H.P. Gavin, R.D. Hanson, F.E. Filisko, "Electrorheological dampers, part I: analysis and design", Journal of Applied Mechanics 63 (1996) 669–675.

[44]. R.Y. Hong, Z.Q Ren, Y.P. Han, H.Z. Li, Y. Zheng, J. Ding, "Rheological proprieties of water – based Fe_3O_4 ferrofluids", Chemical Engineering Science 62 (2007) 5912 – 5924.

[45]. N. M. Wereley, Pang, L, "Nondimensional Analysis Of Semi- Active Electrorheological And Magnetorheological Dampers Using Approximate Parallel Plate Models", Smart Materials and Structures 7 (1998) 732–743.

[46]. S.R. Hong, S.B. Choi, Y.T. Choi, N.M. Wereley, "Non-dimensional analysis for effective design of semi-active electrorheological damping control systems", Proceedings of the Institution of Mechanical Engineers, J. of Aut. Eng. 217 (2003) 1095–1106.

[47]. W. Hu, N. M. Wereley, "Nondimensional Damping Analysis of Flow – mode Magnetorheological and Electrorheological Dampers", Proceedings of IMECE (2003) Washington.

[48]. N.M. Wereley, J.U Cho, Y. T. Choi, S. B. Choi, "Magnetorheological dampers in shear mode", Smart Materials And Structures 17 (2008).

[49]. D.J. Peel, R. Stanway, W.A. Bullough, "Dynamic modelling of an ER vibration damper for vehicle suspension applications", Smart Materials and Structures 5 (1996) 591–606.

[50]. W. W. Chooi, S. O. Oyadiji, "Design, modelling and testing of magnetorheological (MR) dampers using analytical flow solutions", Computers and Structures 86 (2008) 473–482.

[51]. L. Zipser, L. Richter, U. Lange, "Magnetorheologic fluids for actuators", University of Applied Sciences Dresden, Germany (2000).

[52]. X. Wang, F. Gordaninejad, "Flow Analysis of Field-controllable, Electro- and Magneto-rheological Fluids Using Herschel-Bulkley Model", Journal of Intelligent Systems and Structures 10 (1999) 601– 608.

[53]. D. Y. Lee, N. M.Wereley, "Analysis of Electro- and Magnetorheological Flow Mode Dampers Using Herschel-Bulkley Model", Proceedings of SPIE Smart Structure and Materials Conference 3989 (2000) 244–252.

[54]. G. Yang, "Large-Scale Magnetorheological Fluid Damper for Vibration Mitigation: Modeling, Testing and Control," Ph.D. Dissertation, University of Notre Dame (2001).

[55]. N.M Kwok, Q.P Ha, M.T. Nguyen, J. Li, B. Samali, "Bouc–Wen model parameter identification for a MR fluid damper using computationally efficient GA", ISA Transactions 46 (2007) 167-179.

[56]. G. M. Kamath, M. K. Hurt, N. M.Wereley, "Analysis and Testing of Bingham Plastic Behavior in Semi-Active Electrorheological Fluid Dampers", Smart Materials and Structures, 5 (1996) 576–590.

[57]. A. Dominguez, R. Sedaghati, I. Stiharu, "A new dynamic hysteresis model for the magnetorheological dampers", Smart Mater Struct. 15 (2006) 1179–89

[58]. B. Sapinski, "Linearized characterization of a magneto-rheological fluid damper", Mechanics 24 (2005).

[59]. C.C. Chang, P. Roshke, "Neural network modeling of a magnetorheological damper" J Intell Mater Syst Struct 9 (1998) 755–64.

[60]. D.H. Wang, W.H. Liao, "Modeling and control of magnetorheological fluid dampers using neural network", Smart Mater. Struct. 14 (2005) 111–126.

[61]. X. Zhou, B. Nielsen D. Qu, "Semi-active control of three-dimensional vibrations of an inclined sag cable with magnetorheological dampers", Journal of Sound and Vibration 296 (2006) 1–22.

[62]. K. Milecki, "Investigation and control of magneto–rheological fluid dampers", International Journal of Machine Tools & Manufacture 41 (2001) 379–391.

[63]. H.H. Tsang, R.K.L. Su, A.M. Chandler, "Simplified inverse dynamics models for MR fluid dampers", Engineering Structures 28 (2006) 327–341.

[64]. D. Carlson, D.M. Catanzarite, K.A. St.Clair, "Commercial Magneto-Rheological Fluid Devices", Lord Corporation.

[65]. C.C. Siew, M. Hill, R. Holmes, "Evaluation of various fluid-film models for use in the analysis of squeeze film dampers with a central groove" Tribology International 35 (2002) 533–547 .

[66]. H. Esmondea, H. Seeb, M.V. Swainb, "Modelling of ER squeeze films at low amplitude oscillations", J. Non-Newtonian Fluid Mech. 161 (2009) 101–108.

[67]. S. R. Honga, S. B. Choia, M. S. Han, "Vibration control of a frame structure using electro-rheological fuid mounts", International Journal of Mechanical Sciences 44 (2002) 2027–2045.

[68]. J. W. Gravatt, "Magneto-Rheological dampers for super – sport motorcycle applications", Master thesis, Virginia Polytechnic Institute and State University (2003).

[69]. W.H. El-Aouar, "Finite element analysis based modelling of magnetorheological dampers", Master thesis, Virginia Polytechnic Institute and State University, (2002).

[70]. B. F. Spencer, G. Yang, J. D. Carlson, M. Sain**, "**Smart dampers for seismic protection of structures: a full – scale study", 2° Conference on Structural Control, Kyoto (1998).

[71]. K. Sunakoda, H. Sodeyama, N. Iwata, H. Fujitani, S. Soda, "Dynamic performance evaluation of 200kN magnetorhological damper", Smart Struct. Mater. Conference (2000).

[72]. J. A. Cortés, L. S. Villarreal-González, M. Martínez, "Characterization, modelling and simulation of magnetorheological damper behaviour under triangular excitation", Journal of Material 1 (2005).

[73]. S. P. Kelso, "Experimental characterization of commercially practical magnetorheological fluid damper technology", SPIE Conference on Smart Structures and Materials 4332-34 (2001).

[74]. P. Lethbridge "Multiphysics Analysis",American Institute of Physics (2005).

[75]. ANSYS Workbench, Release 10.0 Documentation (2005).

[76]. P. Regazzo, A. Ghiotti, "Development of innovative systems based on smart fluids technology for the improvement of the dimensional accuracy in sheet metal forming operations", Proceedings of the 12th ESAFORM Conf. on Material Forming, Enschede THE NETHERLANDS (2009).

[77]. LORD corporation, MRF 132 DG Technical data.

[78]. ASM HANDBOOK, "Materials characterization", volume 18.

[79]. Steward D. E., Leyk Z. "ANSYS 10.0 Documentation" Meschach Library Copyright (1993).

[80]. P. Regazzo, A. Ghiotti, "Improvement of dimensional accuracy and machine service life in sheet metal forming by control systems based on MR fluids", IV ECCOMAS Thematic conference on Smart structures and materials, Porto PORTUGAL (2009).

[81]. H.A Barnes, J.F. Hutton and K. Walters, "An Introduction to Rheology" Elsevier Science Publishers (1989).

[82]. M. Fauri, F. Gnesotto, G. Marchesi, A. Maschio, "Lezioni di elettrotecnica" Esculapio, Bologna (2003)

[83]. Lord corporation, Technical data

[84]. G. Yang, B.F. Spencer, H.J Jung, J.D. Carlson, "Phenomenological model of large-scale MR damper systems", Advanced In Building Technology 1 (2002).

[85]. L. Yang, F Duan, A. Eriksson, "Analysis of the optimal design strategy of a magnetorheological smart structure", smart material and structures 17 (2008).

[86]. ASM HANDBOOK, "Surface engineering", volume 05.

[87]. A. Ghiotti, P. Regazzo, S. Bruschi, P.F. Bariani "Reduction of vibrations in blanking by MR dampers", Cirp Annals 59 (2010) 275–278

[88]. P. Regazzo, A. Ghiotti (2010), "Vibrations reduction in blanking by magneto-rheological shock dampers" Proceedings of 2nd International CIRP Process Machine Interaction (PMI) Conference, Vancouver CANADA (2010)